A&A 674, A18 (2023)
https://doi.org/10.1051/0004-6361/202243964

Astronomy & Astrophysics
Special issue

Gaia Data Release 3

Gaia Data Release 3

Specific processing and validation of all-sky RR Lyrae and Cepheid stars: The RR Lyrae sample⋆

G. Clementini[1,⋆⋆], V. Ripepi[2], A. Garofalo[1], R. Molinaro[2], T. Muraveva[1], S. Leccia[2], L. Rimoldini[3], B. Holl[3], G. Jevardat de Fombelle[3], P. Sartoretti[4], O. Marchal[5], M. Audard[3,6], K. Nienartowicz[3,7], R. Andrae[8], M. Marconi[2], L. Szabados[9,10], D. W. Evans[11], I. Lecoeur-Taibi[3], N. Mowlavi[3], I. Musella[2], and L. Eyer[6]

[1] INAF, Osservatorio di Astrofisica e Scienza dello Spazio di Bologna, Via Piero Gobetti 93/3, 40129 Bologna, Italy
[2] INAF-Osservatorio Astronomico di Capodimonte, Via Moiariello 16, 80131 Naples, Italy
[3] Department of Astronomy, University of Geneva, Ch. d'Ecogia 16, 1290 Versoix, Switzerland
[4] GEPI, Observatoire de Paris, Université PSL, CNRS, 5 place Jules Janssen, 92190 Meudon, France
[5] Observatoire Astronomique de Strasbourg, Université de Strasbourg, CNRS, UMR 7550, 11 rue de l'Université, 67000 Strasbourg, France
[6] Department of Astronomy, University of Geneva, Chemin Pegasi 51, 1290 Versoix, Switzerland
[7] Sednai Sàrl, Geneva, Switzerland
[8] Max Planck Institute for Astronomy, Königstuhl 17, 69117 Heidelberg, Germany
[9] Konkoly Observatory, ELKH Research Centre for Astronomy and Earth Sciences, Eötvös Loránd Research Network, Konkoly Thege Miklós út 15-17, 1121 Budapest, Hungary
[10] CSFK Lendület Near-Field Cosmology Research Group, Konkoly Thege Miklós út 15-17, 1121 Budapest, Hungary
[11] Institute of Astronomy, University of Cambridge, Madingley Road, Cambridge CB3 0HA, UK

Received 5 May 2022 / Accepted 4 July 2022

ABSTRACT

Context. RR Lyrae stars are excellent tracers of the oldest stars (ages $\gtrsim$ 9–10 Gyr) and standard candles for measuring the distance to stellar systems that are mainly composed of an old stellar population. The *Gaia* Third Data Release (DR3) publishes a catalogue of full-sky RR Lyrae stars observed during the initial 34 months of science operations. They were processed through the Specific Object Study (SOS) pipeline, which was developed to validate and characterise Cepheids and RR Lyrae stars (SOS Cep&RRL) observed by *Gaia*.
Aims. The main steps of the SOS Cep&RRL pipeline are described in the documentation and papers accompanying previous *Gaia* data releases. For DR3, the pipeline was modified in its process: in addition to the *Gaia* multiband (G, G_{BP}, G_{RP}) time-series photometry, the epoch radial velocities measured for RR Lyrae and Cepheids with the Radial Velocity Spectrometer (RVS) on board *Gaia* were also processed through the pipeline.
Methods. The SOS Cep&RRL validation of DR3 candidate RR Lyrae stars relies on diagnostics tools that include the period versus G-amplitude diagram and the period versus ϕ_{21} and ϕ_{31} parameters of the G light-curve Fourier decomposition, as defined by a reference sample of bona fide RR Lyrae stars known in the literature (that we named Gold Sample). Great care was devoted to building a large and pure Gold Sample comprising more than 200 000 RR Lyrae stars. The SOS processing led to an initial catalogue of 271779 RR Lyrae stars that are listed in the `vari_rrlyrae` table of the DR3 archive. A thorough cleaning procedure was then performed to produce a final catalogue of SOS-confirmed DR3 RR Lyrae stars by dropping sources that clearly are contaminants or have an uncertain classification.
Results. Multiband time-series photometry and characterisation are published in *Gaia* DR3 for a clean, validated sample of 270 905 RR Lyrae stars (174 947 fundamental-mode, 93 952 first-overtone, and 2006 double-mode RR Lyrae) that were confirmed and fully characterised by the SOS Cep&RRL pipeline. They are distributed throughout the sky, including variables in 95 globular clusters and 25 Milky Way (MW) companions (the Magellanic Clouds, seven dwarf spheroidal galaxies, and 16 ultra-faint dwarf satellites of the MW). RVS time-series radial velocities are also published for 1096 RR Lyrae and 799 Cepheids of different types (classical, anomalous, and type II Cepheids). Of the 270 905 DR3 RR Lyrae stars, 200 294 are already known in the literature (Gold Sample) and 70 611 are new discoveries by *Gaia*, to the best of our knowledge. An estimate of the interstellar absorption is published for 142 660 fundamental-mode RR Lyrae stars from a relation based on the G-band amplitude, the $(G - G_{RP})$ colour and the pulsation period. Metallicities derived from the Fourier parameters of the light curves are also released for 133 559 RR Lyrae stars.
Conclusions. The final *Gaia* DR3 catalogue of confirmed RR Lyrae stars almost doubles the DR2 RR Lyrae catalogue. An increase in statistical significance, a better characterisation of the RR Lyrae pulsational and astrophysical parameters, and the improved astrometry published with *Gaia* EDR3 make the SOS Cep&RRL DR3 sample the largest, most homogeneous, and parameter-richest catalogue of all-sky RR Lyrae stars published so far in the magnitude range from $\langle G \rangle$ = 7.64 mag (the magnitude of RR Lyr itself, the class prototype) to $\langle G \rangle$ = 21.14 mag (the faintest RR Lyrae in the catalogue).

Key words. stars: general – stars: oscillations – stars: variables: RR Lyrae – stars: variables: Cepheids – Magellanic Clouds – methods: data analysis

⋆ Full Tables 2, 5–9, A.1–A.2, and lightcurves are only available at the CDS via anonymous ftp to `cdsarc.cds.unistra.fr` (`130.79.128.5`) or via `https://cdsarc.cds.unistra.fr/viz-bin/cat/J/A+A/674/A18`

⋆⋆ Corresponding author: G. Clementini, e-mail: `gisella.clementini@inaf.it`

1. Introduction

RR Lyrae are low-mass (typical masses around 0.6–0.8 $M_{\odot}$), old (ages exceeding 9–10 billion years) stars whose surface expands and contracts regularly with periods shorter than one day. The pulsation gives rise to a variation in brightness that occurs in two main flavours. The light curves of c-type RR Lyrae (RRc) stars are almost sinusoidal. They repeat in time with periodicities of typically between about 0.2 and 0.42 day (d), and an amplitude in light variation of up to about half a magnitude in the visual band. RRc stars oscillate in the radial first-overtone pulsation mode. The ab-type RR Lyrae (RRab) stars have asymmetrical sawtooth light curves, periods of typically between about 0.42 and 1 d, and visual amplitudes in the *Gaia* G band from above 0.1 to more than one magnitude. They pulsate in the fundamental pulsation mode. In a small fraction of RR Lyrae stars, fundamental and first-overtone pulsation modes are excited at the same time, giving rise to the double-mode (d-type) RR Lyrae (RRd). The characteristic light variation makes RR Lyrae stars easily recognizable even in very crowded regions of the sky or in high-extinction conditions. Their pulsation characteristics (periods, amplitudes, mean magnitudes and colours, etc.) allow an estimate of their metal abundance and reddening, thus bringing invaluable added values (see e.g. Smith 1995; Catelan & Smith 2015, for comprehensive reviews of RR Lyrae stars).

RR Lyrae stars allow measuring the distance to the systems they live in because they follow luminosity–metallicity (LZ) relations in the visual bands (see e.g. Cacciari & Clementini 2003; Clementini et al. 2003; and references therein and e.g. Muraveva et al. 2018; Garofalo et al. 2022; for more recent LZ relations in the Johnson V and *Gaia* G bands, calibrated on *Gaia* parallaxes) and period–luminosity–(metallicity) (PLZ) relations in the infrared (see e.g. Muraveva et al. 2018; Bhardwaj et al. 2021, and references therein for PLZ relations in the K_s and W_1 infrared bands). These variable stars are the only abundant stellar tracers with a small relative distance error (~5%), particularly at large distances. They therefore allow measuring the most accurate distances to old, distant stellar populations. Moreover, at 5–10 kpc from the Milky Way (MW) disc, they are also the stars with the most precise distances.

RR Lyrae stars are also excellent tracers of the oldest stars that witnessed the first epoch of galaxy formation. They can therefore provide indications about the building blocks that contributed to the build-up of galactic haloes (see e.g. Catelan & Smith 2015; Martínez-Vázquez et al. 2019, and references therein). All these properties make the RR Lyrae stars invaluable dynamical tracers of the Galaxy and a crucial tool for a plethora of applications, from Galactic archaeology and the search for the fossil records of the Galactic formation to tidal streams, dynamics, a validation of distances and extinction maps, and the characterisation of small scale extinction. This explains the renewed widespread interest in these stars within the astronomical community.

Previous *Gaia* data releases (Gaia Collaboration 2016, 2018) already showed the great potential of the mission in the field of stellar variability (Gaia Collaboration 2019) and for RR Lyrae stars and Cepheids in particular (Gaia Collaboration 2017; Clementini et al. 2016, hereafter Paper I; Clementini et al. 2019, hereafter Paper II). The potential is based on the multi-epoch nature and almost simultaneous acquisition of the (spectro-)photometry, astrometry and spectroscopy data collected by *Gaia* throughout the celestial sphere.

The small sample of RR Lyrae stars and Cepheids in the Large Magellanic Cloud (LMC; about 3200 sources in total) published with *Gaia* Data Release 1 (DR1; Paper I) were only a teaser of the samples and data products published for these pulsating stars in subsequent *Gaia* releases. Multi-band time-series photometry and pulsation characteristics were published in *Gaia* Data Release 2 (DR2; Gaia Collaboration 2018) for a catalogue of about 140 000 RR Lyrae stars and for about 10 000 Cepheids observed in the whole Galaxy (including 87 globular clusters and 14 MW companions) during the first 22 months of *Gaia* operation (Paper II). The number of RR Lyrae has now almost doubled, and that of Cepheids has increased by 50% compared to DR2 because of the larger amount of data and extended time baseline (34 months) spanned by *Gaia* Data Release 3 (DR3).

On 13 June 2022, *Gaia* DR3 (Gaia Collaboration 2023) multiband (G, G_{BP}, and G_{RP}) light curves were released for 270 905 RR Lyrae stars together with 15 006 Cepheids that were confirmed and fully characterised by the Specific Object Study pipeline for Cepheids and RR Lyrae (hereafter, SOS Cep&RRL; Papers I and II) developed within the *Gaia* Data Processing and Analysis Consortium (DPAC). Radial velocity (RV) time-series measurements obtained with the Radial Velocity Spectrometer (RVS; Cropper et al. 2018) on board *Gaia* for a sub-sample comprising 1096 RR Lyrae stars and 799 Cepheids (Ripepi et al. 2023) validated by the SOS Cep&RRL pipeline are also published with DR3. These numbers all refer to samples that were cleaned from contaminants and sources with an uncertain classification.

In this paper we present the changes that were implemented in the SOS Cep&RRL pipeline with respect to DR2. We describe in particular a new module that was activated to process the RVS time-series data and explain how the RR Lyrae and Cepheid variables with epoch RVs published in DR3 were selected. We then focus on the procedures and validations that led to the production of the final clean sample of confirmed RR Lyrae stars released in DR3. The processing and validation of the confirmed DR3 Cepheids are instead described in a companion paper (Ripepi et al. 2023).

The characteristic parameters derived by the SOS pipeline for the final sample of *Gaia* DR3 RR Lyrae stars that are published in the `vari_rrlyrae` table include the pulsation period(s), peak-to-peak amplitudes of the G, G_{BP}, and G_{RP} [Amp(G), Amp(G_{BP}), Amp(G_{RP})] light curves, classification into type/pulsation mode (RRab, RRc, and RRd), and the mean magnitudes computed as an intensity average over the full pulsation cycle, along with the ϕ_{21}, ϕ_{31}, R_{21}, and R_{31} parameters of the Fourier decomposition of the G-band light curves. Metallicities ([Fe/H]) computed from a relation that was found to exist with the pulsation period and the ϕ_{31} Fourier parameter of the RR Lyrae light curves (Jurcsik & Kovacs 1996; Nemec et al. 2013) and individual absorption values derived from the relation existing with the pulsation period, the colour and the amplitude of the light variation (Piersimoni et al. 2002) are also released for about a half of the whole SOS RR Lyrae sample. Amplitudes of the RV curves and mean RV values that were computed after modelling the RV curves are also provided in the DR3 `vari_rrlyrae` and `vari_cepheid` tables for sub-samples of RR Lyrae stars and Cepheids.

The paper is organised as follows. In Sect. 2 we provide a brief overview of the SOS Cep&RRL pipeline and describe the changes and developments that were implemented

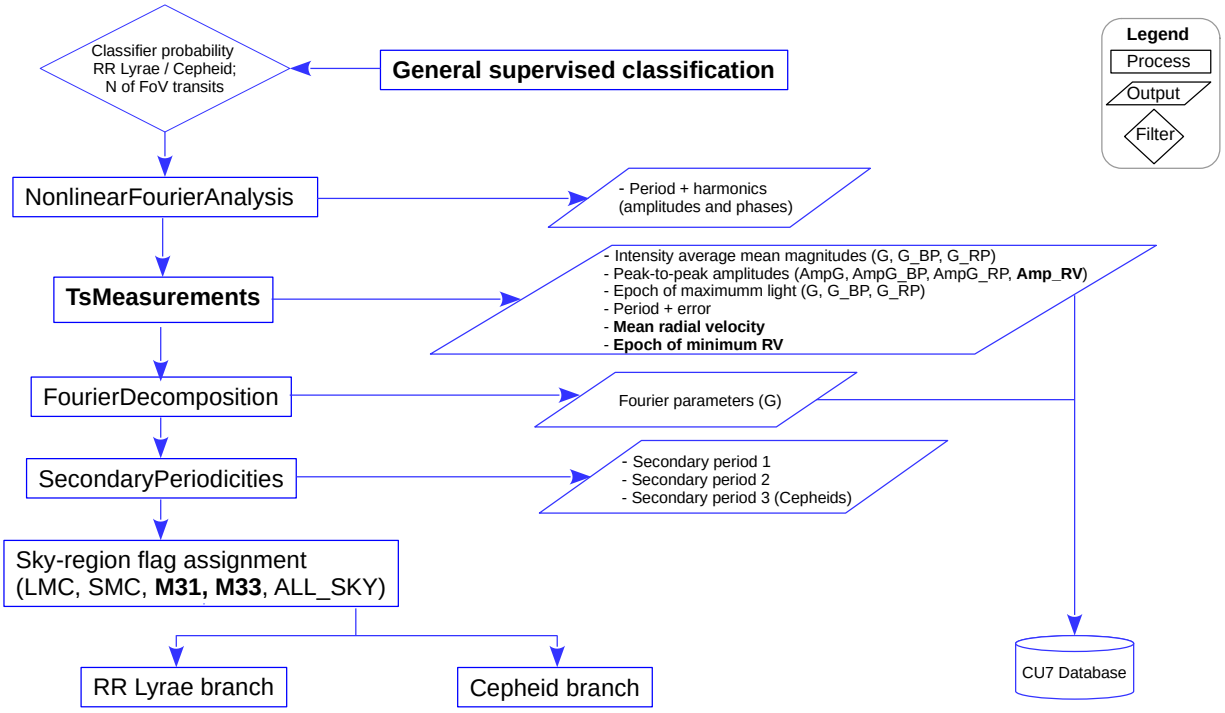

Fig. 1. Schematic view of modules (rectangles) and outputs (parallelograms) of the SOS Cep&RRL pipeline main trunk. The figure is an updated version of Fig. 1 in Paper II. Changes and additions to the pipeline version used in DR2 are highlighted in boldface (see text for details).

to process the *Gaia* DR3 photometry and RV time-series data. Section 3 presents the DR3 input data, the selections that were applied to run the pipeline on the RR Lyrae candidates, and results from the processing. Section 4 focuses on the analysis of the RVS RV time-series data for sub-samples of RR Lyrae stars and Cepheids for which RVS RV curves are published in DR3. Section 5 specifically discusses the astrophysical parameters (metallicity and G-band absorption values) we derived from the pulsation characteristics of RR Lyrae stars. The cleaning from contaminants, reclassifications, and a final validation of the RR Lyrae catalogue are described in Sect. 6. In Sect. 7 we discuss the completeness and purity of the clean catalogue of RR Lyrae stars published in DR3 and present colour-magnitude diagrams and sky maps defined by these RR Lyrae stars. Finally, conclusions and further developments of the SOS Cep&RRL pipeline in preparation for future *Gaia* data releases (DR4 and 5) are briefly discussed in Sect. 8.

2. SOS Cep&RRL pipeline: General overview and changes for DR3

The variability processing (see *Gaia* DR3 Documentation, Rimoldini et al. 2022)[1] is based on the analysis of *Gaia* DR3 calibrated G and integrated G_{BP} and G_{RP} time-series photometry (Riello et al. 2021), and for RR Lyrae stars and Cepheids also on the RVS RV time-series (Sartoretti et al. 2022), through the various steps (modules) of the general variability analysis approach described in Eyer et al. (2017) and in Eyer et al. (2023) specifically for DR3. This includes identification and classification into different types of the variable candidates, which are then fed to the SOS pipelines, each of which is specifically tailored to validate and characterise a certain type of variability. Figure 10.1 in the *Gaia* DR3 Documentation (Rimoldini et al. 2022) shows a schematic view of the general variability processing before the data enter the SOS pipelines.

The SOS Cep&RRL pipeline is designed to validate and characterise all-sky candidate RR Lyrae stars and Cepheids identified in the *Gaia* G, G_{BP}, and G_{RP} time-series photometry by the General Supervised Classification module (Rimoldini et al. 2023) in the variability analysis pipeline. This module uses machine-learning methods and multi-class supervised classifiers to classify *Gaia* time series of candidate variable objects into categories. A full description of the SOS Cep&RRL pipeline can be found in Papers I and II, to which we refer for details. In the following, we summarise steps of the pipeline that are the same for RR Lyrae stars and Cepheids (pipeline main trunk, Fig. 1) and the processing that takes place in the RR Lyrae branch (Fig. 2). The Cepheid branch is discussed in a companion paper (Ripepi et al. 2023).

The steps of the SOS Cep&RRL pipeline main trunk include

- a derivation of the source periodicity (P) with the Lomb-Scargle algorithm (Lomb 1976; Scargle 1982; see Sect. 2.1 in Paper I);
- modelling of the time-series data, folded according to the derived P, using the Levenberg-Marquardt (Levenberg 1944; Marquardt 1963) non-linear fitting algorithm (NonLinearFourierAnalysis module in Fig. 1), which refines the period and model of the light curves;
- a derivation of the main parameters of the variable stars (intensity-averaged mean magnitudes; peak-to-peak amplitudes: Amp(G), Amp(G_{BP}), and Amp(G_{RP}); epoch of maximum light; etc.) from the light curves modelled with the non-linear fitting algorithm;
- Fourier decomposition of the G-band light curve and derivation of the Fourier parameters ϕ_{21}, ϕ_{31}, R_{21}, and R_{31} using a Fourier expansion in cosine functions;
- a search for secondary periodicities.

[1] https://gea.esac.esa.int/archive/documentation/GDR3/

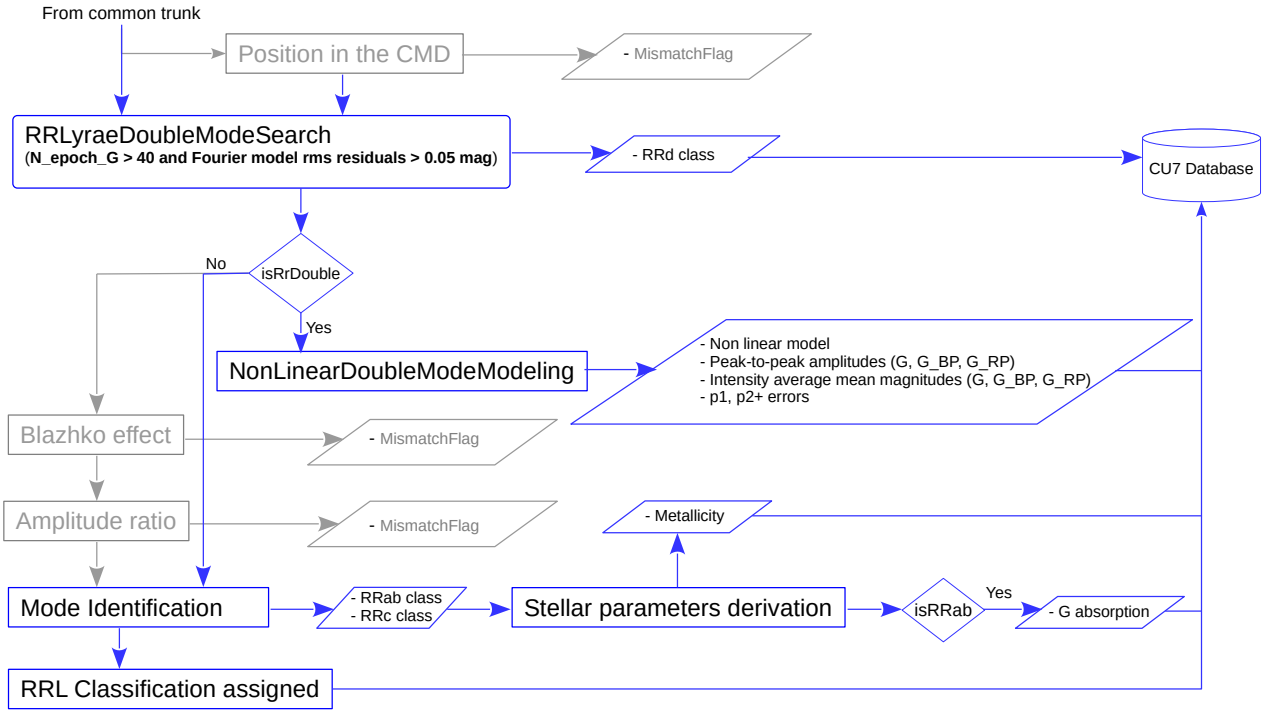

Fig. 2. Modules and outputs of the RR Lyrae branch of the SOS Cep&RRL pipeline. As in Fig. 1, changes with respect to DR2 are highlighted in boldface. Three modules that were not activated for DR3 are shown in grey (see text for details).

The following diagnostic tools and combination of parameters are used in the RR Lyrae branch to extract bona fide RR Lyrae stars from the candidates, classify them into types (RRc, RRab, RRd) and pulsation mode (first overtone, fundamental mode, and double mode), and derive their astrophysical parameters [metallicity – [Fe/H], and absorption in the G-band – $A(G)$],

- pulsation period (P) versus Amp(G) diagram (PA);
- ϕ_{21} versus P diagram;
- R_{21} versus P diagram;
- ϕ_{31} versus P diagram;
- R_{31} versus P diagram;
- [Fe/H] versus P, ϕ_{31} relation;
- $A(G)$ versus Amp(G), P, $(G - G_{RP})$ relation.

A number of changes were implemented and new parts of the pipeline were activated to process the DR3 RR Lyrae and Cepheid candidates. We have highlighted them in boldface in Figs. 1 and 2 and describe below those that occur in (and before) the pipeline main trunk and the RR Lyrae branch. A detailed description of the changes implemented in the Cepheid branch (improved detection of multimode Cepheids, adoption of new period-luminosity and period-Wesenheit relations directly computed in the *Gaia* passbands for the different types of Cepheids, etc.) is presented in Ripepi et al. (2023).

- Optimisation of outlier-removal operators
  Outliers and measurements of poor quality in the *Gaia* photometry and RV time-series data are filtered out by operators of the general variability pipeline, whose configuration parameters can be adapted to the specific type of variable sources under investigation. In the main chain of operators that are applied sequentially to transform and filter the input photometric time series, the `RemoveOutliersFaintAndBrightOperator` (`ROFABO`) that was adopted for DR2, was replaced by the `MultibandOutlierRemovalOperator` (`MORO`) (see Sect. 10.2.3.2 in *Gaia* DR3 Documentation, Rimoldini et al. 2022; Eyer et al. 2023). `MORO` identifies outliers from comparing the measurements in the three *Gaia* photometric bands. However, a `ROFABO` step, with configuration parameters we specifically tailored to RR Lyrae and Cepheid variables, was also added to the operators chain to improve the rejection of poor measurements in the time-series photometry of sources processed through the SOS Cep&RRL pipeline. An `RvsOutlierRemovalOperator` that applies a similar approach as the `ROFABO` was also applied to clean the RVS time-series data (see Rimoldini et al. 2022, for details).
- Processing of RVS radial velocity time series.
  A specific routine was activated that processes the RVS time-series RV measurements. The routine constructs the Fourier model of the RV curve obtained by folding the data according to the period inferred from the G-band time-series photometry and returns the Fourier amplitudes and phases, the peak-to-peak amplitude of the RV curve [Amp(RV)], the mean RV, and the epoch of minimum RV value.
- Error estimate via the bootstrap technique.
  Errors for all the parameters of the RR Lyrae stars and Cepheids that were processed and confirmed by the SOS pipeline for DR3 were estimated via a bootstrap technique that replaced the Monte Carlo simulations (consisting of randomly varying the data within their errors) adopted for DR1 and DR2 (Papers I and II). Specifically, errors on the Fourier fit parameters (period, amplitudes, and phases) and the quantities characterising the light and RV curves (mean magnitudes, mean velocity, peak-to-peak amplitudes, etc.) were estimated by randomly resampling the input data (allowing data point repetitions), and the parameters were recalculated from the resulting simulated sample. The procedure was repeated 100 times, and for each parameter, the error was estimated from the robust standard deviation (1.486 × MAD, where MAD is the median absolute deviation) of the resulting bootstrap distributions. A similar procedure was

also applied to estimate random errors of other attributes released for RR Lyrae stars, such as metal abundances and absorption values.

– New and revised sky sub-regions.
The last module of the main trunk of the pipeline subdivides the sources according to different regions on the sky before sending them to the RR Lyrae and Cepheid branches. This is because different relations are needed to classify the sources depending on their position on the sky (see Paper II). For DR2, we divided the sky into three separate regions: the Large Magellanic Cloud (LMC), the Small Magellanic Cloud (SMC), and all-sky, comprising the remaining part of the sky. The LMC and SMC regions were expanded for DR3. The new region for the LMC is a box centred on the galaxy at $RA_{LMC}(J2000) = 82.5°$, $Dec_{LMC}(J2000) = -68.25°$ and extending from 67.50° to 97.50° in RA and from −75.00° to −62.00° in Dec. Similarly, the new region for the SMC is a box centred at $RA_{SMC}(J2000) = 16°$, $Dec_{SMC}(J2000) = -73°$ and extending from 0.00° to 30.00° in RA and from −76.00° to −70.00° in Dec. Two further regions were also defined, one centred on the Andromeda galaxy (M31) and one around the Triangulum galaxy (M33), to allow the processing of bright Cepheids within the reach of *Gaia* in these galaxies. The details of these two additional regions are provided in Ripepi et al. (2023).

In DR2, a number of Cepheids with a G-band amplitude smaller than 0.5 mag and periods shorter than 1 d were missed or misclassified as RR Lyrae stars. A change was implemented in the SOS pipeline for DR3 by which sources classified as RR Lyrae stars at the end of the common trunk in Fig. 1 were sent to both the RR Lyrae and the Cepheid branches if they belonged to the region of the sky and satisfied the conditions described below.

– All-Sky sources with an available parallax were always sent to both branches;
– Sources in the LMC and in the SMC sub-regions (as defined above) with an amplitude smaller than 0.5 mag, periods shorter than 1 d, and a mean G magnitude brigther than 18.5 and 19 mag in the LMC and SMC, respectively;
– All sources with $P \leq 1$ d in the M31 and M33 sub-regions.

This procedure caused a number of sources to have a double classification. They were checked and finally classified into just one class (RR Lyrae star or Cepheid; see Sects. 3.2 and 3.3).

Two main changes were implemented in the RR Lyrae branch (Fig. 2) of the SOS pipeline. They are briefly described below.

– Improvement of double-mode RR Lyrae detection
The module to search for a secondary periodicity in the time-series photometry of RR Lyrae stars was activated only for sources with more than 40 measurements (FoV transits) in the G-band time-series data and when residuals from the Fourier model that best fits the G-band light curve folded with the primary period were higher than 0.05 mag. This allowed us to reduce the number of spurious double-mode RR Lyrae detections significantly.
– Implementation of new thresholds in the PA diagnostic
The PA diagram is used by the SOS pipeline to separate fundamental-mode and first-overtone RR Lyrae stars (see Fig. 4 in Paper II). For DR1 and DR2, we applied a straight line to separate the RRab and RRc regions. For DR3, we have defined new boundaries of the two regions in order to properly distinguish high-amplitude short-period RRab from RRc stars. The new boundaries are shown as red segments (described by the condition $\mathrm{Amp}(G) \leq 0.64$ mag for $P \leq 0.34$ d) that replaced the dotted portion of the straight black line in Fig. 3. All sources below the red segments and the solid black line are classified as RRc stars, and sources above these lines are RRab stars. However, the new thresholds were not able to capture all such short-period RRab stars (see Sect. 6.1). A more efficient procedure will be implemented for *Gaia* DR4 that specifically takes into account the much steeper rise to maximum light of RRab compared to RRc stars. This will help to better distinguish the two types.

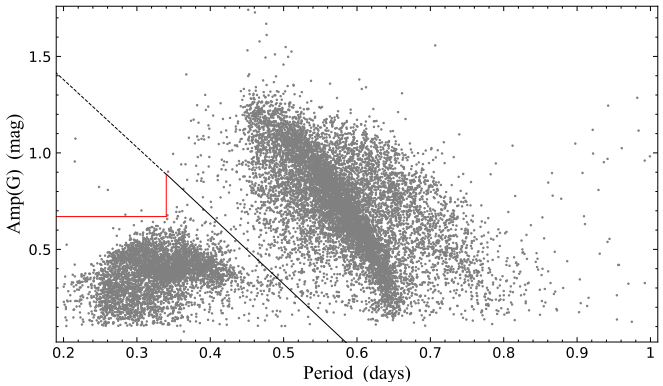

Fig. 3. New boundaries of the RRab and RRc regions in the PA diagram defined by a sample of about 15 000 RR Lyrae stars that was randomly selected from the final RR Lyrae catalogue published in the `dr3_vari_rrlyrae` table of *Gaia* DR3. The dotted portion of the black line separating RRab from RRc stars was replaced by the broken red line in order to properly classify high-amplitude RRab stars with pulsation periods in the same domain as RRc stars (see text for details).

Finally, we show in grey in Fig. 2 three modules that were not activated for DR3. The amplitude ratio routine, although not operational during the SOS processing, was used during validation to compute $\mathrm{Amp}G/\mathrm{Amp}G_{BP}$, $\mathrm{Amp}G/\mathrm{Amp}G_{RP}$, and $\mathrm{Amp}G_{BP}/\mathrm{Amp}G_{RP}$ ratios and to identify eclipsing binaries that contaminate the RR Lyrae sample (see Sect. 6).

3. Application of the SOS Cep&RRL pipeline to the DR3 dataset: Input data and source selections

Input data fed into the SOS Cep&RRL pipeline in DR3 consisted of FoV G and integrated G_{BP} and G_{RP} (when available) time-series photometry of all-sky variable sources classified as RR Lyrae (and Cepheids; see Ripepi et al. 2023) candidates with various probability values by the General Supervised Classification module (Rimoldini et al. 2023; see Fig. 1) of the variability pipeline, as well as RV time-series data from the RVS for small subsamples of these sources with a mean magnitude brighter than $G_{RVS} \sim 14$ mag[2]. The photometry and RV datasets comprise observations collected by *Gaia* over 34 months, from 25 July 2014 to 28 May 2017. For the confirmed RR Lyrae stars discussed in this paper, *Gaia* obtained about 38–39 useful photometric measurements in the G band on average in this time frame (with minimum and maximum values between 12 and 257 measures, depending on the source position on sky; Fig. 4, centre panel), which is to be compared with ∼30 G measures in DR2 and about 30 measurements in G_{BP} (with minimum and maximum values between 0 and 258; Fig. 4, left panel) and G_{RP}

[2] G_{RVS} is the *Gaia* magnitude of the flux collected in the RVS passband: 845–872 nm. For the transformation from G_{RVS} to G magnitude, see Eq. (2) in Gaia Collaboration (2018). In practice, $G - G_{RVS} \sim 0.48$ and 0.45 mag for RRc and RRab stars, respectively.

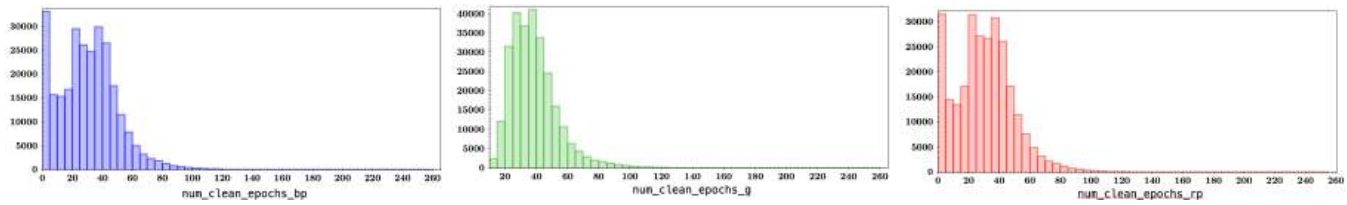

Fig. 4. Distribution in number of epochs in the *Gaia* G_{BP} (left), G (centre), and G_{RP} (right) passbands of the 271 779 RR Lyrae stars confirmed by the SOS Cep&RRL pipeline.

(with minimum and maximum values between 0 and 254; Fig. 4, right panel). Similarly, the *Gaia* RVS time-series data for the sub-samples of RR Lyrae and Cepheids presented in Sect. 4 comprise an average of about 23 RV measurements (minimum and maximum values between 5 and 77). The following criteria were applied to select RR Lyrae candidates to process with the SOS Cep&RRL pipeline :

- sources classified as RR Lyrae candidates by the classifiers of the General Supervised Classification module, with minimum probability thresholds chosen to maximise the recovery of RR Lyrae stars known from different surveys in the literature (see Sect. 3.1);
- sources with at least 12 G FoV transits after the `MOROO` and `ROFABO` outlier removal operators were applied (see Fig. 4);
- at least five measurements for the publication of the RV time series and at least seven transits for the modelling of the folded RV curve;
- a peak-to-peak amplitude >0.1 mag in the G band;
- periods in the range of $0.2 \leq P < 1.0$ d.

3.1. Training sets and literature reference catalogues

Candidate RR Lyrae stars to be processed through the SOS Cep&RRL pipeline were selected on the basis of their probability score to maximise the recovery of RR Lyrae stars that are already known in the literature. A preliminary step was the creation of a reference database of known RR Lyrae stars by collecting catalogues of these variables from major surveys in the literature, including those in 152 different stellar systems: the Magellanic Clouds, 107 globular clusters, nine dwarf spheroidal galaxies (dSphs; Carina, Draco, Fornax, Leo I, Leo II, Sagittarius, Sculptor, Sextans, and Ursa Minor) and 34 ultra-faint dwarfs (UFDs). This large catalogue, homogenised by eliminating duplicates, contains more than 425 000 unique all-sky RR Lyrae entries and spans a range of about 16 mag from RR Lyr itself ($\langle V \rangle$ = 7.76 mag; Fernley et al. 1998) to V6, the lone RR Lyrae star identified in Leo T (Clementini et al. 2012), an ultra-faint dwarf galaxy located at about 400 kpc in distance from the MW. The mean magnitude of V6, $\langle V \rangle$ = 23.59 mag, is lower than the *Gaia* faint limit by about 3 mag. However, we note that 97% of the sources in our custom RR Lyrae catalogue are within the limiting magnitude of *Gaia* and have a counterpart in the EDR3 `source_table` (see below). To build our custom catalogue, we primarily used the OGLE catalogues for RR Lyrae stars as reference (version IV of the survey; Soszyński et al. 2014, 2019), which have a high completeness and purity for the LMC, SMC, and the MW bulge and disc, along with the *Gaia* DR2 RR Lyrae catalogue in the `gaiadr2.vari_rrlyrae` table (Paper II), CATALINA (Drake et al. 2013, 2014, 2017; Torrealba et al. 2015), KEPLER (Molnár et al. 2018), the *Zwicky* Transient Facility (ZTF; Chen et al. 2020), the All-Sky Automated Survey (ASAS; Pojmanski 2000, 2002; Pigulski et al. 2009), the All-Sky Automated Survey for Supernovae (ASAS-SN; Jayasinghe et al. 2019), LINEAR (Palaversa et al. 2013; Sesar et al. 2013), the Palomar Transient Factory (PTF; Sesar et al. 2014), the VISTA Variables in the Via Lactea survey (VVV; Contreras Ramos et al. 2018; Dékány et al. 2018), the fifth edition of the General Catalogue of Variable Stars (GCVS; Samus' et al. 2017), and the PanSTARRS1 3π survey (PS1; Sesar et al. 2017). To integrate our compilation with known RR Lyrae stars in Galactic globular clusters (GCs), we used an updated version of the Variable Stars in Galactic Globular Clusters catalogue (Clement et al. 2001) as main reference, and for RR Lyrae stars in the MW UFDs, we used the compilation in Vivas et al. (2020). For the MW dSphs, we used the RR Lyrae collections by Muraveva et al. (2020) for Draco, Martínez-Vázquez et al. (2016) for Sculptor, Bersier & Wood (2002) for Fornax, Coppola et al. (2015) for Carina, Siegel & Majewski (2000) for Leo II, Stetson et al. (2014) for Leo I, Vivas et al. (2019) for Sextans, Kunder et al. (2008) for Sagittarius, and the collections by Nemec et al. (1988) and Bellazzini et al. (2002) for Ursa Minor.

We specifically note that in building our custom RR Lyrae catalogue, we gave preference to inclusiveness. We therefore did not make any cut for purity. For the selection procedures described in the following sections, we used a version frozen at December 2020 of our custom RR Lyrae catalogue. However, the catalogue is being regularly updated as soon as new RR Lyrae compilations appear in the literature, and we plan to make a most recently updated version available online after *Gaia* DR3 (Garofalo et al., in prep.).

We performed a spatial cross-match within a 2.5″ paring radius of our custom RR Lyrae catalogue and sources in the `gaia_source` table of the *Gaia* EDR3 archive (`gaiaedr3.gaia_source`) and found a counterpart in the EDR3 main catalogue for 414 082 (97%) of the RR Lyrae stars in our collection[3]. The classifiers of the General Supervised Classification module in the variability analysis pipeline returned these 414 082 sources as RR Lyrae candidates with probabilities starting from very low values. More than 75% (311 798) were classified as RR Lyrae by the SOS Cep&RRL pipeline. Characteristic parameters (P, pulsation mode, etc.) consistent with the literature were recovered for about 65% of them.

3.2. Gold Sample and validation criteria

In order to validate the unexpectedly large number of candidate RR Lyrae produced by the classifiers and confirmed by the SOS Cep&RRL pipeline and to extract a bona fide sample to release in DR3, we adopted a strategy based on our custom

[3] We refer to Gavras et al. (2023) for a comprehensive catalogue of known variable sources cross-matched with *Gaia* DR3. This also extends our catalogue to other types of variability.

Gaia SOS

OGLE IV	RRab	RRc	RRd	Sum
RRab	71489 99.2%	478 0.7%	83 0.1%	72050 100%
RRc	231 ~0.9%	26581 99%	15 ~0.1%	26827 100%
RRd	134 5.3%	1663 65.9%	726 28.8%	2523 100%

Fig. 5. Confusion matrix for the RR Lyrae stars. We used as a control sample all sources classified as RR Lyrae stars by the OGLE-IV catalogue of variable stars in the LMC, SMC, and MW bulge that have a cross-match within a radius of 2.5″ with the SOS-confirmed RR Lyrae stars published in our *Gaia* DR3 catalogue for a total of 101 400 objects. Rows refer to literature results, and columns list results of the SOS Cep&RRL pipeline. The corresponding success percentage is shown in the diagonal cells.

RR Lyrae reference catalogue and the RR Lyrae diagnostic tools summarised in Sect. 2. Our strategy consisted of two main steps:

1. we divided the sources into known (311 798 sources) and potentially new RR Lyrae stars based on our custom catalogue;
2. we used the diagnostic tools of known RR Lyrae stars that were correctly characterised by the SOS Cep&RRL pipeline (we named these RR Lyrae stars Gold Sample) as a reference to select and validate potentially new RR Lyrae stars.

Much effort was devoted to build a Gold Sample as large and pure as possible based on the initial sample of 311 798 known RR Lyrae stars that were recovered and characterised by the SOS Cep&RRL pipeline. We started by selecting the sources from the 311 798 known RR Lyrae stars whose SOS pulsation properties simultaneously satisfied the following conditions:

- $|P_{\rm SOS} - P_{\rm Literature}| \leq 0.001$ d;
- the ϕ_{21} Fourier parameter within the range appropriate for RR Lyrae stars: $3.0 \leq \phi_{21} \leq 5.8$ rad, in the ϕ_{21} versus P diagram, for sources with G light curves modelled with at least two harmonics.

Then, for sources whose G light curves were modelled with only one harmonic, we used the PA diagram to reject those outside the regions that are appropriate for RR Lyrae stars. We also relaxed the period criterion (to $|P_{\rm SOS} - P_{\rm Literature}| \leq 0.003$ d and to $|P_{\rm SOS} - P_{\rm Panstarrs}| \leq 0.01$ d) in a number of cases (5617 sources in total) after visual inspection of the light curves. With this procedure, the original sample of 311 798 known RR Lyrae stars was reduced to 201 173 sources. Of these, 369 were found to be eclipsing binaries based on the ratios of the G, G_{BP}, and G_{RP} light-curve amplitudes (see the end of Sect. 2), which were then further confirmed by visual inspection of the light curves; and 168 sources with a double classification were reclassified as Cepheids (see also Sect. 6).

This led us to a final Gold Sample comprising 200 636 bona fide known RR Lyrae stars. They include 101 400 RR Lyrae stars that were observed by OGLE in the LMC, SMC, and the Galactic bulge and disc, 71 489 of which are classified as RRab, 26 581 as RRc, and 726 as RRd stars in both the SOS Cep&RRL pipeline and OGLE. Figure 5 shows a confusion matrix for the Gold Sample RR Lyrae stars that is drawn using the OGLE-IV RR Lyrae catalogue as the control sample.

Figure 6 shows the sky distribution (using galactic and equatorial coordinates in the top and bottom panels, respectively) of the RR Lyrae stars in the Gold Sample. The three panels of Fig. 7 show their PA, ϕ_{21} versus P and ϕ_{31} versus P diagrams, in which the RR Lyrae stars in common with OGLE (101 400 sources) are plotted using different colours for RRab (blue), RRc (magenta), and RRd (black) stars.

3.3. Potentially new RR Lyrae stars

We have used the Gold Sample as a training set to select bona fide RR Lyrae stars from the remaining very large sample of potentially new RR Lyrae candidates provided by the classifiers and processed through the SOS Cep&RRL pipeline. Specifically, we used the PA, ϕ_{21} versus P and ϕ_{31} versus P diagrams defined with the Gold Sample RR Lyrae stars (see Fig. 7) to select potentially new bona fide RR Lyrae stars in sequential steps. This is briefly outlined below.

- From the sources whose G light-curves were modelled with three or more harmonics, we retained only those as bona fide RR Lyrae stars whose ϕ_{31} parameters lay in the proper region of the ϕ_{31} versus P diagram, as defined by the Gold Sample RR Lyrae stars ($0.6 \leq \phi_{31} \leq 5.1$ rad; see the bottom panel of Fig. 7).
- Bona fide RR Lyrae stars were selected from sources whose G light curves were modelled with only two harmonics by making a 2D Cartesian cross-match between their (P, ϕ_{21}) parameters and those of the Gold Sample RR Lyrae stars as reference (see the centre panel of Fig. 7) and verifying afterwards that they were properly located in the Gold Sample PA diagram as well (see the upper panel of Fig. 7).
- Finally, bona fide RR Lyrae stars were selected from sources whose G light curves were modelled with only one harmonic by making a 2D Cartesian cross-match between their [P, Amp(G)] parameters and those of the Gold Sample RR Lyrae stars as reference (see the upper panel of Fig. 7).

Some of sources that were retained as bona fide new RR Lyrae stars according to the above selection procedures have a double classification. This occurred for sources with $P < 1$ d and Amp(G) < 0.5 mag (see Sect. 2), which could either be c-type RR Lyrae stars or first-overtone classical Cepheids (DCEP_1O). The light curves of these sources were visually inspected and their position on the period-luminosity, period-Wesenheit relations for DCEPs (see Ripepi et al. 2023) was checked to finally classify them into one or the other class. At the end of these extensive selection and cleaning procedures, the sample contained 72 167 new (to the best of our knowledge) bona fide RR Lyrae stars.

To summarise, the total number of DR3 RR Lyrae stars that was confirmed and fully characterised by the SOS Cep&RRL pipeline adds to 272 803 sources (this number includes known RR Lyrae stars in the Gold Sample and new discoveries by *Gaia*). These sources were first cross-matched with catalogues of different types of variable stars produced by other SOS variability pipelines to search for possible overlaps. A number were found with ellipsoidal variables (ELL; Gomel et al. 2023), eclipsing binaries (ECL; Mowlavi et al. 2023), and active galactic nuclei (AGN; Carnerero et al. 2023). They were solved by assigning the overlapping sources to a unique variability class after visual inspection of the light curves. The resulting RR Lyrae catalogue then went through an iterative process of cross-validation aimed to ensure consistency and quality of the different data products (astrometry, photometry, variability, etc.) published for the *Gaia* DR3 sources. By this whole procedure, the RR Lyrae catalogue was trimmed to 271 779 sources, 200 589 of which are in the Gold Sample and 71 190 are potentially new RR Lyrae stars that are published in the DR3 `vari_rrlyrae` table. Examples of the G, G_{BP}, and G_{RP} light

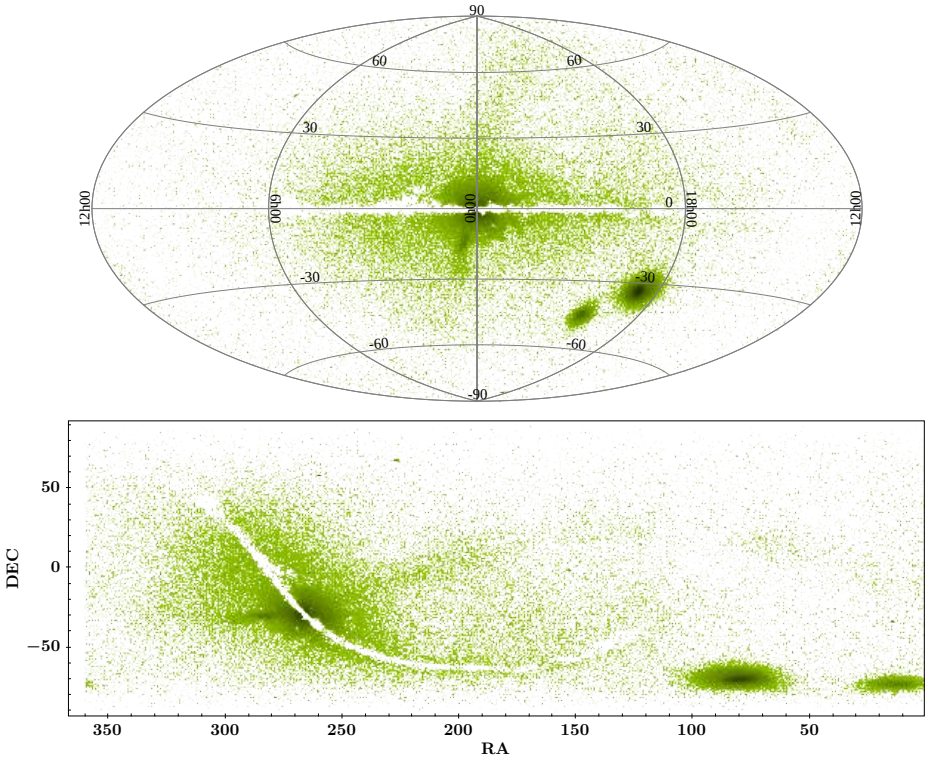

Fig. 6. Sky distributions in galactic coordinates (top panel) and equatorial coordinates (bottom panel) of 200 636 RR Lyrae stars in the Gold Sample.

curves for DR3 RR Lyrae stars with different pulsation modes (RRab, RRc, and RRd) in the MW field and in a number of different stellar systems (the GCs M3 and M62, the LMC and the SMC, the Sculptor dSph, and the Phoenix II and Tucana II UFDs) are presented in Figs. 8 and 9.

The catalogue of 271 779 RR Lyrae stars was further cleaned from contaminants and sources affected by issues that emerged after the final export of the DR3 `vari_rrlyrae` table. This final cleaning procedure is described in Sect. 6.

4. RVS radial velocity time series for RR Lyrae stars and Cepheids

With DR3, epoch RVs measured from the RVS spectra are published for a small sample of RR Lyrae stars and Cepheids for the first time. This small dataset provides a first quality assessment of the RVS per-transit RVs. At the same time, it anticipates RVS data-products that will become available with next *Gaia* releases. In the following subsections we describe how this sample was selected (Sect. 4.1), was processed by the SOS pipeline (Sect. 4.2), and was validated with the literature (see Sect. 4.3 for the RR Lyrae stars, and Sect. 6.6 in Ripepi et al. 2023 for the Cepheids).

4.1. Target selection

The `gaia_source` table in the DR3 archive provides RV values[4] for 5096 RR Lyrae stars and 3190 Cepheids that were confirmed by the SOS Cep&RRL pipeline. From these, we selected sources with five or more epoch RV measurements and a mean G magnitude brighter than ∼15.5 mag. A further selection was made by visual inspection of the light curves and RV curves, which produced a sample of 1100 RR Lyrae stars and 798 Cepheids.

The intensity-averaged G mean magnitudes (as computed by the SOS pipeline) of the 1 100 RR Lyrae stars lie in the range of $7.64 \leq G \leq 14.33$ mag (Fig. 10, grey histogram), and the number of individual RVS measurements ranges from 5 to 77 (Fig. 11, grey histogram). The intensity-averaged G mean magnitudes of the 798 Cepheids lie in the range of $3.75 \leq G \leq 15.46$ mag (Fig. 10, cyan histogram), and the number of valid RVS individual measurements ranges from 5 to 74 (Fig. 11, cyan histogram).

The epoch RVs were computed using the RVS pipeline described in the online documentation Sartoretti et al. (2022, Chap. 6). In practice, they were derived by comparing each cleaned and calibrated RVS spectrum with the synthetic reference template of a star with similar atmospheric parameters. See Sartoretti et al. (2022, Sect. 6.4.8) and Sartoretti et al. (2018, Sect. 7) for a detailed description of how epoch RVs are calculated, and Sartoretti et al. (2022, Fig. 6.13) for the median precision of epoch measurements as a function of $G_{\rm RVS}$. The quality of the epoch RVs depends on several factors: the $G_{\rm RVS}$ magnitude of the star (because the fainter the star, the noisier the spectrum); the appropriate match with a synthetic reference template (see Sartoretti et al. 2022, Sect. 6.4.8.3 for how template spectra are associated with RVS spectra); the quality of astrometric data; and potential limitations of the processing software (e.g. for deblending or the identification of peculiar stars). The epoch RVs published in DR3 are only those of the 1100 RR Lyrae stars and 798 Cepheids described in this paper, which are available via the *Gaia* archive `vari_epoch_radial_velocity` table. Typical uncertainties of the epoch RVs for these sources are $\lesssim$1 km s^{-1} for $G \sim$ 9–9.5 mag ($G_{\rm RVS} \sim$ 8.5–9 mag for RR Lyrae stars) and $\lesssim$6.5 km s^{-1} for $G \sim$ 13 mag ($G_{\rm RVS} \sim$ 12.5 mag for

[4] The RV values of RR Lyrae stars and Cepheids in the DR3 `gaia_source` table are combined RVs obtained in two different ways depending on the $G_{\rm RVS}$ magnitude of the star. For bright stars ($G_{\rm RVS} \leq$ 12 mag), the combined RV is the median of the single-transit RVs. For faint stars, for which the single-transit RVs are less precise, the single-transit cross-correlation functions are averaged. The mean cross-correlation function obtained in this way is then used to measure the stellar RV.

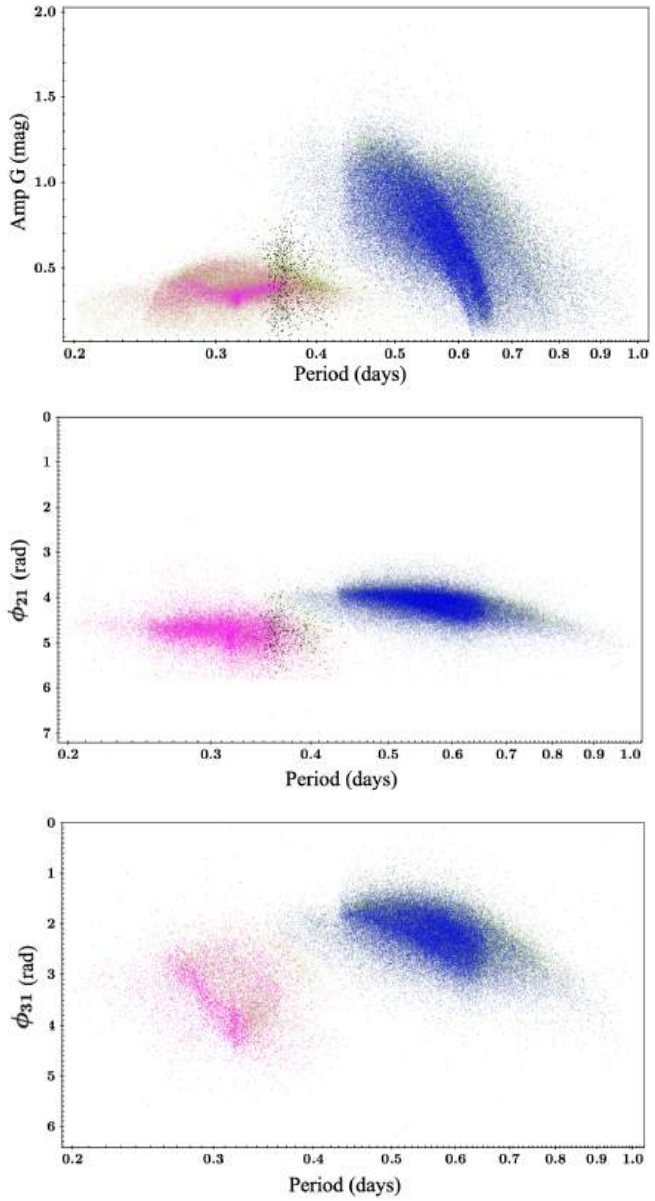

Fig. 7. PA, ϕ_{21} versus P and ϕ_{31} versus P diagrams of the 200 636 RR Lyrae stars in the Gold Sample. The 101 400 sources in common with OGLE are plotted using different colours for RRab (blue), RRc (magenta), and RRd (black) stars, respectively.

RR Lyrae stars) (see Sartoretti et al. 2022, Fig. 6.13). The epoch data of all remaining stars will be published in DR4. The other RVS-pipeline products published in DR3 are at source level (i.e. obtained by combining data from all epochs). They are listed in Table 6.1 of the online documentation and are available via the *Gaia* archive `gaia_source` table. These products include, for example, information about the $G_{\rm RVS}$ magnitude of the star (called `grvs_mag` in the *Gaia* archive) and the atmospheric parameters of the synthetic reference template used to derive the star epoch RVs (called `rv_template_teff`, `rv_template_logg` and `rv_template_feh`, and `rv_atm_param_origin`). Source-level RVS pipeline products are not also published for all the 1100 RR Lyrae stars and 798 Cepheids whose epoch RVs are published in DR3. Source-level information is lacking for 51 Cepheids and 45 RR Lyrae stars, for which the all-epoch-combined RV was deemed of insufficient quality (see Katz et al. 2023, for the filters applied to the all-epoch-combined RVs). In most cases, the reason was the detection of potential variability, such as double lines in more than 10% of the epoch spectra, variability in spectral-sample flux from epoch to epoch, or a large dispersion in epoch RV (`radial_velocity_error` > 40 km s^{-1}). In other cases, the spectra were deemed too noisy, or the effective temperature $T_{\rm eff}$ was found to exceed the limit for good-quality RV measurements (i.e. 7000 K for $G_{\rm RVS}$ > 12 mag and 14 500 K for $G_{\rm RVS}$ ≤ 12 mag). However, we note that most of the above issues are normal features for high-amplitude variable sources such as RR Lyrae stars and Cepheids, whose RV curves typically exhibit amplitudes of tens of km s^{-1}. We carefully inspected the RV curves of these 51 Cepheids and 45 RR-Lyrae stars, and none of them was found to have a peculiar shape. In contrast, the large majority of these sources have very regular and well defined RV curves. Therefore, we kept them for publication, and in Appendix A.1, we provide information about their $G_{\rm RVS}$ magnitudes and the atmospheric parameters of the associated templates. We also explain why no source-level RVS pipeline products are published for them.

4.2. Processing of the RV data through the SOS Cep&RRL pipeline, and results

The time-series RV data of the 1100 RR Lyrae stars and 798 Cepheids were processed by the SOS Cep&RRL pipeline. For sources with more than seven transits (1097 out of 1100 RR Lyrae stars and 785 out of 798 Cepheids), the RV curves obtained by folding the data with the periods inferred from the G-band photometry were modelled with truncated Fourier functions. The mean RV ($\langle$RV$\rangle$), the peak-to-peak RV amplitude [Amp(RV)], and the epoch of minimum RV were computed from the modelled RV curves and are published in the DR3 `vari_rrlyrae` and `vari_cepheid` tables. From top to bottom, Fig. 12 shows examples of G_{BP}, G, and G_{RP} light curves and RV curves for RR Lyrae stars that are released in DR3. The RV curves have the typical specular shape with respect to the light curves for which the minimum value in RV corresponds to the maximum stellar brightness.

An atlas of the light and RV curves for the full sample of 1100 RR Lyrae stars whose time-series RVs are published in DR3 is presented in Appendix A.3. Examples of RV curves and an atlas of the light curves and RV curves for the 798 Cepheids are presented in Ripepi et al. (2023).

Figure 13 shows the error distribution of the mean RV values computed with the SOS pipeline ($\sigma\langle$RV$\rangle$) for the 1097/1100 RR Lyrae stars, whereas Fig. 14 shows $\sigma\langle$RV$\rangle$ as a function of the mean G magnitude of these sources. The uncertainty ranges from 0.48 km s^{-1} to 84.88 km s^{-1} for $\langle G\rangle$ ranging from 7.64 to 14.30 mag, with a peak between 3 and 6 km s^{-1}. This peak corresponds to the bulk of RR Lyrae stars that have a mean G magnitude between 12 and 13 mag in Fig. 14 and is consistent with Fig. 6.13 in Sartoretti et al. (2022). Fewer than 20 sources have $\sigma_{\langle \rm RV\rangle}$ > 25 km s^{-1}. They correspond to sources in the faint magnitude tail of Fig. 14.

Finally, Fig. 15 shows the P versus Amp(RV) diagram of the 1097 RR Lyrae stars. A few sources have very high Amp(RV) values. Three of them are contaminants (filled green circles), and the others have very few RV measurements and hence very uncertain Amp(RV) values.

A comparison was made of the SOS mean RV values of the 1097 RR Lyrae stars and the combined RV values for these stars in the *Gaia* DR3 `gaia_source` table. The two RV values are available for 1054 RR Lyrae stars. This comparison is shown in

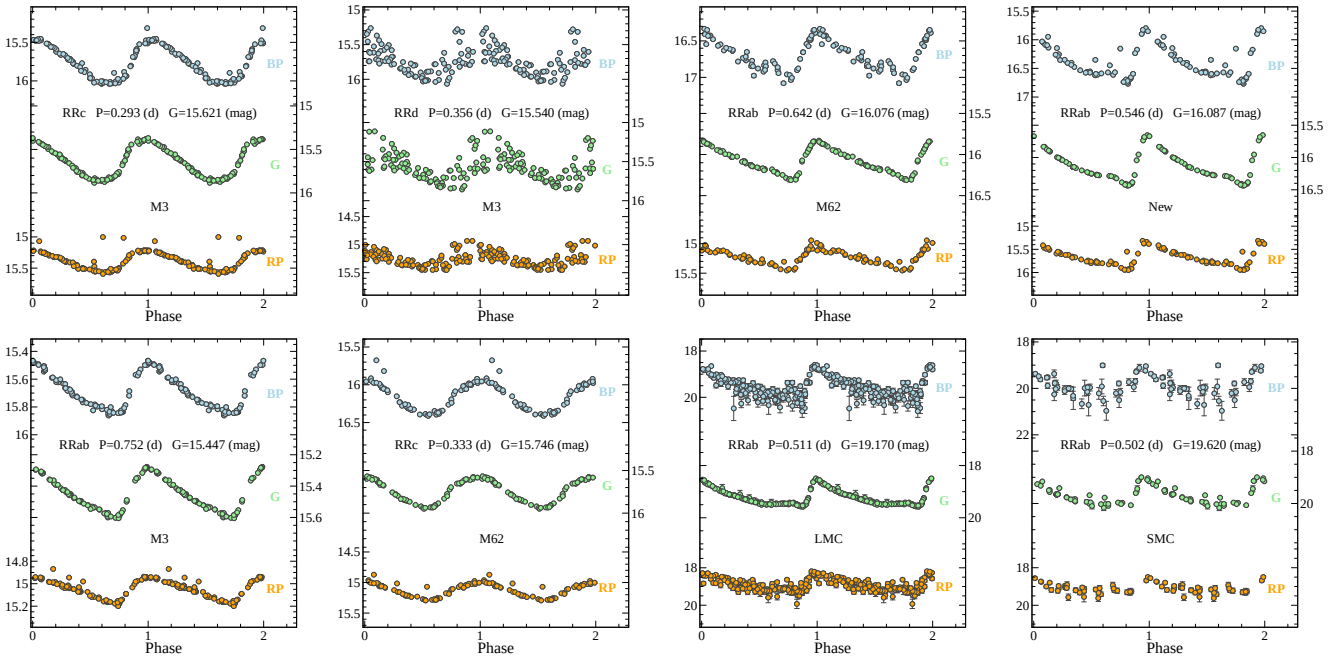

Fig. 8. Examples of light curves for SOS-confirmed DR3 RR Lyrae stars in the globular clusters M3 and M62, in the LMC and the SMC, and a new all-sky RR Lyrae star.

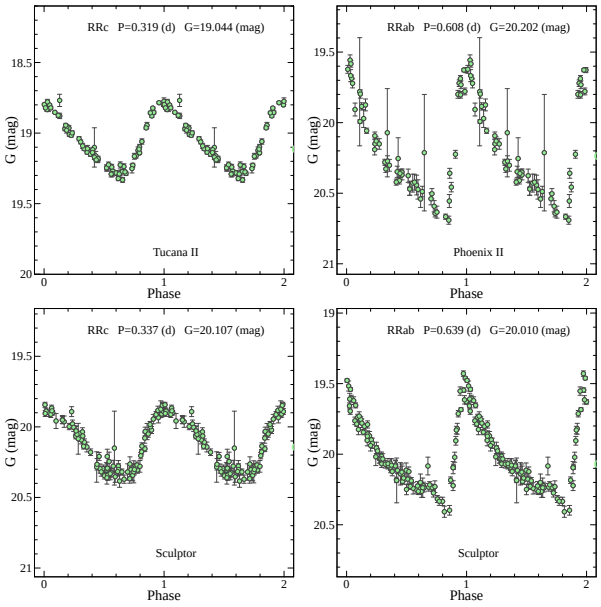

Fig. 9. Same as in Fig. 8, but for RR Lyrae stars in the Sculptor dSph galaxy and in the Phoenix II and Tucana II MW UFDs. Only the G-band light curves are shown because the S/N of the G_{BP} and G_{RP} time-series data is poor at the faint magnitudes of the RR Lyrae stars in these systems.

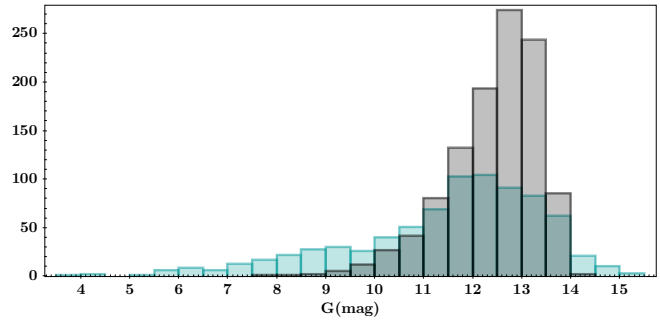

Fig. 10. G magnitude distribution of the 1100 RR Lyrae stars (grey histogram) and 798 Cepheids (cyan histogram) whose RV time series are published in *Gaia* DR3.

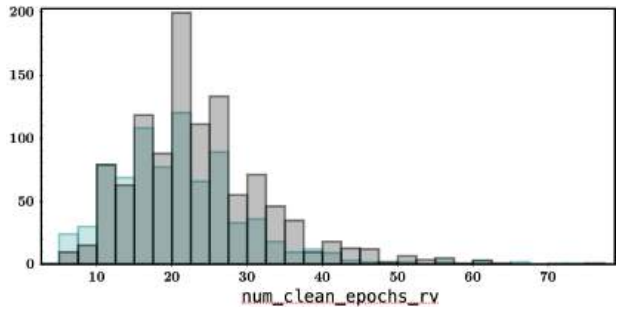

Fig. 11. Number of available individual measurements in the RV time-series data for the 1100 RR Lyrae stars (grey histogram) and 798 Cepheids (cyan histogram) subsamples.

Fig. 16. The agreement within the errors of the two sets of RV measurements is good.

The median and mean difference of the two average values is 5.21 and 6.88 km s^{-1} (with 6.35 km s^{-1} standard deviation), respectively. Finally, Fig. 17 shows the RV map defined by 1097 out of 1100 RR Lyrae stars in the DR3 `vari_rrlyrae` (righ panel), and in the left panel, the map defined by the 5096 RR Lyrae stars in the DR3 `gaia_source` table, for comparison. The sources are colour-coded according their mean RV values. The two distributions are very well consistent, as expected from the good agreement between the two sets of RV values (see Fig. 16). RR Lyrae stars are distributed at all galactic latitudes and populate the maps with RVs ranging from high negative to high positive values.

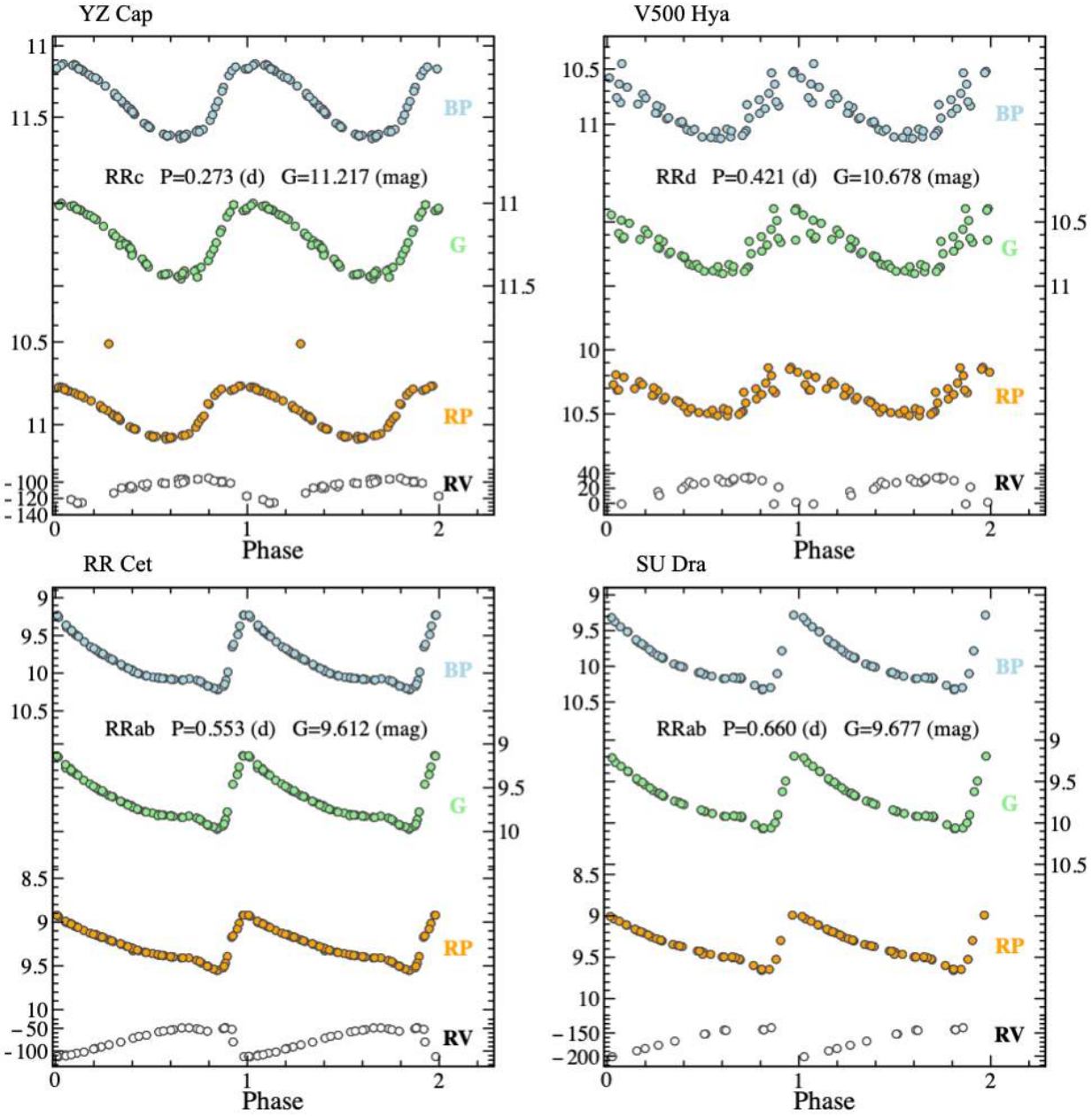

Fig. 12. Examples of light curves and RV curves for RR Lyrae stars released in DR3. From top to bottom in each panel, we show G_{BP}, G, and G_{RP} light curves and RV curve. The error bars of the photometric and RV measurements are smaller than or comparable to the symbol size. In the upper row from left to right, the sources are a first-overtone (RRc) and a double-mode (RRd) star; in the lower row, we show two fundamental-mode (RRab) RR Lyrae stars.

4.3. Validation with the literature

A number of RR Lyrae stars and Cepheids for which epoch RVs are published in DR3 were analysed in the past with the Baade–Wesselink (B–W) technique (e.g. Cacciari et al. 1992, and references therein, for different versions of the B-W method applied to RR Lyrae stars, and Gieren & Barnes 1989; Ripepi et al. 1997, for B–W analyses of Cepheids). Hence, high-accuracy RV measurements either obtained with the CORAVEL spectrophotometer (Baranne et al. 1979) or from high-resolution spectra are available in the literature for these stars. We selected 19 RR Lyrae stars with 10 or more epoch RVS measurements in the RV curves and have made a detailed comparison with the high-accuracy RVs covering the whole stellar pulsation cycle that are available for these variable stars in the literature. We mainly used data taken from the most recent literature for our comparison, as datasets collected in/before the early eighties often have very large uncertainties. A similar comparison for a sample of DCEPs is presented in Ripepi et al. (2023).

The 19 RR Lyrae stars used for this test are listed in Table A.3. In the table we indicate the literature data we used for the comparison, the mean astrophysical stellar parameters ($\langle T_{\rm eff}\rangle$, $\langle \log g\rangle$, and iron abundance: [Fe/H]), which in general are the values that are adopted for or derived from the B-W analyses. The sample comprises 17 RRab and 2 RRc stars. They span a range in [Fe/H] of more than 2 dex. Three of them are known or suspected to be affected by Blažko effect (Blažko 1907), a periodic modulation of the amplitude and shape of the light (and

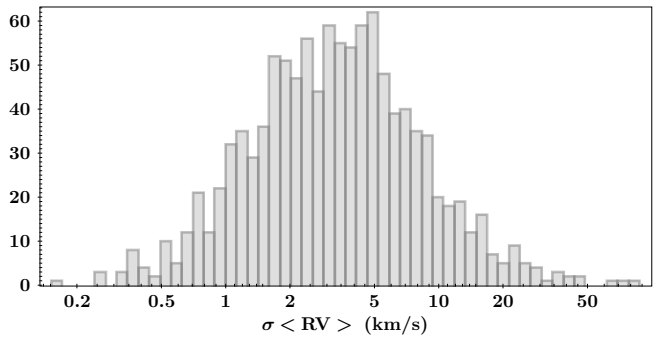

Fig. 13. Error distribution of the mean RV values computed with the SOS pipeline for 1097 out of 1100 RR Lyrae stars.

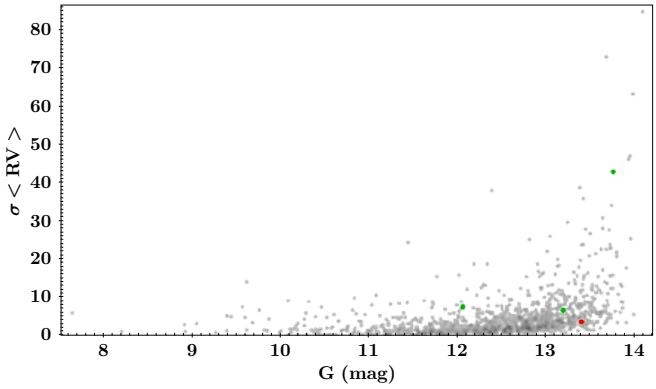

Fig. 14. Uncertainty of the mean RV values as a function of the SOS mean $\langle G \rangle$ magnitude for 1097 out of 1100 RR Lyrae stars (filled grey points). We plot in different colours one DCEP (red symbol) and three ECLs (green symbols) that contaminate the 1097 RR Lyrae sample (see Sect. 6 for details).

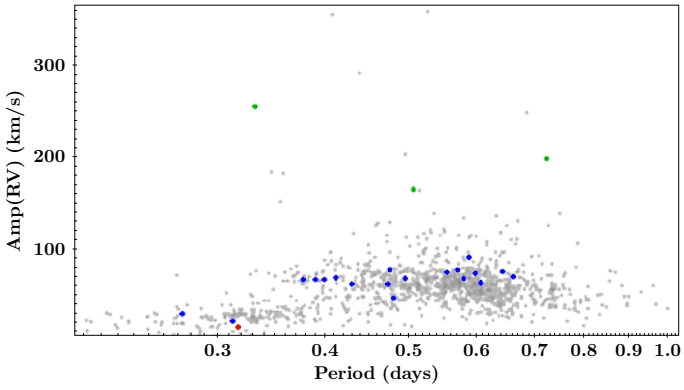

Fig. 15. P vs. Amp(RV) diagram of 1097 out of 1100 RR Lyrae stars. Symbols and colour-coding are the same as in Fig. 14. The filled blue points show 19 RR Lyrae stars with high-accuracy RV curves in the literature that were used to validate the *Gaia* RVs (see Sect. 4.3).

RV) curve, occurring with periodicities from tens to hundreds of days; one (V32) is a member of a globular cluster (NGC 6121 – M4), and UU Vir is an RR Lyrae star suspected to be in a binary system, according to anomaly detected in the *Gaia* DR2 proper motions for the source (Kervella et al. 2019). The 19 RR Lyrae stars have $0.273 \leq P \leq 0.660$ d, $9.56 \leq \langle G \rangle \leq 12.90$ mag, and 10 or more (up to 37) individual RVS measurements, with errors in the range from 0.41 to 16 km s^{-1} depending on the magnitude and pulsation phase.

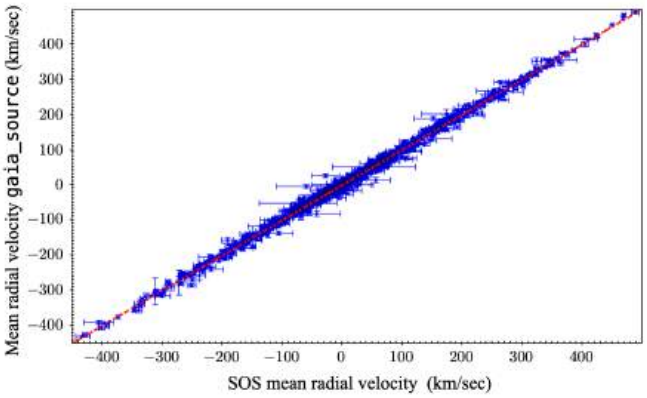

Fig. 16. Comparison of the mean RV values in the DR3 `vari_rrlyrae` table, which are computed with the SOS Cep&RRL pipeline from the modelled RV curves of the RR Lyrae stars, and the combined RV values in the DR3 `gaia_source` table for the 1054 RR Lyrae stars for which both values are available. The median and mean difference between the two average values is 5.21 and 6.88 km s^{-1} (with a standard deviation of 6.35 km s^{-1}), respectively.

The RVS measurements of these 19 RR Lyrae stars are reasonably well distributed over the pulsation cycle. More than one RV dataset is often available in the literature to make the comparison.

The literature RVs and the *Gaia* RVS measurements of the stars in Table A.3 span time intervals of up to a few decades, and the literature periods often do not allow an optimal phasing of all the available RV datasets. We therefore performed a new period search on each combined (literature plus *Gaia*) RV dataset with the package Graphical Analyzer of Time Series (GRATIS; custom software developed at the Bologna Observatory by P. Montegriffo, see e.g. Clementini et al. 2000) and defined periods that allowed us to optimally match the *Gaia* and the literature RV curves for all sources used for this comparison[5]. No photometry was involved in the procedure, but we note that the differences between the periods derived for the 19 RR Lyrae stars from the combined RV datasets ($P_{\rm RV}$) and the periods derived by the SOS pipeline ($P_{\rm SOS}$) from the DR3 time-series photometry are in the range of 2.8×10^{-8} d $< |P_{\rm RV} - P_{\rm SOS}| < 2.0 \times 10^{-5}$ d for 18 of the 19 stars in our sample. Only for V440 Sgr (source_id= 6771307454464848768) is $P_{\rm SOS}$ 0.048 d shorter than the period derived from the combined RV dataset, and it is clearly incorrect because this star has only sparsely sampled light curves and RV curves. The correct period for V440 Sgr is provided in Table A.3.

As an example, Fig. 18 shows the radial velocity curves of the RRc star YZ Cap and the RRab stars RS Boo, W Crt, RR Cet, V32 in M4, and W Tuc using different colours for the literature and the *Gaia* RVS data. The RV curves of the remaining 13 RR Lyrae stars are presented in Fig. A.1. This comparison shows that the shape and amplitude of the *Gaia* RVS and the literature RV curves agree well for 14 of the 19 RR Lyrae stars in the sample, which shows the good quality of the RVS epoch RV data for these sources. Specifically, the agreement is good for YZ Cap, RS Boo, W Tuc, V Ind, DX Del, UU Cet V440 Sgr, and also for V32 in M4, TV Boo, AV Peg, TW Her, and UU Vir when their RVS curves are rigidly shifted by +5 km s^{-1} for the first two, −3 km s^{-1} for the third source, and by −4 km s^{-1} for the last two sources so that the literature curves are better matched.

[5] As far as we know, none of the 19 RR Lyrae stars considered for our comparison is known to present significant period changes. The period of some of these RR Lyrae stars is known to be fairly constant.

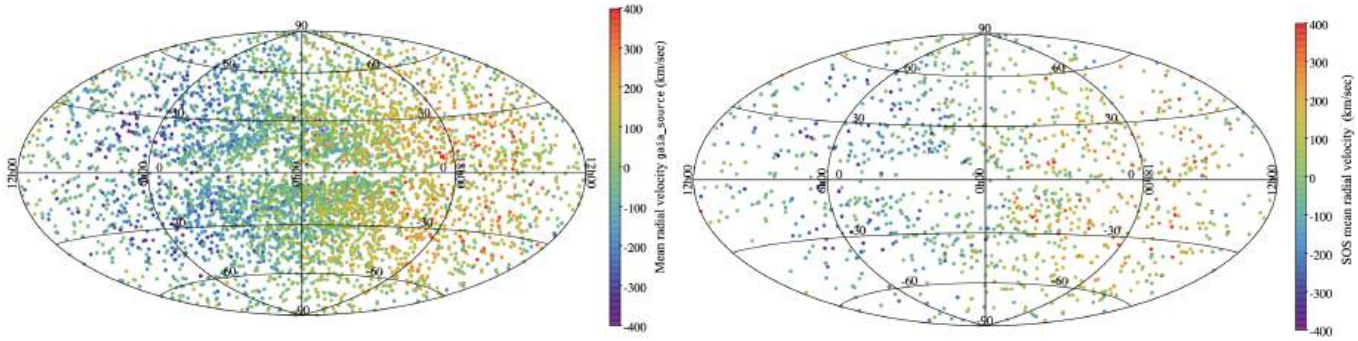

Fig. 17. Radial velocity maps defined by 1097 out of 1100 RR Lyrae stars in the DR3 `vari_rrlyrae` (righ panel) and 5096 RR Lyrae stars in the `gaia_source` table (left panel). The sources are colour-coded according to their mean RV values, as encoded in the colour bar on the right.

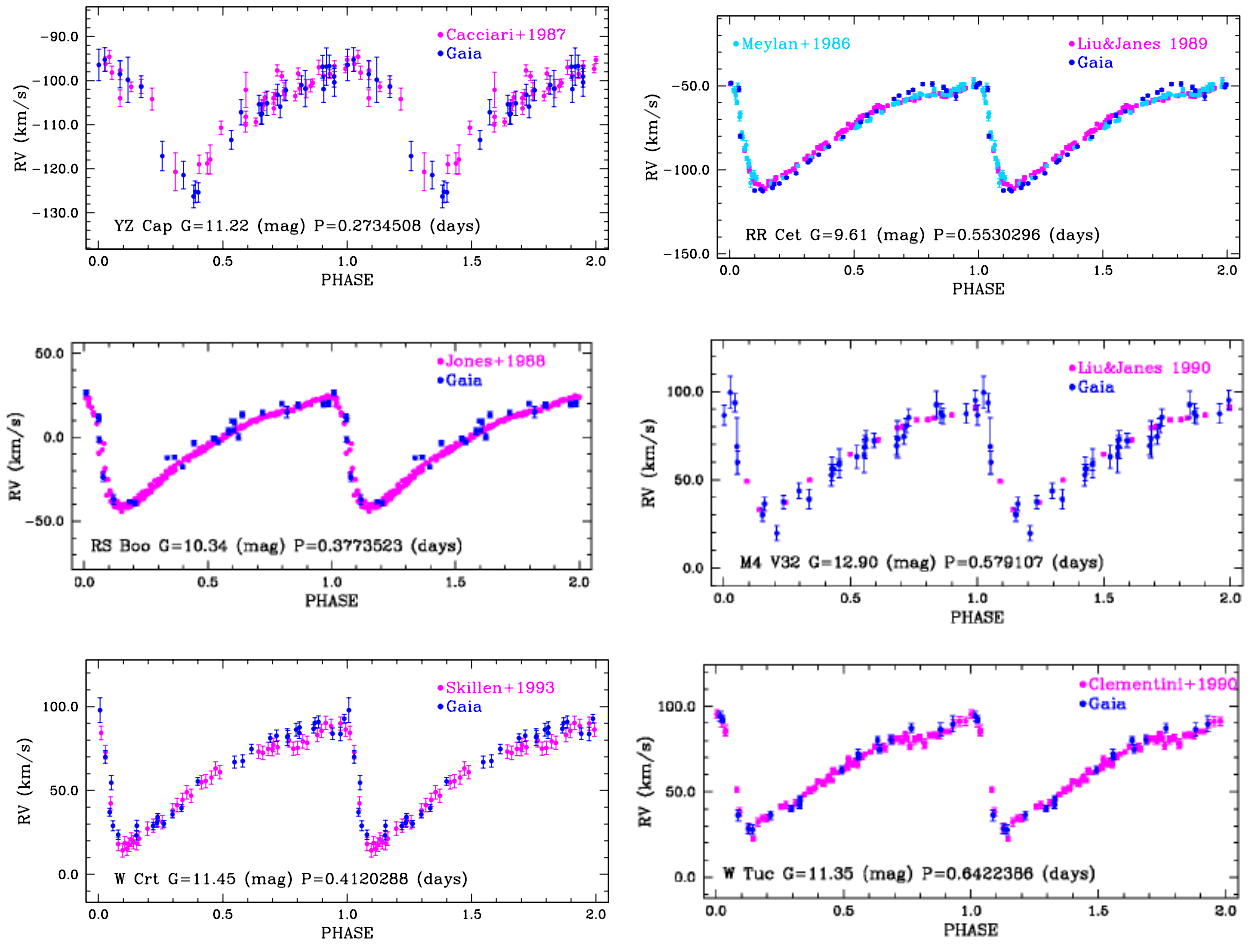

Fig. 18. Comparison of the *Gaia* RVS radial velocities (filled blue circles) with literature RV datasets (filled magenta and cyan circles) for the RRc star YZ Cap (top left) and the RRab stars RS Boo (middle left), W Crt (bottom left), RR Cet (top right), V32 in the GC M4 (middle right), and W Tuc (bottom right). We also show the pulsation period (as rederived in our analysis) and the intensity-averaged G-band mean magnitude (as derived by the SOS Cep&RRL pipeline). The *Gaia* RV curve of V32 in M4 was shifted by -5 km s^{-1} to better match the literature RV curve.

The agreement is also acceptable for RV Phe and SS For, despite the large scatter caused by the Blazhko effect in these two stars. Conversely, there are noticeable differences between the literature and *Gaia* RV curves for RR Cet, RX Eri, SU Dra, SW Dra, and to a lesser extent, also for W Crt. These differences are most apparent around the bump just before the RV maxima, around phases 0.7–0.9, where the *Gaia* RVS curves reach higher velocities than the literature curves. Investigating the reason for these differences is beyond the purposes of this paper, but we note that shock waves are known to propagate in the atmosphere of RR Lyrae stars in correspondence with the hump (phase ∼0.9) and bump (phase ∼0.7) in the light and RV curves (Gillet & Crowe 1988; Clementini et al. 1994; Gillet & Fokin 2014, and references therein) that cause flux redistribution, H line emission, and U-excess. The RVS measurements seem to reflect the flux redistribution caused by shocks propagating in the atmospheres of these 5 RR Lyrae stars better than the literature RVs.

5. Astrophysical parameters

The `StellarParametersDerivation` module of the SOS Cep&RRL pipeline (see Fig. 2) computes two main astrophysical parameters for the confirmed RR Lyrae stars: 1. a photometric estimate of individual metal abundance ([Fe/H]) for RRab and RRc stars whose light curves have been Fourier-modelled with at least three harmonics, and 2. a G -band absorption [$A(G)$] for RRab stars for which the $(G - G_{RP})$ colour is available. The `StellarParametersDerivation` module is fully described in Sect. 2.1 of Paper II. Here, we only note that unlike in DR2, uncertainties in metallicity and $A(G)$ values (as well as for any other parameter derived by the SOS pipeline) in DR3 were calculated with the bootstrap method.

In the following, we present the [Fe/H] abundances (Sect. 5.1) and $A(G)$ values (Sect. 5.3) computed from the pulsation characteristics of the confirmed RR Lyrae stars, and compare them with values in the literature and with the astrophysical parameters derived by the *Gaia* pipeline that processes the RVS spectra and the *BP*, *RP* low-resolution prism spectra (Apsis; Creevey et al. 2023; Sects. 5.2 and 5.4).

5.1. Metallicity

In the *Gaia* DR3 `vari_rrlyrae` table, individual photometric metallicities ([Fe/H]) are published for 133 557 RR Lyrae stars. They were computed by the `StellarParametersDerivation` module from the pulsation period P and the ϕ_{31} parameter of the G light-curve Fourier decomposition, using the relations for RRab and RRc stars derived in Nemec et al. (2013). These relations are calibrated on [Fe/H] values obtained from an abundance analysis of high-resolution spectra ($R \sim 36\,000$ and $65\,000$) of 41 field RR Lyrae stars.

Figure 19 shows the error distribution of the photometric metallicities for the 133 557 RR Lyrae in the sample.

Mean and median metallicity errors are 0.46 dex (with 0.33 dex std) and 0.36 dex, respectively. Errors were computed by adding the uncertainty estimated with the bootstrap method and the scatter around the calibration relations of 0.084 dex and 0.13 dex for RRab and RRc stars, respectively (Nemec et al. 2013), in quadrature and by adopting a rather generous systematic error of 0.2 dex that likely led to an overestimation of the metallicity uncertainties.

To validate the photometric metallicities, we first determined how well they reproduce the metal abundance of the Nemec et al. (2013) calibrators. This is shown in Fig. 20, where the [Fe/H] metallicities derived by the SOS Cep&RRL pipeline are compared with the metal abundances from high-resolution spectra of 39 RR Lyrae of the Nemec et al. (2013) calibrators for which both estimates are available. The agreement is good within the errors, confirming that the SOS photometric metallicities of RR Lyrae stars are closely tied to the metallicity scale from the abundance analysis of Nemec et al. (2013). We note, however, that the photometric metallicity of RR Lyr, the prototype and brightest star of the class, is significantly discrepant and poorly determined, as shown by the very large error bars. The reason likely is a poor determination of the ϕ_{31} parameter for the star.

As already noted in Paper I, the photometric metallicities inferred from the [Fe/H], P, and ϕ_{31} relation better represent the mean metal abundance of a population of RR Lyrae stars than the metallicy of the individual sources. Furthermore, new calibrations of this relation have appeared in the recent literature

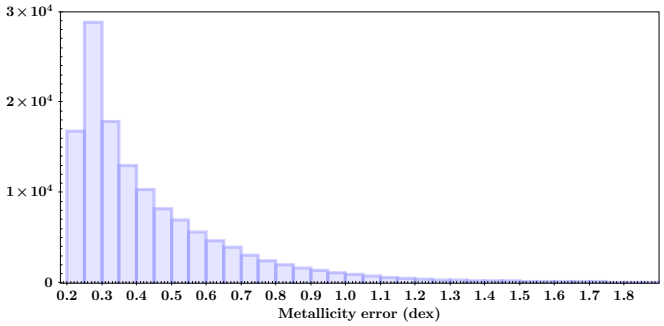

Fig. 19. Error distribution of the metallicities derived for 133 557 DR3 RR Lyrae stars by the SOS pipeline. The mean and median metallicity errors are 0.46 dex (0.33 dex std) and 0.36 dex, respectively. We show only sources with $\sigma_{[Fe/H]} \leq 2.0$ dex (i.e. 99.6% of the sample). We also note that for 71% of the sources in the plot, $\sigma_{[Fe/H]} \leq 0.5$ dex.

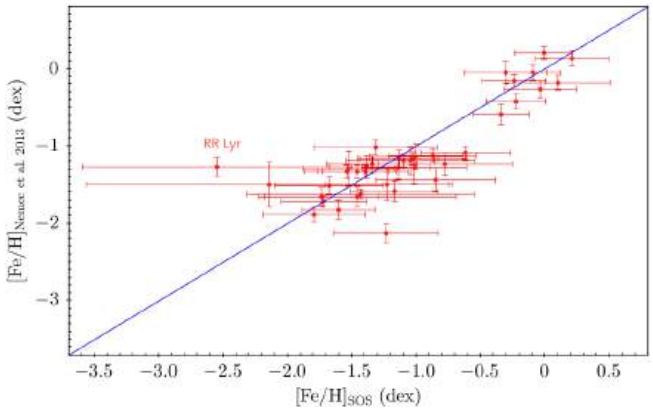

Fig. 20. Comparison of the photometric metallicities derived by the SOS Cep&RRL pipeline and the metallicities from high-resolution spectra of 39 RR Lyrae stars of the Nemec et al. (2013) calibrators.

(e.g. Iorio & Belokurov 2021; Mullen et al. 2021)[6]. Claims have been made by Iorio & Belokurov (2021) that metallicities based on the Nemec et al. (2013) calibrations are biased toward high metallicities. Conversely, Mullen et al. (2021) found an excellent agreement for higher metallicities in the Nemec et al. (2013) calibration range ($-1.5 \lesssim$ [Fe/H] $\lesssim 0.03$ dex), while estimates diverge for lower metallicities.

In order to test the reliability of the RR Lyrae metallicities computed with the SOS pipeline, we compared them with the metal abundances from high-resolution spectroscopy available in the literature for different samples of RR Lyrae stars. Because the Mullen et al. (2021) relations are calibrated on the RR Lyrae metallicities from high-resolution spectra ($R \sim 35\,000$) of Crestani et al. (2021), we discuss the comparison with Crestani et al. (2021) in the following. A comparison with other abundance analyses of RR Lyrae stars in the literature is presented in Appendix B.1.

First we compared the metal abundances from high-resolution spectra for RR Lyrae stars in common between Nemec et al. (2013) and Crestani et al. (2021). This comparison is shown in the left panel of Fig. 21 and seems to confirm that the Nemec et al. (2013) metallicities may be 0.1–0.2 dex higher than those of Crestani et al. (2021) for [Fe/H] ~ -1.5 dex.

[6] We recall that the pipelines processing the *Gaia* data are frozen well in advance of releases. Specifically, the SOS Cep&RRL pipeline adopted to process the DR3 data was frozen in early 2020.

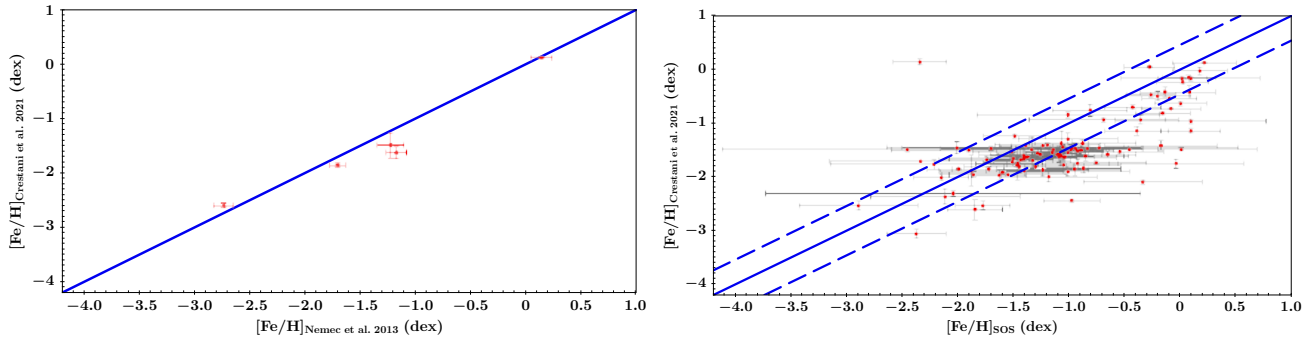

Fig. 21. Left panel: comparison of the metallicity from high-resolution spectra for five RR Lyrae stars in common in Nemec et al. (2013) and Crestani et al. (2021). Right panel: comparison of the photometric metallicities derived by the SOS pipeline and the spectroscopic metallicities from high-resolution spectra derived by Crestani et al. (2021) for 105 RR Lyrae stars in common in the two samples. The two dashed lines are offset by ±0.46 dex, the mean error of the photometric metallicities (see Fig. 19), from the one-to-one line.

Table 1. Metallicity and absorption in the G band for a sample of GCs and dSphs, obtained by averaging individual values derived by the SOS pipeline for the RR Lyrae stars in these systems.

Name	$[Fe/H]_{C09}$ (dex)	RRLs (N_1)	$[Fe/H]_{Gaia}$ (dex)	St. dev. $[Fe/H]_{Gaia}$ (dex)	RRLs (N_2)	$A(G)$ (mag)	St. dev. $[A(G)]$ (mag)	$A(G)$ (*) (mag)	Ref.
NGC 1261	−1.27	14	−1.13	±0.49	12	1.32	±1.47	0.02	(1)
NGC 1851	−1.18	21	−1.11	±0.48	18	1.27	±1.06	0.05	(2)
NGC 288	−1.32	1	−1.24	±0.33	1	0.07	±0.08	0.08	(3)
NGC 3201	−1.59	73	−1.27	±0.36	77	0.73	±0.30	0.62	(4)
NGC 5024	−2.10	25	−1.66	±0.57	25	0.49	±0.69	0.05	(5)
NGC 5139-OCen	−1.53	36	−1.42	±0.63	39	0.43	±0.36	0.31	(6)
NGC 5272-M3	−1.50	125	−1.38	±0.39	105	0.89	±1.52	0.01	(7)
NGC 6266-M62	−1.18	105	−0.73	±0.36	88	2.77	±1.81	1.23	(8)
IC 4499	−1.53	64	−1.45	±0.48	58	0.66	±0.23	0.60	(9)
NGC 7078-M15	−2.37	44	−1.95	±0.54	30	0.89	±0.83	0.26	(10)
Sculptor	−1.68	289	−1.64	±0.50	275	0.53	±0.63	0.05	(11)
Draco	−1.93	258	−1.79	±0.67	216	0.54	±0.43	0.08	(12)
Ursa Major I	−2.18	5	−2.38	±0.43	5	1.94	±2.00	0.02	(13)
Ursa Major II	−2.47	1	−2.24	±0.45	3	0.26	±0.04	0.25	(14)

Notes. (*)A(G)values obtained by transforming the $A(V)$ values in the literature using the following ratio of extinction coefficients $A(G)/A(V)$ = 0.840 from Bono et al. (2019). N_1 and N_2 are the number of RR Lyrae stars on which the mean $[Fe/H]_{Gaia}$ and $A(G)$ values were computed, with the corresponding standard deviation of the mean in Cols. 5 and 8, respectively.
References. (1) Salinas et al. (2016); (2) Walker (1998); (3) Kaluzny et al. (1997), Arellano Ferro et al. (2013); (4) Layden & Sarajedini (2003), Arellano Ferro et al. (2014); (5) Cuffey (1966), Goranskij (1976), Arellano Ferro et al. (2011); (6) Braga et al. (2018); (7) Benkő et al. (2006); (8) Contreras et al. (2010); (9) Walker & Nemec (1996); (10) Corwin et al. (2008); (11) Martínez-Vázquez et al. (2016);(12) Muraveva et al. (2020); (13) Garofalo et al. (2013); (14) Vivas et al. (2020).

The right panel of Fig. 21 shows the comparison of the photometric metallicities derived with the SOS Cep&RRL pipeline and the metal abundances from high-resolution spectra from Crestani et al. (2021) for 105 RR Lyrae stars in common in the two studies. As expected, this confirms the metallicity offset seen in the left panel of the figure, but the two sets of estimates are still generally consistent within the admittedly large errors of the SOS metallicities.

In Table 1 we compare available metallicities for a sample of globular clusters (GCs) and dwarf spheroidal galaxies (dSphs) with the metal abundances obtained by averaging individual photometric estimates from the SOS pipeline for RR Lyrae stars in these systems. The agreement is satisfactory, and except for M62, it is always within the standard deviations of the mean values estimated from the RR Lyrae stars.

Finally, the metallicity distributions of RR Lyrae stars in the all-sky, LMC, and SMC regions are shown with different colours in Fig. 22. A photometric metallicity estimate is available for 114 653 RR Lyrae in the all-sky region, for 16 295 in the LMC region, and for 2634 in the SMC region. The metallicity distributions peak at mean values of [Fe/H] = −1.07± 0.63, −1.31 ± 0.62, and −1.66 ± 0.66 dex for the all-sky, LMC, and SMC variables, respectively. The mean value estimated for the LMC variables is confirmed to be about 0.2 dex higher than reported by Gratton et al. (2004) from low-resolution ($R \simeq 800$) spectra of 98 RR Lyrae stars in the bar of the LMC: [Fe/H]= −1.48 ± 0.03 dex (on the Harris 1996 metallicity scale) and by Borissova et al. (2006), [Fe/H] = −1.53 ± 0.02 dex, from 78 RR Lyrae stars, covering a wide range of distances out to 2.5 degrees from the LMC centre.

5.2. Comparison with GSP_Spec metallicities

The `astrophysical_parameters` table in the *Gaia* DR3 archive contains metallicities derived with specific modules of the Apsis pipeline (Creevey et al. 2023) that analyse the *Gaia*

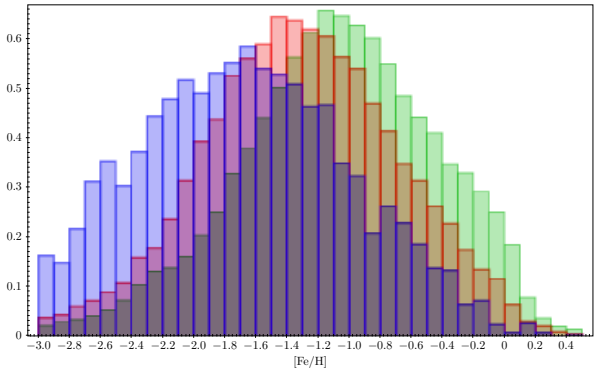

Fig. 22. Normalised metallicity distribution of the 133 577 RR Lyrae stars with photometric metallicities computed with the SOS pipeline. The sources are divided into the three separate regions (all-sky, LMC, and SMC) defined in Sect. 2. Green, red, and blue histograms represent all-sky, LMC, and SMC variables, respectively. The three distributions peak at mean values of [Fe/H] = −1.07±0.63, −1.31±0.62, and −1.66± 0.66 dex for the all-sky, LMC, and SMC variables, respectively.

RVS spectra and the low-resolution *BP*, *RP* prism spectra. Of particular interest for our comparison are the metal abundances produced by `GSP_Spec`, the module that processes the RVS spectra (Recio-Blanco et al. 2023).

The [M/H] metal abundances computed by the GSP_Spec module (`mh_gspspec`) are available for 288 RR Lyrae stars in the sample with a photometric metallicity computed by the SOS pipeline. Following recommendations in Recio-Blanco et al. (2023), we applied the GSP_spec quality flag (`flags_gspspec`) to filter out sources with lower-quality GSP_Spec abundances. This reduced the sample to 193 RR Lyrae stars. The left panel of Fig. 23 shows the comparison of the [M/H] abundances from GSP_Spec and the [Fe/H] metallicities computed with the SOS pipeline for these 193 RR Lyrae stars. The agreement between the two sets of metallicities is satisfactory throughout the entire range from [Fe/H] ∼ −2.5 to ∼+0.3 dex. About 70% of the sources lie within ±0.46 dex (the mean metallicity error in Fig. 19) from the one-to-one line, and 93% lie within ±0.5 dex. This gives us confidence in the reliability of the photometric metallicities obtained with the SOS Cep&RRL pipeline.

The [M/H] metal abundances computed by GSP_Phot (`mh_gsphot`), the Apsis module that processes the low resolution *BP*, *RP* prism spectra (Andrae et al. 2023) are also available for several thousand RR Lyrae stars confirmed by the SOS pipeline. However, the GSP_phot metallicities of RR Lyrae stars appear to be affected by very large uncertainties and systematic effects. In particular, for the 193 RR Lyrae stars discussed previously, the GSP_Phot metallicities are systematically offset from both the GSP_Spec and the SOS estimates by more than 1 dex towards higher abundances. The reason for this likely are the unusually large flux errors in the time-averaged *BP*/*RP* spectra of RR Lyrae stars compared to non-variable sources of the same spectral type (see Fig. B.3 in Appendix B), as well as issues of the instrument model of the *BP*/*RP* spectra due to a lack of calibrators with emission lines below 400 nm (see Montegriffo et al. 2023, for details). We return to this issue below when we discuss the GSP_Phot *G* absorption in Sect. 5.4.

5.3. G-band absorption

An estimate of individual interstellar absorption in the *G* band [$A(G)$] was obtained by the `StellarParametersDerivation` module for 142 867 fundamental-mode RR Lyrae stars from an empirical relation of the amplitude of the *G* light curve [Amp(G)], the pulsation period (P), and the ($G - G_{RP}$) colour of these RRab stars (see Sect. 2.1.2 in Paper II for details). Typical uncertainties in $A(G)$ are about ±0.4 mag, corresponding to the mean of the absorption uncertainty (`g_absorption_error`) values in the `vari_rrlyrae` table for the 142 867 RR Lyrae stars. Figure 24 shows the error distribution in $\sigma_{A(G)}/A(G)$ of the $A(G)$ values. For 30% of the 142 867 RRab stars, $\sigma_{A(G)}$ is lower than 10%, for 47% of the sample, it is lower that 20%, and for 68% of the sample, it is lower than 50%. Finally, for 19% of the sample, $\sigma_{A(G)}$ is higher than 100%.

In the right part of Table 1 we compare the $A(G)$ values obtained by transforming the $A(V)$ values in the literature for a sample of GCs and dSphs using the ratio of the extinction coefficients in different bands by Bono et al. (2019) (see the notes to Table 1) with the $A(G)$ values obtained by averaging the individual *G*-absorption estimates computed with the SOS pipeline for RR Lyrae stars in these systems. The mean A(G) measurements and relative standard deviations listed in Table 1 were computed for the entire sample of RR Lyrae stars contained in each system. However, the innermost RR Lyrae stars in the GCs are affected by significant crowding effects that impact the G_{RP} magnitudes in particular, and may thus lead to unreliable (high) $A(G)$ values. When RR Lyrae stars within the half-light radius of each cluster are excluded, the derived mean $A(G)$ values are more compatible with the literature values and their standard deviations are reduced by up to 50%. We also recommend to use the $A(G)$ values obtained with the SOS pipeline for RR Lyrae stars fainter than $G \geqslant 18.5 - 19$ mag with caution. These sources may have very uncertain G_{RP} magnitudes, which also leads to unreliable $A(G)$ values. This is the case for some of the dSphs listed in Table 1. Of these, Ursa Major II, the only dSph in Table 1 containing bright RR Lyrae stars ($G \sim 18$ mag), has in fact a mean $A(G)$ value with small std that perfectly agrees with the literature estimation. Finally, an absorption map drawn from the 142 867 RRab stars is presented in Sect. 7.

5.4. Comparison with GSP_phot absorption values

The `astrophysical_parameters` table in the *Gaia* DR3 archive contains $A(G)$ values (`ag_gspphot`) derived by the GSP_Phot module of the Apsis pipeline (Creevey et al. 2023). GSP_Phot $A(G)$ values are available for 84 501 of the RRab stars with an $A(G)$ estimate from the SOS pipeline. In Fig. 25 we show the comparison of the two independent $A(G)$ estimates. The $A(G)$ values are colour-coded according to the intensity-averaged *G* magnitudes of the RR Lyrae stars. Two sequences are clearly visible above the one-to-one line. These bright sequences are composed of a mixture of RR Lyrae stars for which absorption values were either computed with the `ESP_HS` module of Apsis, the routine designed to derive astrophysical parameters of bright ($G < 17.65$ mag) O-, B-, and A-type stars, or by the GSP_Phot module (see panel (a) of Fig. B.4 in Appendix B). The misidentification of the RR Lyrae as OB stars in the brightest sequence in Fig. 25 is the reason for the overestimated (`ESP_HS`) absorption values for these sources. On the other hand, as discussed in Appendix B, the peak-to-peak variability of about one magnitude in *G* (Amp(G) parameter in the `vari_rrlyrae` table) of the RRab stars is absorbed as increased flux uncertainties in the time-averaged *BP*/*RP* spectra that were used to estimate the GSP_Phot absorption. Because of the unusually large *BP*/*RP* flux uncertainties, the χ^2 is flattened, thus opening the room for degeneracies. In particular, this appears to be most

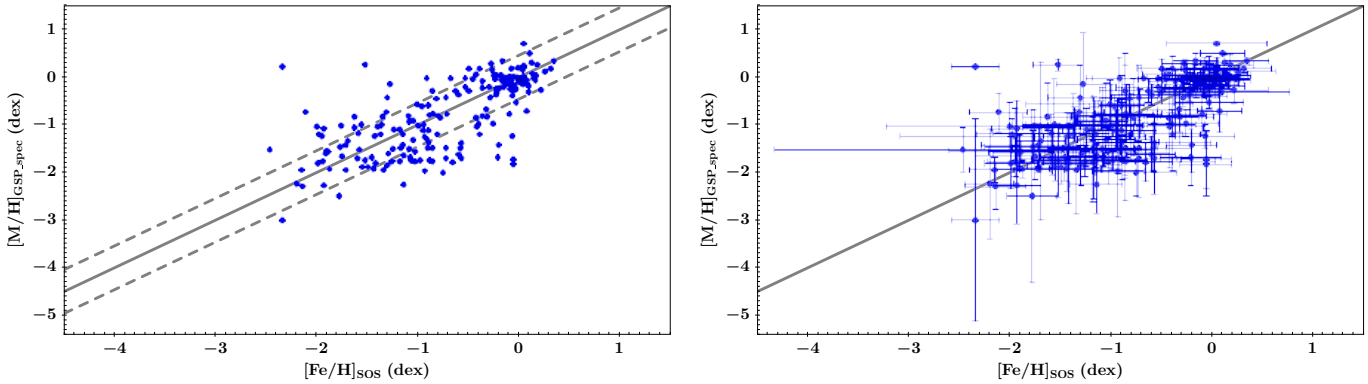

Fig. 23. Left panel: comparison of the [M/H] metal abundances (`mh_gspspec`) computed with the GSP_Spec module of Apsis and [Fe/H] metallicities computed with the SOS Cep& RRL pipeline for 193 RR Lyrae stars for which both values are available. The two dashed lines are offset by ±0.46 dex, the mean error of the photometric metallicities (see Fig. 19), from the one-to-one line; right panel: same as in the left panel, but also showing the error bars of the $[M/H]_{GSP\_Spec}$ and $[Fe/H]_{SOS}$ metallicities.

likely an extreme case of temperature-extinction degeneracy due to GSP_Phot adopting incorrect mean temperatures for these RR Lyrae stars.

To conclude, as already pointed out for the GSP_Phot metallicities (Sect. 5.2), the comparison of the $A(G)$ values shows the difficulty of correctly inferring astrophysical parameters for high-amplitude variables, such as the RR Lyrae stars, based on time-averaged BP/RP spectra. We recommend that for RR Lyrae stars (or for any other type of high amplitude pulsating variable stars) the epoch BP/RP spectra are used individually (if their S/N allows for it) along with epoch $T_{\rm eff}$ and $\log g$ values, and to then average the results to obtain more reliable GSP_Phot metallicities and absorption values. On the other hand, as further discussed in Appendix B, the SOS Cep&RRL and GSP_Phot absorption values agree within $\simeq\pm0.2$ mag for RR Lyrae stars for which the GSP_Phot module uses $T_{\rm eff}$ values in the proper range for fundamental-mode RR Lyrae stars (e.g. $6300 \lesssim T_{\rm eff} \lesssim 6800$ K; see Col. 11 in Table A.3 and the top panel of Fig. B.5). This is likely the case for about 14 000 RR Lyrae stars of the 84 501 sources for which both absorption estimates are available. We also find that for these same RR Lyrae strars, the SOS Cep&RRL [Fe/H] values and the GSP_Phot metallicities agree within ±0.5 dex.

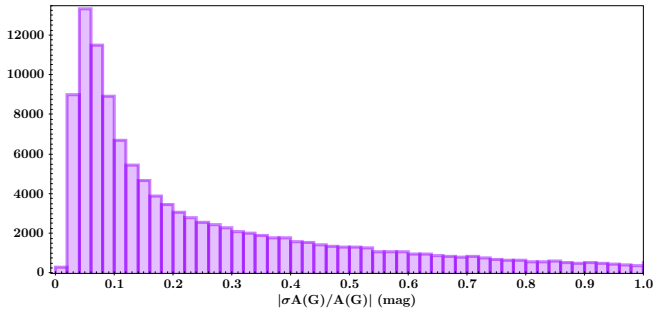

Fig. 24. Error distribution in $\sigma_{A(G)}/A(G)$ of the $A(G)$ values computed with the `StellarParametersDerivation` module for 142 867 fundamental-mode RR Lyrae stars. Only sources for which $\sigma_{A(G)}$ is lower than 100% (81% of the RR Lyrae stars with an estimate of $A(G)$) are shown in the plot.

6. Final cleaning and validation of the DR3 RR Lyrae catalogue

During the final validation of the catalogue of 271 779 RR Lyrae stars that were confirmed and characterized with the SOS pipeline, a number of issues, misclassifications, and uncertain classifications were detected. In this section we discuss them and provide tables with the identifiers of the affected sources. A final statistics of the SOS confirmed DR3 RR Lyrae stars, corrected for the issues described in this section, is presented in Sect. 7.

6.1. Mode identification for short-period RR Lyrae stars

Short-period RRab stars with $P \lesssim 0.4$ d overlap with RRc stars in the PA diagram. In DR3 we have adopted new boundaries of the RRab and RRc regions in the PA diagram to separate the fundamental-mode from the first-overtone RR Lyrae stars (see Sect. 2 and Fig. 3). However, some RRab stars were not captured by the new boundaries and were incorrectly classified as RRc stars. This is the case of the RRab stars 4297554691689496192 (P = 0.366 d) and 1826975050760883072 (P = 0.357 d). We caution that there may be a few more cases like these in the DR3 `vari_rrlyrae` table.

6.2. Double-mode RR Lyrae stars with Pf ≃ P1O

The parameters of 2007 double-mode RR Lyrae stars are published in the DR3 `vari_rrlyrae` table. For 121 of them, the two periodicities Pf and $P1O$ that are listed in the table differ by less than 0.01 d. This was likely caused by a remapping problem of $p1$ and $p2$, the two periodicities detected in the time-series photometry of these sources, into Pf (fundamental pulsation period) and $P1O$ (first-overtone pulsation period). For all these 121 sources, the $p1$ and $p2$ values differ and are in the proper ratio for double-mode RR Lyrae stars. We provide the correct Pf and $P1O$ values computed by the SOS pipeline for these 121 double-mode RR Lyrae stars in Table 2.

6.3. RR Lyrae stars with large or null errors for the main parameters

The `peak_to_peak_bp`, `peak_to_peak_rp`, `int_average_bp`, and `int_average_rp` parameters of a number of RR Lyrae stars in the DR3 `vari_rrlyrae` table have very large errors (see e.g. for source 4660156103061766400) or

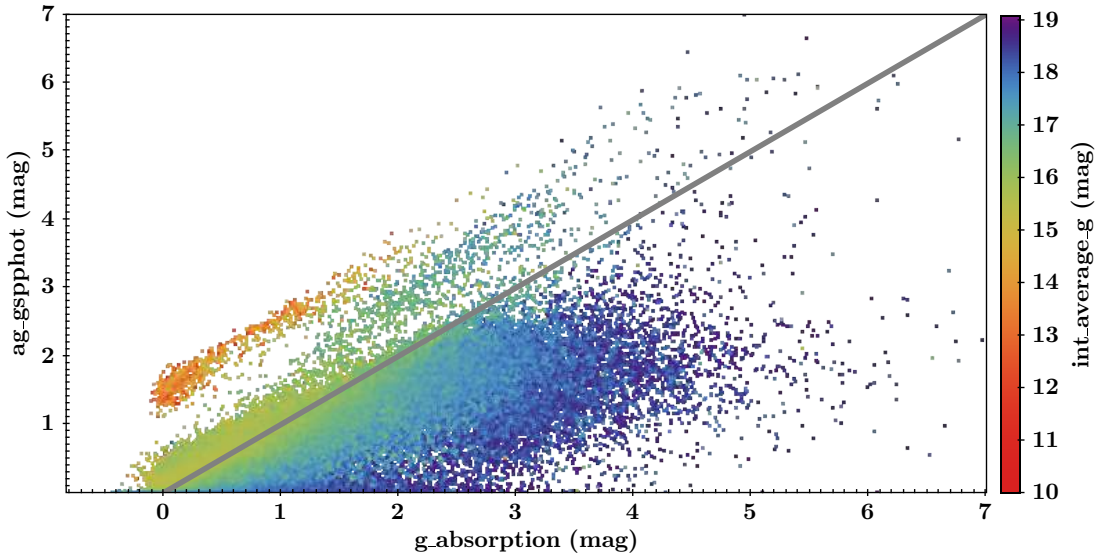

Fig. 25. Comparison of G absorption values derived by the GSP_Phot module of the Apsis pipeline (`ag_gspphot`; Creevey et al. 2023) and the values derived by the SOS pipeline (`g_absorption`) for 84 501 RRab stars for which both estimates are available. The $A(G)$ values are colour-coded according to the intensity-averaged G magnitudes of these RR Lyrae stars, as encoded in the colour scale on the right (see text for details).

Table 2. Correct Pf and $P1O$ periods for 121 double-mode RR Lyrae stars for which the two periodicites published in the *Gaia* DR3 `vari_rrlyrae` table differ by less than 0.01 d.

Gaia sourceid	Pf	$P1O$
408895729987233536	0.373330688241618	0.512642740772834
501173342860631808	0.356601096360751	0.479398897708066
510602690164934528	0.450007942826883	0.333771875260333
711991473282863616	0.405938896214094	0.544093988121247
799159586901582464	0.41546585867929	0.556716992103652
1009169258447656576	0.373435128605576	0.501424952889536
1019488037636107136	0.377019820562923	0.505549683973198
1300079698489198464	0.401148054398303	0.537722672814259
1323028808262955264	0.478288427372862	0.35013538941965
...	...	...

Notes. This table is available in its entirety at the CDS.

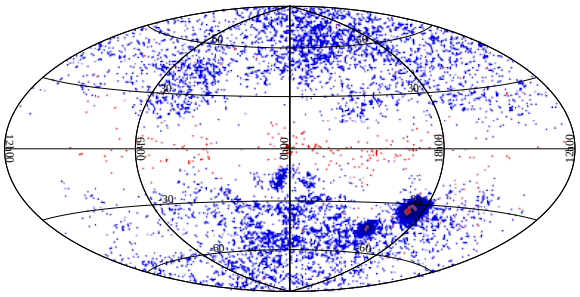

Fig. 26. Sky distribution in galactic coordinates of 9 503 RR Lyrae stars with low/negative $A(G)$ values (blue symbols) and 286 RR Lyrae stars with $A(G)$ values higher than 10 magnitudes (red symbols).

errors set to zero (see e.g. sources 4660223379454198144, 4685971467924582144, and 5027218748491264768). This happens for bona fide RR Lyrae stars with a mean G magnitude (`int_average_g`) fainter than 18.5–19 mag and sparse measurements with large errors in the G_{BP} and G_{RP} light curves. The affected sources are mainly in the Magellanic Clouds, in the Galactic bulge, and in a number of MW dSphs and UFDs.

Additionally, the R_{21} (`r21_g`) and R_{31} (`r31_g`) Fourier parameters of the G light curves for ~4400 DR3 RR Lyrae stars exceed the expected range of [0,1]. However, these limits are fully respected if the rather large errors associated with the R_{21}, R_{31} parameters of these sources are taken into account.

6.4. RR Lyrae stars with negative or very high A(G) values

The G absorption ($A(G)$; `g_absorption` parameter) is negative (with values ranging from 0 to −1.279 mag) for 9503 DR3 RR Lyrae stars, corresponding to 6.3% of the 142 867 RR Lyrae stars with an $A(G)$ value in the `vari_rrlyrae` table (see Sect. 5.3), and it is higher than 10 mag (up to 3367.32 mag for source 5847675733921242624) for 286 sources (i.e. 0.2% of the RR Lyrae stars with an $A(G)$ estimate).

As discussed in Sect. 5.3, 19% of the RR Lyrae stars with an $A(G)$ estimate have $|\sigma_{A(G)}/A(G)| > 1$. This is the case of all the 9503 sources with a negative $A(G)$. Of these, 8033 have $-0.1 < A(G) < 0$ mag, 9 297 have $-0.2 < A(G) < 0$ mag, and 9487 have $-0.5 < A(G) < 0$ mag. The remaining sources (0.2%) with $A(G) < -0.5$ mag are fainter than $G \sim 19$ mag and therefore have uncertain $(G-G_{RP})$ colours that affected the $A(G)$ estimations.

Two hundred and eighty-six RRLyrae stars have high positive $A(G)$ values, discarding the extreme case of 5847675733921242624, which clearly has an incorrect $A(G)$ value. Of these, 77% have $0.007 < |\sigma_{A(G)}/A(G)| < 0.2$ and 91% have $0.007 < |\sigma_{A(G)}/A(G)| < 0.5$. The sky distribution of the RR Lyrae stars with low/negative or very high $A(G)$ values is shown in Fig. 26 with blue symbols for the former and red symbols for the latter. As expected, the RR Lyrae stars with very high $A(G)$ values are mainly confined in the Galactic disc and in regions with the highest reddening in the Magellanic Clouds, while RR Lyrae stars with a low/negative $A(G)$ value are mainly located at high latitudes in the MW halo.

Table 3. 31 RR Lyrae stars in the *Gaia* DR3 `vari_rrlyrae` table that have a different classification in the OGLE catalogue.

Gaia sourceid	$\langle G \rangle$ (mag)	Revised type (this paper)	Type (OGLE-IV)
4121189659364789632	18.407 ± 0.040	RRab	ACEP 1O
6724031478150071680	14.782 ± 0.007	RRab	ACEP 1O
3325594070648057344	13.304 ± 0.007	DCEP_1O	CEP 1O/2O
5259472605426820864	17.174 ± 0.002	DCEP_1O	CEP 1O/2O
5337626858335118080	17.471 ± 0.002	DCEP_1O	CEP 1O
5861856101075703552 (*)	13.398 ± 0.010	DCEP_MULTI	CEP F/1O
6025724977547669120	15.533 ± 0.010	DCEP_1O	CEP F/1O
4086063080350131968	13.863 ± 0.025	ACEP_F	ACEP F
4088429190686315136	16.836 ± 0.021	ACEP_F	ACEP F
4099638849167163648	13.514 ± 0.024	ACEP_1O	ACEP 1O
4123275364279164672	14.546 ± 0.004	ACEP_1O	ACEP 1O
5253954057825909504	17.249 ± 0.005	ACEP_F	ACEP F
5333097209687948032	19.000 ± 0.007	ACEP_F	ACEP 1O
5343906650256155392	15.834 ± 0.002	ACEP_1O	ACEP 1O
5355902184686008832	14.863 ± 0.003	ACEP_1O	ACEP 1O
5625331663591871104	17.862 ± 0.002	ACEP_1O	ACEP 1O
5949793765379361152	17.784 ± 0.006	ACEP_1O	ACEP 1O
5956690971798673664	15.261 ± 0.020	ACEP_F	ACEP F
5970892843763951104	17.397 ± 0.003	ACEP_F	ACEP F
5978313726930066048	16.533 ± 0.004	ACEP_1O	ACEP 1O
5979051907235436160	17.042 ± 0.004	ACEP_F	ACEP F
6026530163731660928	15.445 ± 0.009	ACEP_F	ACEP F
6029981290235791232	15.607 ± 0.002	ACEP_1O	ACEP 1O
6724250895118108928	15.294 ± 0.003	ACEP_1O	ACEP 1O
4048728299707790976	15.562 ± 0.014	ACEP_1O/RRab?	ACEP 1O
4101192497784043520	14.931 ± 0.010	ACEP_1O/RRab?	ACEP 1O
4107356012051364480	15.654 ± 0.020	ACEP_1O/RRab?	ACEP 1O
5956833835251660800	15.975 ± 0.014	RRab/ACEP_F?	ACEP F
5968150764841574912	18.733 ± 0.005	ACEP_1O/RRab?	ACEP 1O
5980267829660152960	17.404 ± 0.005	ACEP_1O?/RRab?	ACEP 1O
6061867986376466688	16.290 ± 0.005	ACEP_F/RRab?	ACEP F

Notes. Based on a number of attributes, including their *Gaia* EDR3 parallax, the sources listed in the table are either confirmed as fundamental-mode RR Lyrae stars (2 sources), are reclassified as DCEPs (5 sources) or ACEPs (17 sources), or have an uncertain classification between RRab stars and ACEPs (7 sources). (*)This source is one of the 1100 RR Lyrae stars with RVS time-series RVs published in DR3.

6.5. RR Lyrae stars with a different classification in the OGLE catalogue

The *Gaia* DR3 `vari_rrlyrae` table lists 31 sources that the classifiers of the General Supervised Classification module in the variability analysis pipeline (Rimoldini et al. 2023) classified only as RR Lyrae candidates. They were therefore only processed through the RR Lyrae branch of the SOS Cep&RRL pipeline, which confirmed their classification as RR Lyrae stars. However, these sources are classified as Cepheids (5 as DCEPs and 26 as ACEPs) in the OGLE-IV catalogue of variable stars. Based on their *Gaia* EDR3 parallaxes, these sources were plotted on the period-luminosity (PL) and period-Wesenheit (PW) relations of DR3 Cepheids (see Table 2 in Ripepi et al. 2023). For two of them, the classification as RRab stars was confirmed, while 22 were reclassified as Cepheids (5 DCEPs and 17 ACEPs), and 7 have an uncertain classification between ACEPs or RRab stars. The sourceids of these 31 sources are provided in Table 3 along with their final classifications. One of the sources that was reclassified as DCEP (source 5861856101075703552) is included in the list of 1100 RR Lyrae stars with RVS time-series RVs published in DR3. Owing to this reclassification, the number of RR Lyrae stars with epoch RVs drops to 1099 and the Cepheid number increases to 799 (but see also Sect. 6.9).

6.6. RR Lyrae stars missing in the vari_rrlyrae table

The catalogue of 271 779 RR Lyrae stars does not contain 14 bona fide RR Lyrae stars that were confirmed by the SOS Cep&RRL pipeline. They were mistakenly removed from the SOS final catalogue, but are listed in the `vari_classifier_result` table. Table 4 gives the sourceids of these 14 RR Lyrae stars, and in Table C.1 we provide the parameters (P, peak-to-peak G, G_{BP}, G_{RP} amplitudes, mean magnitudes, etc.) that were computed by the SOS pipeline for these sources.

6.7. Overlaps with pipelines that process galaxies and QSOs

A total of 1139 sources in the `vari_rrlyrae` table are classified as galaxies by other DPAC pipelines. After visual inspection of their light curves, 618 of them were confirmed as RR Lyrae stars, more than 400 of which are known RR Lyrae stars in the OGLE-IV catalogue or in the catalogue of variable stars

Table 4. 14 bona fide RR Lyrae stars that were mistakenly removed from the SOS RR Lyrae catalogue.

Gaia DR3 sourceid
4092009204924599040
4120414435009794048
4144246349481643392
5797652730842515968
5797917193442176640
5846086424210395520
5917239841741208576
5991733644318583424
6017924835910361344
6069336998880602240
6707009423228603904
5935214760885709440
4362766825101261952
5967334102579505664

Notes. The sources in this table do not appear in the `vari_rrlyrae` table, but are listed in the `vari_classifier_result` table. The SOS Cep&RRL parameters for these 14 RR Lyrae stars are provided in Table C.1.

Table 5. 521 sources in the *Gaia* DR3 `vari_rrlyrae` table that are classified as galaxies or non-single/extended objects by other DPAC pipelines.

Gaia DR3 source id	Tentative class (*)
252947980027906048	RR Lyrae?
367375357718907776	galaxy/QSO
392996452549916416	...
406587893736299136	...
419307353484601472	...
3206068021312873728	...
1056196096618040960	...
5571533079335954816	...
4685908211622296576	...
4928220400858440704	...
...	...

Notes. The entries in this table either are clearly not RR Lyrae stars or are sources for which the SOS Cep&RRL pipeline classification as RR Lyrae stars is uncertain (see Col. 2). (*)Tentative classification after visual inspection of the light curves. The table is available in its entirety at the CDS.

in GCs. The remaining 521 sources are listed in Table 5. The majority of them are rather faint sources ($G > 20$ mag) and are either clearly not RR Lyrae stars or have an uncertain classification.

About 57 000 RR Lyrae stars in the `vari_rrlyrae` table are classified as QSOs by other DPAC pipelines. Of these, 55 448 are known RR Lyrae stars (~30 000 from the OGLE-IV catalogue and ~25 400 from other main catalogues of RR Lyrae stars in the literature). We visually inspected the light curves of the remaining 1635 sources and confirmed the classification as RR Lyrae stars for 1353 of them (80 of them are classified as RR Lyrae stars in the SIMBAD database as well; Wenger et al. 2000). The remaining 282 sources that are listed in Table 6 are either clearly not RR Lyrae stars or have an uncertain classification.

Table 6. 282 sources in the *Gaia* DR3 `vari_rrlyrae` table that are classified as QSOs by other DPAC pipelines.

Gaia DR3 sourceid	Class (*)
5710645592594769280	ECL
5246357493290558336	ECL
4661507982702013312	...
5116113679481496832	...
2456881998103809280	...
1305269977485608192	...
6242394047412731520	...
...	...

Notes. The entries in this table either are clearly not RR Lyrae stars or are sources with an uncertain classification. (*)Classification after visual inspection of the light curves. This table is available in its entirety at the CDS.

Table 7. Eighty bona fide RRab stars in the *Gaia* DR3 `vari_rrlyrae` table that are identified as non-single star by the `SEAPipe` pipeline.

Gaia DR3 source id
4061010604884154624
4097861458597689856
4043627562186192768
1827951859436521728
6045465845526924544
...

Notes. This table is available in its entirety at the CDS.

6.8. Non-single star sources identified with SEAPipe

The DPAC-Source Environment Analysis Pipeline (`SEAPipe`; Harrison 2011; Harrison et al., in prep.) was run on the catalogue of 271 779 RR Lyrae stars confirmed by the SOS Cep&RRL pipeline to determine whether additional sources are present in the vicinity (within a radius of ~2″) that might contaminate the light of the RR Lyrae stars. SEAPipe returned a list of 80 RR Lyrae stars that were found to be non-single sources. These 80 sources mainly lie in the MW bulge and disc, 79 of them are RR Lyrae stars already known in the literature (67 are in the OGLE-IV catalogue and 12 in the ZTF and *Gaia* DR2 catalogues), only one is a new discovery. Visual inspection of the light curves allowed us to confirm that they are all *ab*-type RR Lyrae stars, with different levels of noise particularly in the G_{BP} and G_{RP} light curves that is often also accompanied by a reduced amplitude of the G-band light curve. These are clear signatures of contamination and blending by neighboring stars (see e.g. Fig 16 in Di Fabrizio et al. 2005) that can affect the estimated mean magnitude and peak-to-peak amplitudes of these RR Lyrae stars, but not the derived periods. We list these 80 RRab stars in Table 7 and caution about the use of amplitudes, mean magnitudes, Fourier parameters, and derived quantities of these sources.

6.9. Contamination by binaries and other types of variable stars

RR Lyrae stars in the `vari_rrlyrae` with *Gaia* EDR3 parallaxes accurate to better than 5% were plotted on a $PW(G, G_{BP} - G_{RP})$ relation along with DR3 Cepheids with same parallax accuracy (see Ripepi et al. 2023, for details). A group of 147

Table 8. Sources in the *Gaia* DR3 `vari_rrlyrae` table that are reclassified as ECLs or possible ECLs (55 in total) and variable stars with poor light curves and uncertain classification into type (17 sources).

Gaia DR3 sourceid	Class [(*)]	Lit_Survey
87159184382553088	ECL	CATALINA
568221222620689024	ECL	ASAS-SN
326383086038685952	ECL	GCVS
6812645960632807296	ECL	ASAS
5292689405748796160	ECL	CATALINA
...	...	...

Notes. [(*)]Classification after visual inspection of the light curves. This table is available in its entirety at the CDS.

Table 9. *Gaia* DR3 sourceids of the 888 sources that were rejected during the final validation of the catalogue of 271 779 RR Lyrae stars that are published in the DR3 `vari_rrlyrae` table.

Gaia DR3 sourceid
72425797289881344
87159184382553088
252947980027906048
271665825465872256
279252868010888960
...

Notes. This table is available in its entirety at the CDS.

RR Lyrae stars appear to be fainter by ~0.5 to ~8.5 mag than expected in this plot. These sources are all known RR Lyrae stars that were classified by various different surveys: OGLE (44 sources), ASASSN (40), CATALINA (25), PS1(5) and ZTF, DR2, GCVS, and the catalogue of variable stars in GCs (33 sources altogether). The light curves of these 147 sources were visually inspected and often found to exhibit large scatter, split branches, and other issues, even though they are all rather bright sources. On the basis of a visual inspection of the light curves, the sample contains 75 bona fide RR Lyrae stars or most likely RR Lyrae stars (59 RRab and 16 RRc stars), 55 ECLs[7] that contaminate the RR Lyrae sample or have an uncertain classification between an ECL and a RR Lyrae star or between an ECL and a non-RR Lyrae source, 8 sources show a very prominent bump before the minimum in the light curve, and the light curves of 9 sources are so poor that a classification into type is not possible. We provide the identifiers of the 72 sources in this sample that we reclassify as ECLs or possible ECLs (55 in total) and variable stars with poor light curves and uncertain classification in type (17 sources) in Table 8.

Finally, three of the sources that are reclassified as ECLs (sources 4130380472726484608, 3062985235999231104, and 5734183009797858176) are included in the list of 1100 RR Lyrae stars whose RVS time-series RVs are published in DR3. Owing to their reclassification and the reclassification as DCEP of the source discussed in Sect. 6.5, the number of bona fide RR Lyrae stars with epoch RVs finally drops to 1096.

6.10. Correlation of scan angle and period

A clear correlation was found to exist between the scan angle of the *Gaia* observations and the detection of spurious periods for variable stars of different types. A detailed analysis of this correlation and the parameters defined to assess the reliability of the periods derived from the time-series data analysis of variable sources are presented in Holl et al. (2023). The SOS sample of 271 779 RR Lyrae stars was checked and correlation-value plots were produced, showing that perhaps a few percent of the sources in the sample are affected by possible scan-angle effects at most. This is a low, but perhaps not fully negligible percentage.

[7] The classification as an ECL was based on the value of the ratio of the peak-to-peak amplitudes of the G_{BP} and G_{RP} light curves (this ratio for eclipsing binaries is typically $\mathrm{Amp}(G_{BP})/\mathrm{Amp}(G_{RP}) = 1.0 \pm 0.2$ and is ~1.6 for RR Lyrae stars) and on the visual inspection of the light curves folded with once and twice the period determined by the pipeline.

7. Results and final accounting

The validation process described in Sect. 6 allowed us to clean the catalogue of 271 779 RR Lyrae stars that are published in the DR3 `vari_rrlyrae` table by rejecting 888 sources that are contaminants (mainly ECLs) and objects with an uncertain classification (Sects. 6.5, 6.7, and 6.9). This led to a clean sample of 270 891 confirmed RR Lyrae stars. To this number, we added the 14 RR Lyrae stars (4 RRab and 10 RRc stars) discussed in Sect. 6.6. This led to a final sample of 270 905 DR3 bona fide RR Lyrae stars, of which 200 294 are RR Lyrae already known in the literature (Gold Sample) and 70 611 are new discoveries with *Gaia*. To facilitate use, we collect in Table 9 the sourceids of the 888 sources that were rejected during the final validation process described in Sect. 6. We also note that the periods of a fraction of the 888 sources we rejected during the final cleaning may indeed be affected by the scan-angle effects mentioned in Sect 6.10.

Figure 27 shows the G magnitude distribution of the clean sample of 270 905 DR3 RR Lyrae stars that were confirmed with the SOS pipeline. The magnitude distribution of the 70 611 new RR Lyrae stars is highlighted in black.

Table 10 summarises some statistics of the SOS DR3 RR Lyrae sample, namely, the subdivision between known (Gold Sample) and new discoveries by *Gaia*; the number of RRab, RRc, and RRd types; the number in the LMC, SMC and all-sky regions; how many RR Lyrae stars have a metallicity or G absorption estimate, and, finally, the number of RR Lyrae stars (and Cepheids) with RVS time-series RVs published in DR3.

We note that 1676 RR Lyrae stars of the 270 905 clean sample are distributed among 95 GCs, and 1114 are spread among 7 dSph galaxies (505 of which lie in Sculptor) and 16 UFD satellites of the MW.

The following parameters computed with the SOS Cep&RRL pipeline are released for the clean sample of 270 891 RR Lyrae stars (and for the 888 sources that were filtered out in Sect. 6) in the *Gaia* DR3 `vari_rrlyrae` table, along with the related uncertainties:

- source pulsation period(s) (main and secondary periodicity, if any);
- intensity-averaged mean G, G_{BP}, G_{RP} magnitudes;
- mean RV (for 1096 RR Lyrae stars, one RR Lyrae star reclassified as DCEP_1O, and three sources reclassified as ECLs);
- epochs of maximum light in the three passbands;
- epoch of minimum RV;
- ϕ_{21} and R_{21} Fourier parameters of the G light curve;
- ϕ_{31} and R_{31} Fourier parameters of the G light curve;
- peak-to-peak G, G_{BP}, G_{RP}, RV amplitudes [Amp(G), Amp(G_{BP}), Amp(G_{RP}), Amp(RV)];

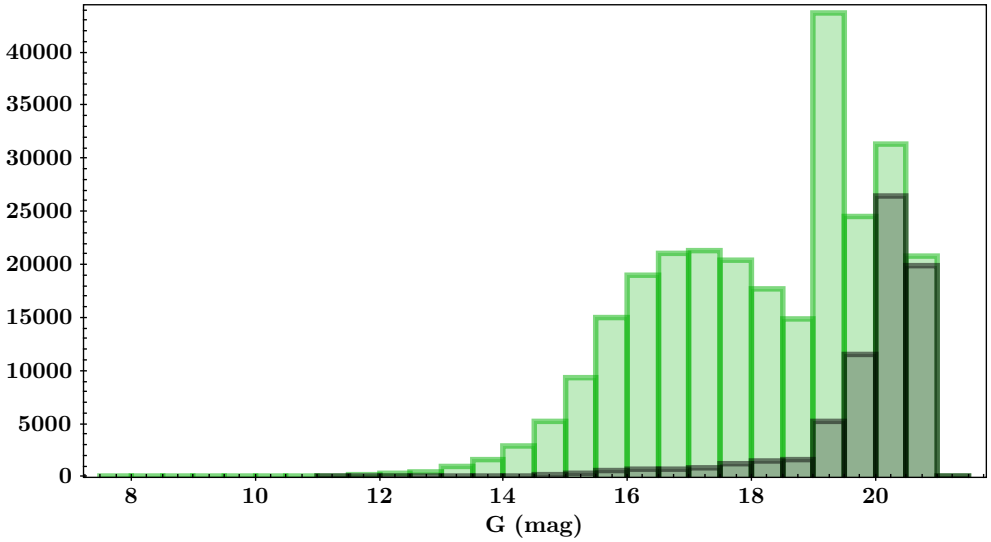

Fig. 27. Distribution in G magnitude of the clean sample of 270 905 DR3 RR Lyrae stars confirmed with the SOS Cep&RRL pipeline. The peaks at $G \sim 19.2, 19.7$ mag correspond to RR Lyrae stars in the LMC and SMC, respectively. The magnitude distribution of the 70 611 new RR Lyrae stars is highlighted in black.

Table 10. Statistics of the RR Lyrae stars confirmed by the SOS Cep&RRL pipeline that are published in DR3.

Sample	$N(-14)$ `vari_rrlyrae`	$N_{\rm clean}(-14)$	$N_{\rm clean}(+14)$
Gold Sample	200 589	200 293	200 294
New discoveries [(a)]	71 190	70 598	70 611
Total number of RR Lyrae stars	271 779	270 891	270 905
LMC region [(b)]	31 535	31 379	31 379
SMC region [(b)]	4828	4788	4788
All-Sky region [(b)]	235 416	234 724	234 738
Fundamental mode (RRab) [(c)]	175 350	174 943	174 947
First overtone (RRc) [(c)]	94 422	93 942	93 952
Double mode (RRd)	2007	2006	2006
[Fe/H] values (RRab and RRc)	133 577	133 558	133 559
$A(G)$ values (RRab only)	142 867	142 656	142 660
RV time series (RR Lyrae) [(d)]	1100	1096	1096
RV time series (Cepheids) [(d)]	798	799	799
RV time series (other type)	...	3	3
Total number of sources with RV time series data	1898	1898	1898

Notes. Numbers in Cols. 2 and 3 correspond to the samples before and after the validation and cleaning described in Sect. 6, respectively. Numbers in Col. 4 are after adding the 14 RR Lyrae stars discussed in Sect. 6.6. [(a)]"New" means "new to the best of our knowledge". [(b)]Regions for the LMC, SMC, and all-sky are as defined in Sect. 2. [(c)]Numbers of RRab and RRc stars in column $N_{\rm clean}(-14)$ are corrected for the reclassifications in Sect. 6.1. [(d)]Numbers of RR Lyrae and Cepheids with RV time-series data published in DR3 are corrected in column $N_{\rm clean}(-14)$ for the reclassifications in Sects. 6.5 and 6.9.

– RR Lyrae subclassification into RRab, RRc, and RRd types;
– absorption in the G band, $A(G)$, for RRab stars; and
– photometric metallicity, [Fe/H], for RRab and RRc stars.

The SOS Cep&RRL parameters for the 14 bona fide RR Lyrae stars that do not appear in the `vari_rrlyrae` table (see Sect. 6.6) are instead provided in Table C.1.

Gaia sourceids, coordinates, G, $G_{\rm BP}$, and $G_{\rm RP}$ time-series photometry for each of the 270 905 RR Lyrae stars (and for the 888 rejected sources) and RVS time-series RVs for 1895 sources between RR Lyrae stars and Cepheids and for three RR Lyrae stars that were reclassified as ECLs can be retrieved from the *Gaia* data release archive[8] and its mirror nodes. The archives also provide tools for queries and a cross-match of *Gaia* data with other catalogues in the literature.

We provide in Table 12 the specific link to the `vari_rrlyrae` table of the *Gaia* DR3 archive and summarise the names of the parameters computed with SOS Cep&RRL that can be retrieved for RR Lyrae stars from the archive table. Finally, in Appendix E, we give examples of queries to retrieve some of the quantities and parameters listed in Table 12.

[8] `http://archives.esac.esa.int/gaia/`

7.1. Completeness and purity of the DR3 RR Lyrae sample

The final clean catalogue of 270 905 RR Lyrae stars confirmed with the SOS pipeline released in *Gaia* DR3 almost doubles the DR2 RR Lyrae catalogue. This is possible through the improved sky coverage, the increased statistic, and the longer time baseline (34 months) covered by the DR3 time-series data (see Sect. 3), which all contributed to improving the completeness and purity of the DR3 RR Lyrae catalogue. This is well shown by comparing the DR3 and the OGLE-IV catalogues of RR Lyrae stars that we use in the following to estimate the completeness, contamination, and percentage of new RR Lyrae stars in the LMC, SMC, and Galactic bulge regions. We also note that while the completeness of our catalogue can be easily estimated in these regions because our reference catalogue, OGLE-IV, is complete at more or less the same magnitude as the *Gaia* data, the completeness in the all-sky region is much more difficult to establish because we still lack a likewise complete and homogeneous catalogue as OGLE for all-sky RR Lyrae stars. In principle, we could use our custom catalogue of 414 082 literature RR Lyrae stars with a counterpart in the EDR3 `gaia_source` table, as reference for the all-sky region, and specifically, the subsample of 311 798 sources confirmed as RR Lyrae stars with the SOS Cep&RRL pipeline. However, this reference catalogue is a compilation of many different surveys, each with a rather different sky coverage, depth/limiting magnitude, completeness, and contamination.

With these caveats in mind to estimate the completeness of our clean final catalogue of 270 905 DR3 RR Lyrae stars, we used the following catalogues that cover different regions of the sky as reference:

(i) OGLE IV for the RR Lyrae stars in the LMC, SMC and the Galactic Bulge (red areas in Fig. D.1);

(ii) the All-Sky catalogue in the DR2 `vari_rrlyrae` table (hereafter, *Gaia* DR2 catalogue) corrected for contaminant galaxies (139 801 RR Lyrae stars, see Paper II);

(iii) the ASAS-SN catalogue, which contains 28 337 RR Lyrae stars with magnitudes in the range $10.4 < V < 17.4$ mag, distributed throughout the sky, as shown in Fig. D.2;

(iv) the CATALINA catalogue, which contains 42 775 RR Lyrae stars with magnitudes in the range $11.0 < V < 21.1$ mag, distributed nearly throughout the entire sky, as shown in Fig. D.3; and

(v) the catalogue of 311 798 all-sky known RR Lyrae stars (extracted from our custom catalogue of literature RR Lyrae stars (see Sect. 3.1) that the SOS pipeline confirms as RR Lyrae stars, along with the 200 294 RR Lyrae stars in the clean Gold Sample for which periods are correctly recovered by the SOS pipeline[9]. The results are summarised in Table 11. The completeness values in Col. 2 correspond to the recovery percentages from a cross-match within 2.5″ between RR Lyrae stars in the DR3 clean catalogue and the reference catalogues as listed in Col. 1. Percentages of new discoveries in Col. 3 correspond to the percentage of additional sources in the DR3 catalogue with respect to the number of recovered sources in each reference catalogue. The contamination in Col. 4 is estimated only for the new sources in the DR3 catalogue by determining how many of the new sources have a non-RR Lyrae classification in the SIMBAD catalogue. It corresponds to the percentage of contaminants over the number of new sources with respect to each reference catalogue.

Table 11. Completeness, contamination, and new discoveries of our final clean catalogue of 270 905 DR3 RR Lyrae stars in different sky regions from the comparison with different literature surveys.

	Completeness	New [(a)]	Contamination
OGLE-IV [(b)]			
LMC	83%	4%	<1.8%
SMC	94%	6%	<8%
Bulge-up	79%	20%	<0.15%
Bulge-down	82%	40%	...
Gaia DR2 [(c)]	90%	103%	<0.12%
ASAS-SN [(b)]	73.7%		
CATALINA [(b)]	85.5%		
All Surveys [(d)]	64.2%		

Notes. [(a)]New means "new sources to the best of our knowledge". [(b)]Regions used for the comparison with OGLE-IV are shown in red in Fig. D.1, for ASAS-SN, they are shown in Fig. D.2, and for CATALINA, they are shown in Fig. D.3. [(c)]Comparison with the 139 801 sources in the DR2 RR Lyrae catalogue after correcting for contaminant galaxies. [(d)]Comparison of the 311 798 all-sky known RR Lyrae stars and the Gold Sample RR Lyrae stars whose periods are correctly recovered by the SOS pipeline.

7.2. Colour-magnitude diagrams

Figure 28 shows colour-magnitude diagrams (CMDs) in apparent G versus $(G_{BP} - G_{RP})$ magnitudes defined by RR Lyrae stars in the DR3 clean catalogue. In particular, the left panel shows the CMD of RR Lyrae stars in GCs (red symbols) and the RR Lyrae stars in dSphs and UFDs for which the $(G_{BP} - G_{RP})$ colours are available (blue symbols). The middle panel instead shows the CMD of the whole sample of 215 115 (out of 270 905) RR Lyrae stars for which $(G_{BP} - G_{RP})$ colours are available, using different colours for variables in the LMC, SMC, and all-sky regions as defined in Sect. 2. Finally, the right panel shows the CMD of the whole sample (grey symbols). Red, green, and blue symbols show RR Lyrae stars with parallaxes better than 10%, 20%, and 50%, respectively. In the left panel of Fig. 29, we instead show the HR diagram in G absolute magnitude (M_{G_0}) and dereddend $(G_{BP} - G)_0$ colour of 915 RRab stars that have a parallax with $\sigma_\varpi/\varpi < 0.1$, RUWE < 1.4[10], and $A(G) < 0.2$ mag. The right panel shows 620 RRab stars from the same sample, but with $A(G) < 0.1$ mag. The observed mean G magnitudes were dereddened using the $A(G)$ values estimated by the SOS pipeline, while the G_{BP_0} magnitudes were derived from the observed G_{BP} values using the relations $A(G)/A(V) = 0.840$ and $A(G_{BP})/A(V) = 1.086$ from Bono et al. (2019). The RR Lyrae stars are colour-coded according to their metallicity as computed by the SOS pipeline and appear to be a mixture of a metal-poor and bluer component and a more metallic and redder component. We overplot the HR diagrams in Fig. 29 with the boundaries of theoretical instability strips (ISs) for fundamental-mode RR Lyrae stars of three different chemical compositions ($Z = 0.0001$; $Z = 0.001$; and $Z = 0.02$) from the suite of

[9] We note that a large fraction of the 311 798 known RR Lyrae stars that were confirmed with the SOS Cep&RRL pipeline (see Sect. 3.1) were finally rejected because the SOS periods for these sources differ by more than 0.001 d from the literature periods. Some of these rejected sources are listed in the `vari_classifier_result` table.

[10] See Sect. 14.1.2 of the *Gaia* Data Release 2 Documentation release 1.2; https://gea.esac.esa.int/archive/documentation/GDR2/.

Table 12. Links to the *Gaia* archive table to retrieve pulsation characteristics, metallicity, and absorption in the G band computed by the SOS Cep&RRL pipeline for 270 891 confirmed RR Lyrae stars (and for 888 rejected sources listed in Table 9) that are released in *Gaia* DR3.

Table URL	https://gea.esac.esa.int/archive/
RR Lyrae main parameters computed by the SOS Cep&RRL pipeline	
Table name	gaiadr3.vari_rrlyrae
Source ID	source_id
Type	best_classification (one of RRc, RRab or RRd)
$Pf, P1O$	p_f, p1_o
$\sigma(Pf, P1O)$	pf_error, p1_o_error
E [(a)](G, G_{BP}, G_{RP}, RV)	epoch_g, epoch_bp, epoch_rp, epoch_rv
σE(G, G_{BP}, G_{RP}, RV)	epoch_g_error, epoch_bp_error, epoch_rp_error, epoch_rv_error
$\langle G\rangle, \langle G_{BP}\rangle, \langle G_{RP}\rangle, \langle RV\rangle$	int_average_g, int_average_bp, int_average_rp, average_rv
$\sigma\langle G\rangle$, $\sigma\langle G_{BP}\rangle$, $\sigma\langle G_{RP}\rangle$, $\sigma\langle RV\rangle$	int_average_g_error, int_average_bp_error, int_average_rp_error, average_rv_error
Amp(G, G_{BP}, G_{RP}, RV)	peak_to_peak_g, peak_to_peak_bp, peak_to_peak_rp, peak_to_peak_rv
σ[Amp(G)], σ[Amp$(G_{BP}]$, σ[Amp$(G_{RP}]$, σ[Amp(RV)]	peak_to_peak_g_error, peak_to_peak_bp_error, peak_to_peak_rp_error, peak_to_peak_rv_error
$\phi_{21}(G)$	phi21_g
$\sigma[\phi_{21}(G)]$	phi21_g_error
$R_{21}(G)$	r21_g
$\sigma[R_{21}(G)]$	r21_g_error
$\phi_{31}(G)$	phi31_g
$\sigma[\phi_{31}(G)]$	phi31_g_error
R_{31}	r31_g
$\sigma[R_{31}(G)]$	r31_g_error
[Fe/H] [(b)]	metallicity
σ ([Fe/H])	metallicity_error
A(G) [(c)]	g_absorption
σ A(G)	g_absorption_error
$N_{obs}(G$ band)	num_clean_epochs_g
$N_{obs}(G_{BP}$ band)	num_clean_epochs_bp
$N_{obs}(G_{RP}$ band)	num_clean_epochs_rp
N_{obs}(RV)	num_clean_epochs_rv

Notes. Pulsation characteristics include period(s), epochs of maximum light and minimum radial velocity (E), peak-to-peak amplitudes, intensity-averaged mean magnitudes, mean radial velocity, $\phi_{21}, R_{21}, \phi_{31}, R_{31}$ Fourier parameters with related uncertainties. To facilitate access to the table, we also provide the correspondence between parameter [period(s), E, etc.] and the name of the parameter in the *Gaia* archive table. [(a)]E corresponds to the time of maximum in the light curve and the time of minimum in the RV curve. The BJD of all epochs is offset by JD 2455197.5 d (= J2010.0). [(b)]Photometric metal abundance derived from the period and the ϕ_{31} Fourier parameter of the G light curve of RR Lyrae stars (see Sects. 5.1 and 7). [(c)]Absorption in the G band computed from a relation that links the star intrinsic colour to the period and the amplitude of the G-band light variation of fundamental-mode RR Lyrae stars (see Sects. 5.3 and 7).

theoretical models by Marconi et al. (2015). The RR Lyrae stars nicely fall within the boundaries of the theoretical ISs shown in Fig. 29. The slight discrepancy at the red boundary of the IS between observed RR Lyrae position and the predicted edge might be due to the treatment of convection. As extensively discussed in Di Criscienzo et al. (2004), an increase in the mixing-length parameter from the adopted 1.5 value to 2.0 makes the predicted boundary bluer by about 300 K, which matches the observed stellar distribution far better. We also note that the errors of the SOS metallicity estimates of the few RR Lyrae stars with $(G_{BP} - G)$ colours higher than ~0.3 mag that fall outside the red boundaries of the $Z = 0.001$ and 0.02 ISs are larger than 0.46 and up to 1.5 dex.

7.3. Sky maps

Figure 30 shows the distribution on sky in galactic coordinates of the clean sample of 270 905 DR3 RR Lyrae stars, and Fig. 31 shows their PA, ϕ_{21} versus P and ϕ_{31} versus P diagrams. The two extended RR Lyrae overdensities in the bottom right quadrant of Fig. 30 trace the haloes of the Large and Small Magellanic Clouds. The stream of RR Lyrae stars that crosses the Galactic disc is the disrupting Sagittarius dSph galaxy that becomes visible just left below of the centre of the map. Other lower RR Lyrae overdensities can easily be recognised, for example the Sculptor dSph (with more than 500 RR Lyrae) close to the south Galactic pole, Ursa Minor and Draco dSphs in the upper north-west quadrant, the Sextans dSph in the upper north-east quadrant, and close to the north Galactic pole the concentration of more than 150 RR Lyrae stars of the M3 GC. About 1500 other RR Lyrae stars are concentrated in another 94 different GCs in the map.

The DR3 RR Lyrae clean catalogue contains 70 611 new RR Lyrae stars discovered by *Gaia*. They are mainly faint sources (see Fig. 27), and according to Fig. 32, they are mainly concentrated in high-reddening regions of the Galactic disc and bulge that were poorly sampled with the *Gaia* DR2 scanning law.

Figure 33 presents a map in galactic coordinates that is drawn from 133 559 RR Lyrae stars in the DR3 clean catalogue for which individual photometric metallicities ([Fe/H]) obtained with the SOS Cep&RRL pipeline (see Sect. 5.1) are published in the *Gaia* DR3 `vari_rrlyrae` table. We colour-coded the sources in the map according to their metallicity. The higher metallicity of the RR Lyrae stars in the MW bulge and disc compared to variables in the Galactic halo can easily be appreciated, and the lower metal abundance of the RR Lyrae stars in the SMC compared to the variables in the LMC is also clear. To ensure that the features in Fig. 33 are not an artefact due to measurement errors or to the adopted metallicity calibration (Nemec et al. 2013), we show in Fig. 34 only RR Lyrae stars with metallicity errors $\sigma_{[Fe/H]} \leq 0.46$ dex (the mean error of the SOS Cep&RRL metallicity estimates according to Fig. 19 in Sect. 5.1). The relative difference in metallicity of the RR Lyrae stars in the LMC, SMC, Galactic halo, and in the bulge and thin disc of our Galaxy is still rather clearly visible, and it would

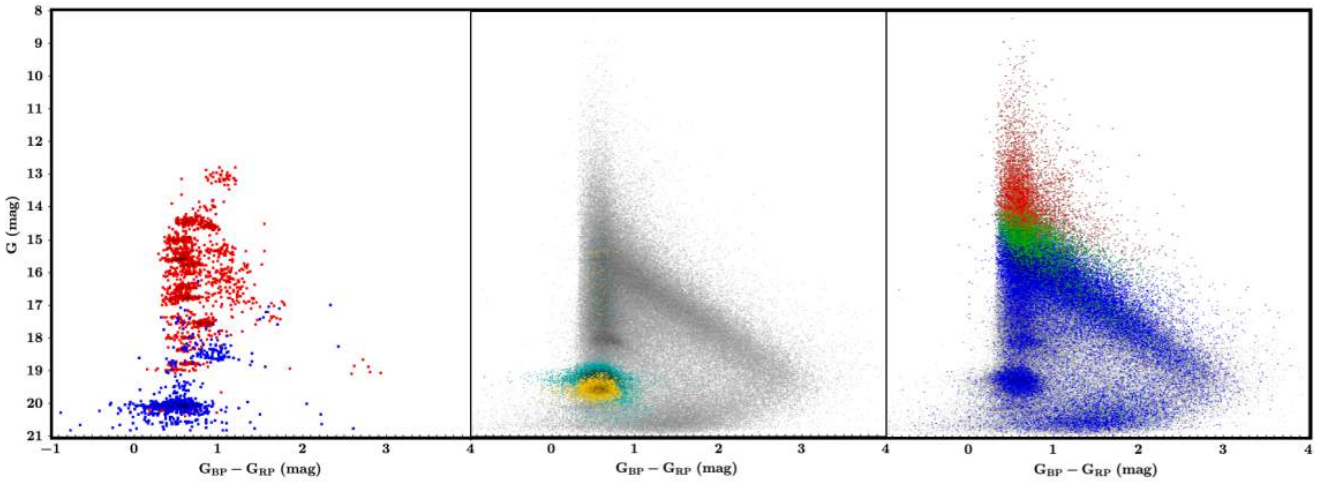

Fig. 28. CMDs in apparent G magnitude vs. $(G_{BP} - G_{RP})$ colour defined by RR Lyrae stars in the DR3 clean catalogue. Left panel: G and G_{BP}−G_{RP} CMD of RR Lyrae stars in the DR3 clean catalogue that lie in GCs (red points) and dSph galaxies (blue points), for which colour information is available (2558 out of 2790 sources). Each concentration of points corresponds to a different system. Middle panel: G and G_{BP}−G_{RP} CMD of the whole sample of RR Lyrae stars for which colour information is available, 215 116 sources (out of 270 905). Different colours show the variable stars in the LMC (26 468 sources; cyan symbols), SMC (4353 sources; yellow symbols), and all-sky (184 280 sources; grey symbols) regions as defined in Sect. 2. Right panel: lower panel same as in the middle panel, but blue, green, and red points mark RR Lyrae stars with $\sigma_{\varpi}/\varpi < 0.5$ (58 018 sources), <0.2 (13 377 sources), and <0.1 (4670 sources), respectively.

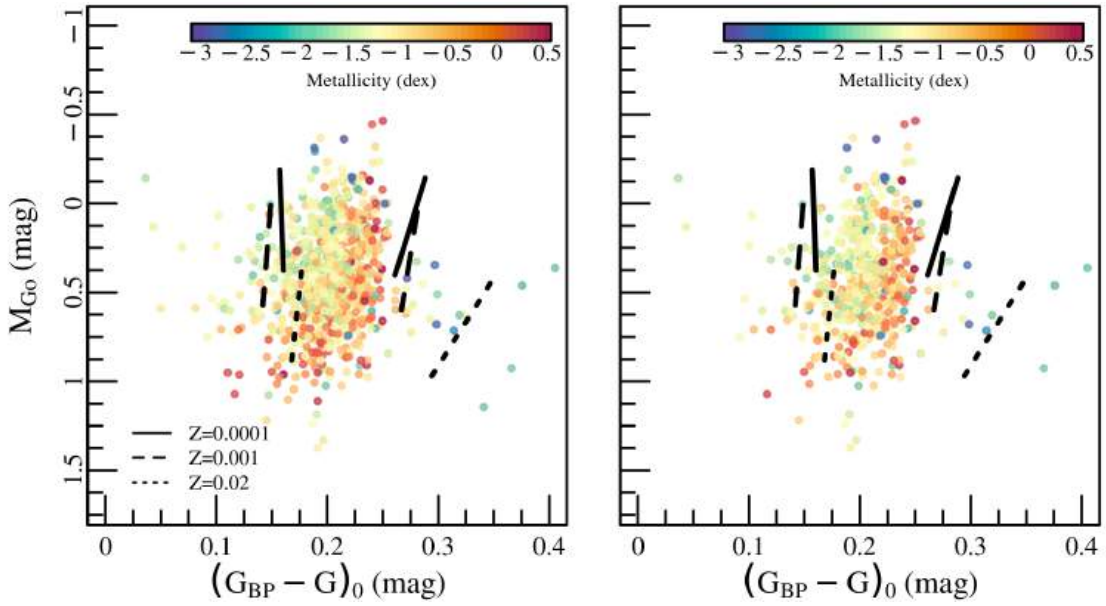

Fig. 29. HR diagram in G absolute magnitude (M_{G_0}) and dereddend $(G_{BP} - G)_0$ colour. Left panel: M_{G_0} $(G_{BP}$−$G)_0$ CMD of 915 DR3 RRab stars that have σ_{ϖ}/ϖ <0.1, RUWE < 1.4, and $A(G)$ <0.2; right panel: same as in the left panel, but for 620 RR Lyrae of the sample for which $A(G) < 0.1$. The sources are colour-coded according to their metallicity. The lines show the boundaries of theoretical ISs for RRab stars of three different chemical compositions ($Z = 0.0001$, solid lines; $Z = 0.001$, dashed lines; and $Z = 0.02$, dotted lines) from Marconi et al. (2015).

not change significantly if we were to adopt the Crestani et al. (2021) metallicity calibration, for instance. Figure 35 shows the PA diagram of the 133 559 RR Lyrae stars with a metallicity estimate. We again colour-coded the sources according to their metal abundance. The colour-coding highlights the difference in metallicity of the various sequences (Oosterhoff loci, Oosterhoff 1939) seen in the PA diagram, in particular the higher metallicity of short-period RRab and RRc stars compared to the lower metal abundance of long-period fundamental-mode and first-overtone RR Lyrae.

Finally, we show in Fig. 36 a map in galactic coordinates of 142 660 fundamental-mode RR Lyrae stars with absorption in the G-band computed with the SOS pipeline (see Sect. 5.3). The sources are colour-coded according to their individual $A(G)$ values. They neatly trace the high-extinction regions along the Galactic plane.

8. Conclusions and future developments

The factor two in statistics with respect to DR2, the better characterisation of the RR Lyrae stars and their pulsational and astrophysical parameters, along with the improved astrometry published with *Gaia* EDR3 (Gaia Collaboration 2021) make the SOS Cep&RRL DR3 sample the largest, most homogeneous, and

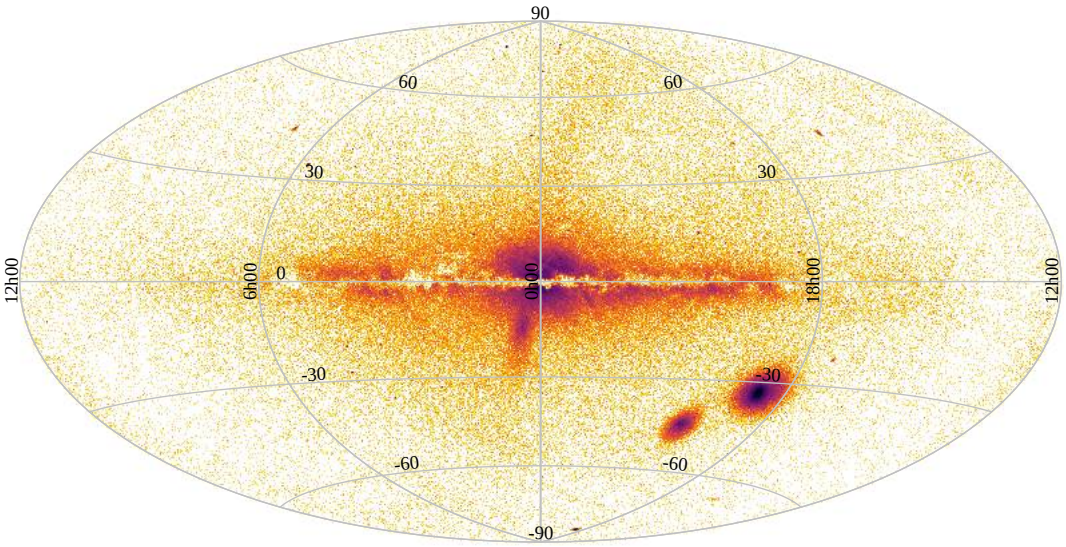

Fig. 30. Distribution on the sky of the clean sample of 270 905 DR3 RR Lyrae stars that were confirmed and characterised with the SOS Cep&RRL pipeline in galactic coordinates. The sample comprises 200,294 known RR Lyrae stars (Gold Sample) and 70,611 new discoveries by *Gaia*.

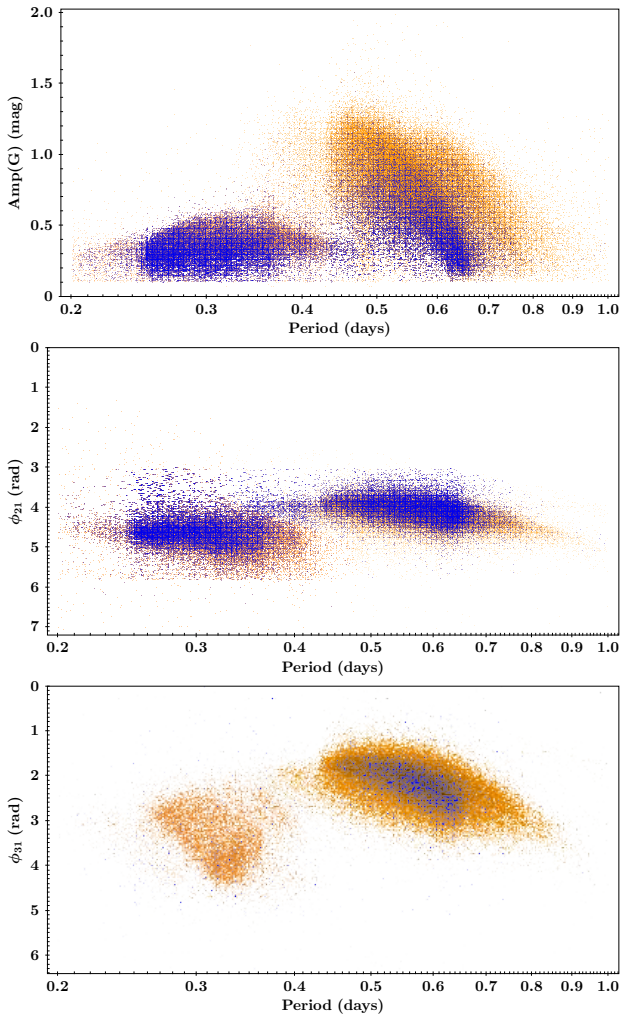

Fig. 31. PA (270 905 sources; top panel), ϕ_{21} vs. P (251 423 sources; centre panel) and ϕ_{31} vs. P (136 015 sources; bottom panel) diagrams of the RR Lyrae stars in the DR3 clean sample. New discoveries by *Gaia* are marked with blue dots; 70 611 are shown in the top panel, 70 447 in the central panel, and 5317 in the bottom panel.

parameter-richest catalogue of all-sky RR Lyrae stars published so far in the magnitude range from $\langle G \rangle = 7.64$ mag (the magnitude of RR Lyr itself; sourceid 2125982599343482624) and $\langle G \rangle = 21.14$ mag (the magnitude of star 658193189673442944, the faintest RR Lyrae in the catalogue). The DR3 RR Lyrae catalogue along with known RR Lyrae stars confirmed with the SOS pipeline, but for which the SOS periods differ from the literature periods (see Sect. 3.1), increases the census of RR Lyrae stars in our Galaxy and its close companions to about 370 000 within the limiting magnitude of *Gaia*

Gaia Data Release 4 (DR4) will be based on 66 months of data. It will therefore allow the SOS Cep&RRL pipeline to better determine the pulsation period(s) and characterise RR Lyrae stars and Cepheids more effectively. The pipeline is currently being redesigned and simplified, and a number of changes will be implemented to improve the processing in view of *Gaia* DR4. Some of these changes are briefly outlined below.

1. Tests are in progress how the algorithm can be improved for the period determination (currently the Lomb-Scargle method, see Sect. 2) so that the number of spurious period detections is reduced, particularly when several peaks of similar power are present in the power spectrum of the sources.
2. The number of harmonics for modelling the light curves of RRc stars with a well-sampled light/RV curve will be increased to more than two to increase the number of RR Lyrae stars for which the ϕ_{31} Fourier parameter is available.
3. The skewness of the light curve and the time of rise to maximum light (ϕ-rise time) will be adopted in addition to the position in the PA diagram to distinguish RRab from RRc stars, particularly in the short-period regime ($P < 0.4$ d).
4. Luminosity-metallicity (LZ) and PW and PW-metallicity (PWZ) relations in the *Gaia* bands, calibrated on *Gaia* parallaxes (e.g. those published by Garofalo et al. 2022) will be adopted in the pipeline to classify RR Lyrae stars with reliable parallax values.
5. CMDs in absolute magnitude, colour-colour diagrams, and the comparison with theoretical instability strips will be used to improve the source classification, the derivation of

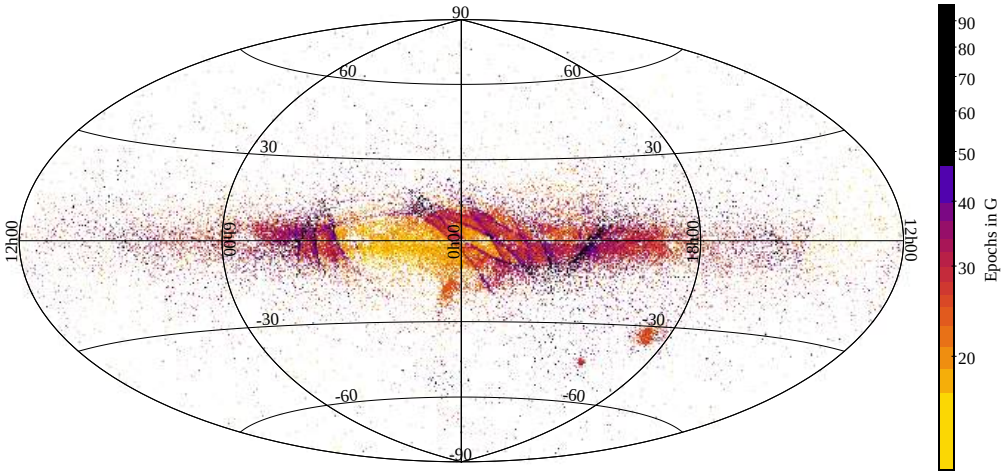

Fig. 32. Distribution on the sky of 70 611 DR3 RR Lyrae stars that are new discoveries by *Gaia* in galactic coordinates. The sources are colour-coded according to the number of epochs in the *G*-band light curves as encoded in the colour scale on the right.

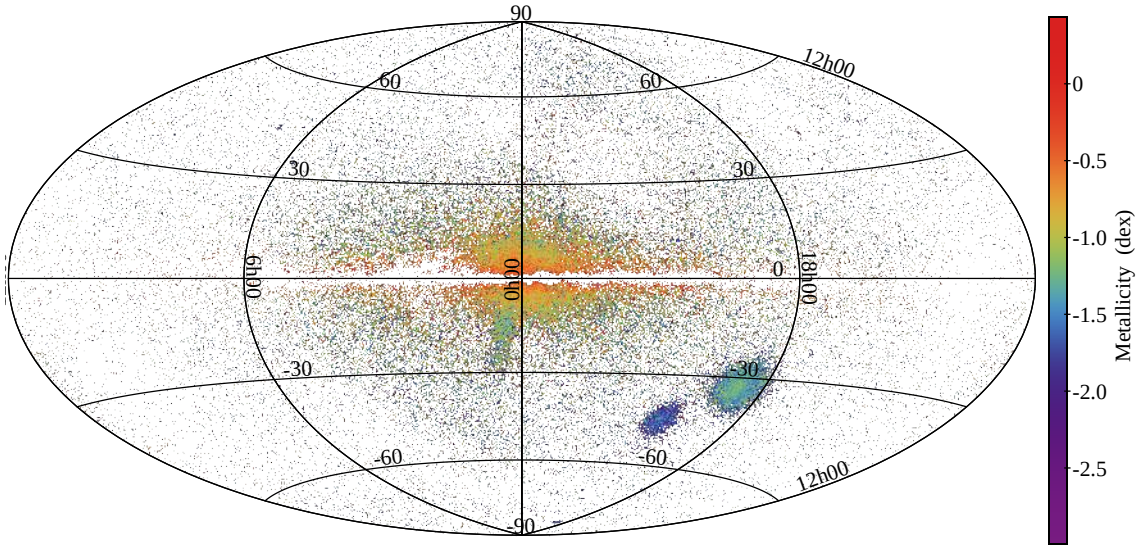

Fig. 33. Map in galactic coordinates of 133 559 RR Lyrae stars in the DR3 clean catalogue for which individual photometric metallicity estimates obtained with the SOS pipeline are published in the *Gaia* DR3 `vari_rrlyrae` table. The sources are colour-coded according to their metallicity ([Fe/H]) as encoded in the colour scale on the right.

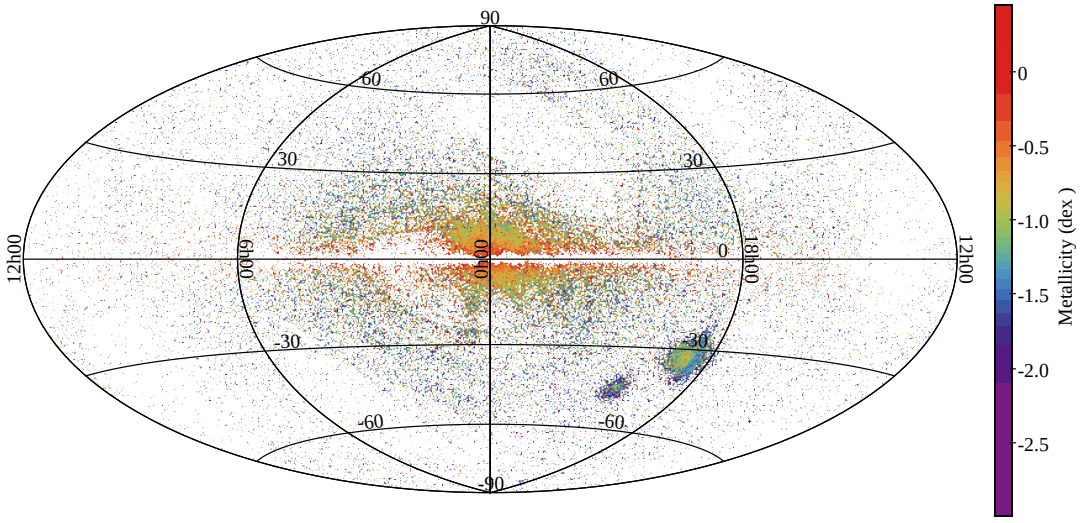

Fig. 34. Same as in Fig. 33, but showing only 88 440 RR Lyrae stars with an error in metallicity $\sigma_{[Fe/H]} \leq 0.46$ dex.

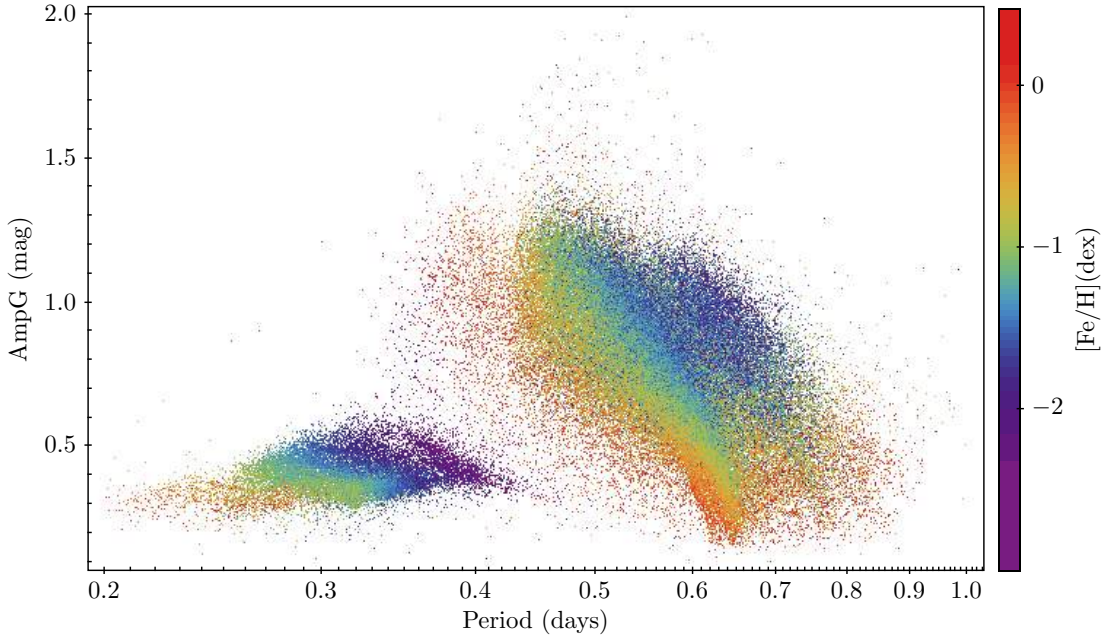

Fig. 35. PA diagram of the 133 559 RR Lyrae stars with a metallicity estimate. The sources are colour-coded according to their metal abundance ([Fe/H]) as encoded in the colour scale on the right.

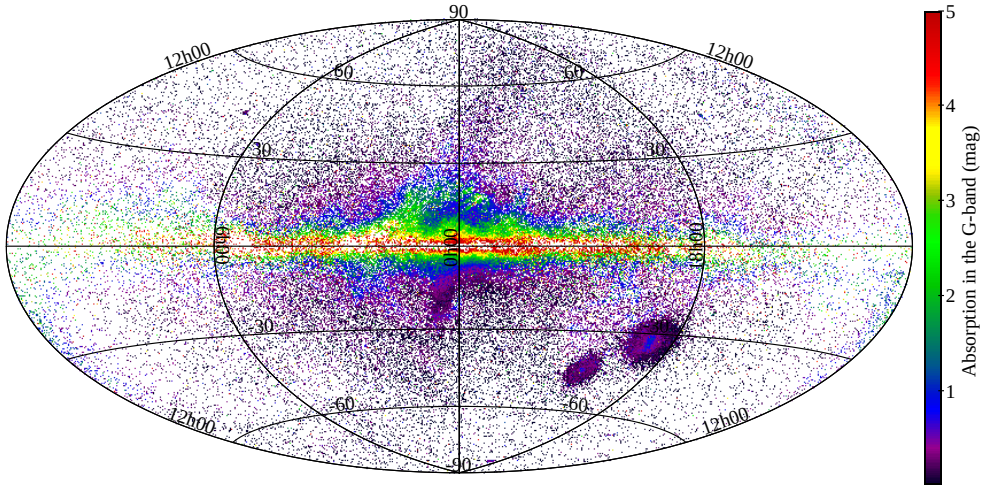

Fig. 36. Map in galactic coordinates of 142 660 RRab stars with individual G absorption values estimated with the SOS pipeline. The sources are colour-coded according to their $A(G)$ values as encoded in the colour scale on the right.

intrinsic parameters (e.g. effective temperatures), and the removal of contaminants.

6. We will test different calibrations of the relations that are used to estimate photometric metallicities from the ϕ_{31} Fourier parameter and the pulsation period of RR Lyrae stars, and we hope to derive new [Fe/H] – ϕ_{31} – P relations that are directly calibrated on the *Gaia* data using a sample of RR Lyrae stars with metallicity determinations from high-resolution spectra covering the whole parameter space spanned by these variable stars.
7. We will revise the computation of errors in metallicity because they may currently be overestimated.
8. Test will be made to derive astrophysical parameters (metallicities, gravities, and $T_{\rm eff}$ values) to best select the template spectra for the cross-correlation to measure radial velocities of RR Lyrae stars. The time series of BP/RP spectra will also be used.

To conclude, the SOS Cep&RRL clean catalogue of 270 905 RR Lyrae stars published with *Gaia* DR3 already represents a significant step forward in the construction of a complete, homogeneous, and parameter-rich catalogue of all-sky RR Lyrae stars within the limiting magnitude of *Gaia.* This has been lacking so far. We anticipate that this RR Lyrae catalogue will be consolidated and further improved with *Gaia* DR4.

Acknowledgements. This work has made use of data from the ESA space mission *Gaia*, processed by the *Gaia* Data Processing and Analysis Consortium (DPAC). Funding for the DPAC has been provided by national institutions participating in the *Gaia* Multilateral Agreement. In particular, the Italian participation in DPAC has been supported by Istituto Nazionale di Astrofisica (INAF) and the Agenzia Spaziale Italiana (ASI) through grants I/037/08/0, I/058/10/0, 2014-025-R.0, 2014-025-R.1.2015 and 2018-24-HH.0 to INAF (PI M. G. Lattanzi), the Swiss participation by the Swiss State Secretariat for Education, Research and Innovation through the "Activités Nationales Complémentaires". The work was supported in part by the French Centre National de la Recherche Scientifique (CNRS), the Centre National d'Etudes Spatiales (CNES), the Institut

des Sciences de l'Univers (INSU) through the Service National d'Observation (SNO) *Gaia*. UK community participation in this work has been supported by funding from the UK Space Agency, and from the UK Science and Technology Research Council. RA has been funded by the DLR (German space agency) via grants 50QG0602, 50QG1001, 50QG1403, and 50QG201. The *Gaia* mission website is: http://www.cosmos.esa.int/gaia. This research has made use of the SIMBAD database, operated at CDS, Strasbourg, France. We warmly thank O. Creevey, A. Recio-Blanco and M. Fouesneau for advises on the use of products from the GSP_Spec and GSP_Phot modules of the Apsis pipeline, D. Harrison for running the SEAPipe pipeline on the catalogue of RR Lyrae stars produced by the SOS Cep&RRL pipeline and P. Montegriffo for the development and maintenance of the GRATIS software. In this study we have largely made use of TOPCAT (Taylor 2005).

References

Andrae, R., Fouesneau, M., Sordo, R., et al. 2023, A&A, 674, A27 (*Gaia* DR3 SI)
Arellano Ferro, A., Figuera Jaimes, R., Giridhar, S., et al. 2011, MNRAS, 416, 2265
Arellano Ferro, A., Bramich, D. M., Giridhar, S., et al. 2013, Acta Astron., 63, 429
Arellano Ferro, A., Ahumada, J. A., Calderón, J. H., & Kains, N. 2014, Rev. Mex. Astron. Astrofis., 50, 307
Baranne, A., Mayor, M., & Poncet, J. L. 1979, Vistas Astron., 23, 279
Barnes Thomas, G. I., Moffett, T. J., Hawley, S. L., Slovak, M. H., & Frueh, M. L. 1988, ApJS, 67, 403
Bellazzini, M., Ferraro, F. R., Origlia, L., et al. 2002, AJ, 124, 3222
Benkő, J. M., Bakos, G. Á., & Nuspl, J. 2006, MNRAS, 372, 1657
Bersier, D., & Wood, P. R. 2002, AJ, 123, 840
Bhardwaj, A., Rejkuba, M., de Grijs, R., et al. 2021, ApJ, 909, 200
Blažko, S. 1907, Astron. Nachr., 175, 325
Bono, G., Iannicola, G., Braga, V. F., et al. 2019, ApJ, 870, 115
Borissova, J., Minniti, D., Rejkuba, M., & Alves, D. 2006, A&A, 460, 459
Braga, V. F., Stetson, P. B., Bono, G., et al. 2018, AJ, 155, 137
Cacciari, C., & Clementini, G. 2003, in Stellar Candles for the Extragalactic Distance Scale, eds. D. Alloin, & W. Gieren, 635, 105
Cacciari, C., Clementini, G., Prevot, L., et al. 1987, A&AS, 69, 135
Cacciari, C., Clementini, G., & Buser, R. 1989a, A&A, 209, 154
Cacciari, C., Clementini, G., Prevot, L., & Buser, R. 1989b, A&A, 209, 141
Cacciari, C., Clementini, G., & Fernley, J. A. 1992, ApJ, 396, 219
Carnerero, M. I., Raiteri, C. M., Rimoldini, L. et al. 2023, A&A, 674, A24 (*Gaia* DR3 SI)
Catelan, M., & Smith, H. A. 2015, Pulsating Stars (Wiley-VCH)
Chen, X., Wang, S., Deng, L., et al. 2020, VizieR Online Data Catalog: J/ApJS/249/18
Clement, C. M., Muzzin, A., Dufton, Q., et al. 2001, AJ, 122, 2587
Clementini, G., Cacciari, C., & Lindgren, H. 1990, A&AS, 85, 865
Clementini, G., Merighi, R., Pasquini, L., Cacciari, C., & Gouiffes, C. 1994, MNRAS, 267, 83
Clementini, G., Carretta, E., Gratton, R., et al. 1995, AJ, 110, 2319
Clementini, G., Cignoni, M., Contreras Ramos, R., et al. 2012, ApJ, 756, 108
Clementini, G., Di Tomaso, S., Di Fabrizio, L., et al. 2000, AJ, 120, 2054
Clementini, G., Gratton, R., Bragaglia, A., et al. 2003, AJ, 125, 1309
Clementini, G., Ripepi, V., Leccia, S., et al. 2016, A&A, 595, A133
Clementini, G., Ripepi, V., Molinaro, R., et al. 2019, A&A, 622, A60
Contreras, R., Catelan, M., Smith, H. A., et al. 2010, AJ, 140, 1766
Contreras Ramos, R., Minniti, D., Gran, F., et al. 2018, ApJ, 863, 79
Coppola, G., Marconi, M., Stetson, P. B., et al. 2015, ApJ, 814, 71
Corwin, T. M., Borissova, J., Stetson, P. B., et al. 2008, AJ, 135, 1459
Creevey, O. L., Sordo, R., Pailler, F., et al. 2023, A&A, 674, A26 (*Gaia* DR3 SI)
Crestani, J., Braga, V. F., Fabrizio, M., et al. 2021, ApJ, 914, 10
Cropper, M., Katz, D., Sartoretti, P., et al. 2018, A&A, 616, A5
Cuffey, J. 1966, AJ, 71, 514
Dékány, I., Hajdu, G., Grebel, E. K., et al. 2018, ApJ, 857, 54
Di Criscienzo, M., Marconi, M., & Caputo, F. 2004, ApJ, 612, 1092
Di Fabrizio, L., Clementini, G., Maio, M., et al. 2005, A&A, 430, 603
Drake, A. J., Catelan, M., Djorgovski, S. G., et al. 2013, ApJ, 763, 32
Drake, A. J., Graham, M. J., Djorgovski, S. G., et al. 2014, ApJS, 213, 9
Drake, A. J., Djorgovski, S. G., Catelan, M., et al. 2017, MNRAS, 469, 3688
Eyer, L., Mowlavi, N., Evans, D. W., et al. 2017, ArXiv eprints [arXiv:1702.03295]
Eyer, L., Audard, M., Holl, B., et al. 2023, A&A, 674, A13 (*Gaia* DR3 SI)
Fernley, J. A., Lynas-Gray, A. E., Skillen, I., et al. 1989, MNRAS, 236, 447
Fernley, J., Barnes, T. G., Skillen, I., et al. 1998, A&A, 330, 515
Gaia Collaboration (Brown, A. G. A., et al.) 2016, A&A, 595, A2
Gaia Collaboration (Clementini, G., et al.) 2017, A&A, 605, A79
Gaia Collaboration (Brown, A. G. A., et al.) 2018, A&A, 616, A1
Gaia Collaboration (Eyer, L., et al.) 2019, A&A, 623, A110
Gaia Collaboration (Brown, A. G. A., et al.) 2021, A&A, 649, A1
Gaia Collaboration (Vallenari, A. et al.) 2023, A&A, 674, A1 (*Gaia* DR3 SI)
Garofalo, A., Cusano, F., Clementini, G., et al. 2013, ApJ, 767, 62
Garofalo, A., Delgado, H. E., Sarro, L. M., et al. 2022, MNRAS, 513, 788
Gavras, P., Rimoldini, L., Nienartowicz, K., et al. 2023, A&A, 674, A22 (*Gaia* DR3 SI)
Gieren, W. P., Barnes, Thomas G., & I., & Moffett, T. J., 1989, ApJ, 342, 467
Gillet, D., & Crowe, R. A. 1988, A&A, 199, 242
Gillet, D., & Fokin, A. B. 2014, A&A, 565, A73
Gomel, R., Mazeh, T., Faigler, S., et al. 2023, A&A, 674, A19 (*Gaia* DR3 SI)
Goranskij, V. P. 1976, Peremennye Zvezdy Prilozhenie, 3, 1
Gratton, R. G., Bragaglia, A., Clementini, G., et al. 2004, A&A, 421, 937
Harrison, D. L. 2011, Exp. Astron., 31, 157
Holl, B., Fabricius, C., Portell, J., et al. 2023, A&A, 674, A25 (*Gaia* DR3 SI)
Iorio, G., & Belokurov, V. 2021, MNRAS, 502, 5686
Jayasinghe, T., Stanek, K. Z., Kochanek, C. S., et al. 2019, MNRAS, 485, 961
Jones, R. V., Carney, B. W., Latham, D. W., & Kurucz, R. L. 1987, ApJ, 314, 605
Jones, R. V., Carney, B. W., & Latham, D. W. 1988, ApJ, 332, 206
Jones, R. V., Carney, B. W., Storm, J., & Latham, D. W. 1992, ApJ, 386, 646
Jurcsik, J., & Kovacs, G. 1996, A&A, 312, 111
Kaluzny, J., Krzeminski, W., & Nalezyty, M. 1997, A&AS, 125, 337
Katz, D., Sartoretti, P., Guerrier, A., et al. 2023, A&A, 674, A5 (*Gaia* DR3 SI)
Kervella, P., Gallenne, A., Remage Evans, N., et al. 2019, A&A, 623, A116
Kunder, A., Popowski, P., Cook, K. H., & Chaboyer, B. 2008, AJ, 135, 631
Lambert, D. L., Heath, J. E., Lemke, M., & Drake, J. 1996, ApJS, 103, 183
Layden, A. C., & Sarajedini, A. 2003, AJ, 125, 208
Levenberg, K. 1944, Quart. Appl. Math., 2, 164
Liu, T., & Janes, K. A. 1989, ApJS, 69, 593
Liu, T., & Janes, K. A. 1990, ApJ, 360, 561
Lomb, N. R. 1976, Ap&SS, 39, 447
Marconi, M., Coppola, G., Bono, G., et al. 2015, ApJ, 808, 50
Marquardt, D. W. 1963, J. Soc. Indust. Appl. Math., 11, 431
Martínez-Vázquez, C. E., Stetson, P. B., Monelli, M., et al. 2016, MNRAS, 462, 4349
Martínez-Vázquez, C. E., Vivas, A. K., Gurevich, M., et al. 2019, MNRAS, 490, 2183
Meylan, G., Burki, G., Rufener, F., et al. 1986, A&AS, 64, 25
Molnár, L., Plachy, E., Juhász, Á. L., & Rimoldini, L. 2018, A&A, 620, A127
Montegriffo, P., De Angeli, F., Andrae, R., et al. 2023, A&A, 674, A3 (*Gaia* DR3 SI)
Mowlavi, N., Holl, B., Lecœur-Taïbi, I. et al. 2023, A&A, 674, A16 (*Gaia* DR3 SI)
Mullen, J. P., Marengo, M., Martínez-Vázquez, C. E., et al. 2021, ApJ, 912, 144
Muraveva, T., Delgado, H. E., Clementini, G., Sarro, L. M., & Garofalo, A. 2018, MNRAS, 481, 1195
Muraveva, T., Clementini, G., Garofalo, A., & Cusano, F. 2020, MNRAS, 499, 4040
Nemec, J. M., Wehlau, A., & Mendes de Oliveira, C. 1988, AJ, 96, 528
Nemec, J. M., Cohen, J. G., Ripepi, V., et al. 2013, ApJ, 773, 181
Oosterhoff, P. T. 1939, The Observatory, 62, 104
Osuna, P., Ortiz, I., Lusted, J., et al. 2008, IVOA Astronomical Data Query Language Version 2.00, IVOA Recommendation 30 October 2008
Palaversa, L., Ivezić, Ž., Eyer, L., et al. 2013, AJ, 146, 101
Pancino, E., Britavskiy, N., Romano, D., et al. 2015, MNRAS, 447, 2404
Piersimoni, A. M., Bono, G., & Ripepi, V. 2002, AJ, 124, 1528
Pigulski, A., Pojmański, G., Pilecki, B., & Szczygieł, D. M. 2009, Acta Astron., 59, 33
Pojmanski, G. 2000, Acta Astron., 50, 177
Pojmanski, G. 2002, Acta Astron., 52, 397
Recio-Blanco, A., de Laverny, P., Palicio, P. A., et al. 2023, A&A, 674, A29 (*Gaia* DR3 SI)
Riello, M., De Angeli, F., Evans, D. W., et al. 2021, A&A, 649, A3
Rimoldini, L., Eyer, L., Audard, M., et al. 2022, Gaia DR3 documentation Chapter 10: Variability, Gaia DR3 documentation, European Space Agency; Gaia Data Processing and Analysis Consortium, Online at https://gea.esac.esa.int/archive/documentation/GDR3/index.html
Rimoldini, L., Holl, B., Gavras, P., et al. 2023, A&A, 674, A14 (*Gaia* DR3 SI)
Ripepi, V., Barone, F., Milano, L., & Russo, G. 1997, A&A, 318, 797
Ripepi, V., Clementini, G., Molinaro, R., et al. 2023, A&A, 674, A17 (*Gaia* DR3 SI)
Salinas, R., Contreras Ramos, R., Strader, J., et al. 2016, AJ, 152, 55
Samus', N. N., Kazarovets, E. V., Durlevich, O. V., Kireeva, N. N., & Pastukhova, E. N. 2017, Astron. Rep., 61, 80
Sartoretti, P., Katz, D., Cropper, M., et al. 2018, A&A, 616, A6
Sartoretti, P., Blomme, R., David, M., & Seabroke, G. 2022, Gaia DR3 documentation, Chapter 6: Spectroscopy, Online at https://gea.esac.esa.int/archive/documentation/GDR3/Data_processing/chap_cu6spe/

Scargle, J. D. 1982, ApJ, 263, 835
Sesar, B., Ivezić, Ž., Stuart, J. S., et al. 2013, AJ, 146, 21
Sesar, B., Banholzer, S. R., Cohen, J. G., et al. 2014, ApJ, 793, 135
Sesar, B., Hernitschek, N., Mitrović, S., et al. 2017, AJ, 153, 204
Siegel, M. H., & Majewski, S. R. 2000, AJ, 120, 284
Skillen, I., Fernley, J. A., Jameson, R. F., Lynas-Gray, A. E., & Longmore, A. J. 1989, MNRAS, 241, 281
Skillen, I., Fernley, J. A., Stobie, R. S., & Jameson, R. F. 1993, MNRAS, 265, 301
Smith, H. A. 1995, RR Lyrae Stars (Cambridge, UK: Cambridge University Press), Cambridge Astrophys. Ser., 27
Soszyński, I., Udalski, A., Szymański, M. K., et al. 2014, Acta Astron., 64, 177
Soszyński, I., Udalski, A., Szymański, M. K., et al. 2019, Acta Astron., 69, 87
Stetson, P. B., Fiorentino, G., Bono, G., et al. 2014, PASP, 126, 616
Taylor, M. B. 2005, in Astronomical Data Analysis Software and Systems XIV, eds. P. Shopbell, M. Britton & R. Ebert, ASP Conf. Ser., 347, 29
Torrealba, G., Catelan, M., Drake, A. J., et al. 2015, MNRAS, 446, 2251
Vivas, A. K., Alonso-García, J., Mateo, M., Walker, A., & Howard, B. 2019, AJ, 157, 35
Vivas, A. K., Martínez-Vázquez, C., & Walker, A. R. 2020, ApJS, 247, 35
Walker, A. R. 1998, AJ, 116, 220
Walker, A. R., & Nemec, J. M. 1996, AJ, 112, 2026
Wenger, M., Ochsenbein, F., Egret, D., et al. 2000, A&AS, 143, 9

Appendix A: RVS radial velocities

A.1. Tables with the source-level parameters of 51 Cepheids and 45 RR Lyrae stars for which this information is lacking in the `gaia_source` table of the *Gaia* DR3 archive.

Table A.1. Source-level information for 51 Cepheids for which the all-epoch-combined RV was deemed of insufficient quality.

Gaia sourceid	rv_template_teff	rv_template_logg	rv_template_feh	rv_atm_param_origin	grvs_mag	grvs_mag_error	radvelinvalidreason
5351161399793209984	5 000	1.5	0.25	222	6.281	0.043	D
5329352998951582976	6 000	1	−0.25	222	6.492	0.056	D
5355057622307185280	5 500	3.5	0	333	6.607	0.038	D
5338036117182452096	6 250	2	0.25	222	6.815	0.070	D
473043922712140928	5 500	4.5	0	333	6.834	0.047	D

Notes. `radVelInvalidReason` provides the reason why the source-level parameters are excluded from publication. D: Double-lined detected in more than 10% of the epochs; P: variations in the spectral-sample flux from epoch to epoch; H: hot star; CF: poor cross-correlation-function; T: potential template mismatch; E=the error of the all-epochs combined radial velocity is larger than 40 km s^{-1} (see Sartoretti et al. 2022, Chap. 6, for details). This table is available in its entirety at the CDS.

Table A.2. Same as in table A.1, but for 45 RR Lyrae stars.

Gaia sourceid	rv_template_teff	rv_template_logg	rv_template_feh	rv_atm_param_origin	grvs_mag	grvs_mag_error	radvelinvalidreason
2857456211775108480	6 500	3	0	222	9.076	0.127	D
2142052889490819328	6 250	3	−0.5	444	9.324	0.083	T
2341083636832476 16	6 500	3	−0.25	555	9.411	0.091	D
6686289122295812736	6 250	3.5	−0.5	444	9.534	0.051	D
1858568795812429056	6 000	3	−0.5	444	10.242	0.059	D

Notes. This table is available in its entirety at the CDS.

Table A.3. Information for 19 RR Lyrae stars with high accuracy RV curves available in the literature.

Source_id	Name	Mode	Period days	$\langle G \rangle$ mag	N_{RVS}	Amp(RV) km s^{-1}	$\gamma_{(RVS+Lit.)}$ km s^{-1}	$\gamma_{Lit.}$ km s^{-1}	[Fe/H]$_{Lit.}$ dex	$\langle T_{eff} \rangle_{Lit.}$ K	$\langle logg \rangle_{Lit.}$ km s^{-1}	Ref1	Ref2	Notes	Ins.
(1)	(2)	(3)	(4)	(5)	(6)	(7)	(8)	(9)	(10)	(11)	(12)	(13)	(14)	(15)	(16)
1286188056265485952	RS Boo	RRab	0.3773523	10.34	28	67.38	−3.96 (2.57)	−3.7	−0.50	6 795	3.261$^{(a,b)}$	8	8	Blaz.	b
1492230556717187456	TV Boo	RRc	0.312551	10.91	34	27.07	−102.44 (5.00)	−104.0	−2.20±0.15	7 057	2.90	1	1	-	b
6884361748289023488	YZ Cap	RRc	0.2734508	11.22	27	26.19	−106.91 (2.29)	−106.5 ± 1.6	−1.25	7 280±100	3.00±0.10	2	10	-	a
2558296724402139392	RR Cet	RRab	0.5530296	9.61	30	62.79	−74.42 (2.50)	−74.6/−75.1	−1.25±0.10	6 434	2.71	1,6	1	-	b
2414817603803476864	UU Cet	RRab	0.6060755	11.94	21	55.71	−113.88 (3.10)	−114.4	−0.87	6 290	2.75$^{(c,b)}$	3	13	-	a
3546458301374134528	W Crt	RRab	0.4120288	11.45	31	75.76	59.87 (3.64)	58.8	−0.70	6 715	2.70$^{(c)}$	4	4	-	c
1760981190300823808	DX Del	RRab	0.4726188	9.81	26	55.48	−55.15 (2.80)	−55.1	−0.25	6 512	2.7±0.2$^{(d,b)}$	5,6	12	-	d,a
1058066262817534336	SU Dra	RRab	0.6604232	9.68	13	60.63	−167.08 (1.87)	−166.9	−1.60±0.20	6 433	2.72	1	1	-	b
1683444631038133248	SW Dra	RRab	0.5696720	10.38	20	62.04	−29.13 (2.57)	−29.8	−0.80/−1.40	6 380±50^{e}	2.78±0.10	2,7	11,8	-	a,b
2981136563934324224	RX Eri	RRab	0.5872470	9.56	26	67.15	67.72 (3.89)	66.4	−1.40±0.20	6 326	2.67	1	1	-	b
5117708899055276416	SS For	RRab	0.49544999	10.10	28	62.81	−109.93 (4.92)	−111.7	−1.50	6 710±50	2.85±0.10	2	11	Blaz.	a
4596935593202765184	TW Her	RRab	0.3996157	11.22	27	72.90	−3.31 (2.66)	−4.5	−0.50	6 770	3.424$^{(a,b)}$	8	8	-	b
6483680332235888896	V Ind	RRab	0.4796017	9.86	12	52.83	202.71 (1.74)	202.5	−1.51	-	-	3	-	-	a
1793460115244988800	AV Peg	RRab	0.3903809	10.39	16	65.68	−58.22 (1.70)	−58.7	0.00±0.10	6 603	2.99	1	1	-	b
6526559499016401408	RV Phe	RRab	0.5963778	11.81	37	59.72	99.72 (6.65)	99.1	−1.50	6 370±50/6 290	2.76±0.10	2	10,13	Blaz.?	a
6771307454464848768	V440 Sgr$^{(f)}$	RRab	0.4774854	10.23	10	76.61	−60.92 (2.95)	−61.6	−1.40	6 810±50	2.87±0.10	2	10	-	a
4709830423483623808	W Tuc	RRab	0.6422386	11.34	18	69.22	64.69 (1.90)	64.60	−1.35	6 440	2.75$^{(c,b)}$	3	13	-	a
3698725337376560512	UU Vir	RRab	0.4756085	10.52	14	72.32	−7.80 (2.07)	−8.2/−7.1	−0.40±0.10/−0.7	6 520/6 570	2.84/3.279$^{(a,b)}$	1,5,8	1,8	Bin.?	b
6045485228725626752	M4-V32$^{(g)}$	RRab	0.5791070	12.90	34	63.50	67.93 (5.31)	66.4	−1.3 ± 0.2	6 324	2.67	9	9	-	b

Notes. Meaning of the different columns is as follows: (1) Gaia DR3 source id; (2) Literature Name; (3) Pulsation mode (RRab=Fundamental; RRc= First Overtone); (4) Pulsation period (P), as re-evaluated in the present analysis; (5) Intensity-averaged G-band mean magnitude, as derived from the SOS Cep&RRL pipeline; (6) number of valid RVS RV measurements; (7) Peak-to-peak amplitude of the combined RVS and literature RV data. The RVS measurements of TV Boo and M4-V32 were shifted by +5km s^{-1}, those of TW Her and UU Vir by −4 km/s, and those of AV Peg by −3 km/s to better match the corresponding literature data; (8) Centre of mass RV (γ) of the curve obtained by combining RVS and literature RV data, with in parentheses the rms scatter of the modelled RV curve; (9) Literature values for γ; (10) Iron abundance; (11) Mean effective temperature; (12) Mean gravity; (13) References for the literature RV; (14) References for the stellar parameters; (15) Notes: Binary (Bin) and/or Blazhko (Blaz.).; (16) Instrument type: a=CORAVEL; b=spectra; c=image-tube spectrograph; d=photoelectric RV meter. The meaning of the numbers in columns (13) and (14) is as follows: 1=Liu & Janes (1989); 2=Cacciari et al. (1987); 3=Clementini et al. (1990); 4=Skillen et al. (1993); 5=Barnes et al. (1988); 6=Meylan et al. (1986); 7=Jones et al. (1987); 8=Jones et al. (1988); 9=Liu & Janes (1990); 10=Cacciari et al. (1989a); 11=Cacciari et al. (1989b); 12=Skillen et al. (1989); 13=Cacciari et al. (1992); The binarity information is taken from Kervella et al. (2019). ^{a}Gravity value at ϕ=0.0. ^{b}Cacciari et al. (1992) derived a mean gravity of 2.83±0.11 dex by averaging the gravity values inferred from the radii and masses published by Jones et al. (1992), which were derived from the B-W analysis of 18 RRab and 2 RRc stars. This mean gravity value can be used in place of $^{(a)}$, $^{(c)}$ and $^{(d)}$ or when a $\langle logg \rangle$ value is missing. ^{c}Constant gravity value adopted in Cacciari et al. (1992) B-W analysis of UU Cet, RV Phe and W Tuc, and in Skillen et al. (1993) analysis of W Crt. ^{d}2.7±0.2 is the 'static' gravity, that is the gravity of an RR Lyrae star were it not pulsating (Fernley et al. 1989). $^{e}\langle T_{eff} \rangle$=6460 K estimated from the $V-K$ colour by (Jones et al. 1988) . ^{f}The period derived by the SOS pipeline for this star (P_{SOS}=0.428933547 d) is incorrect, we provide in the table the correct period (P=0.4774854 d). The $\langle G \rangle$, Amp(RV) and γ_{RVS} values of V440 Sgr listed in the table were computed using the correct period. ^{g} Two RV measurements from *Gaia* RVS around the curve maximum are outliers with large errors. They were discarded when computing the Amp(RV) and γ values in columns (7) and (8).

A.2. Comparison of literature and *Gaia* RV curves for 13 of the 19 RR Lyrae stars for which high-accuracy RVs are available (see Sect. 4.3).

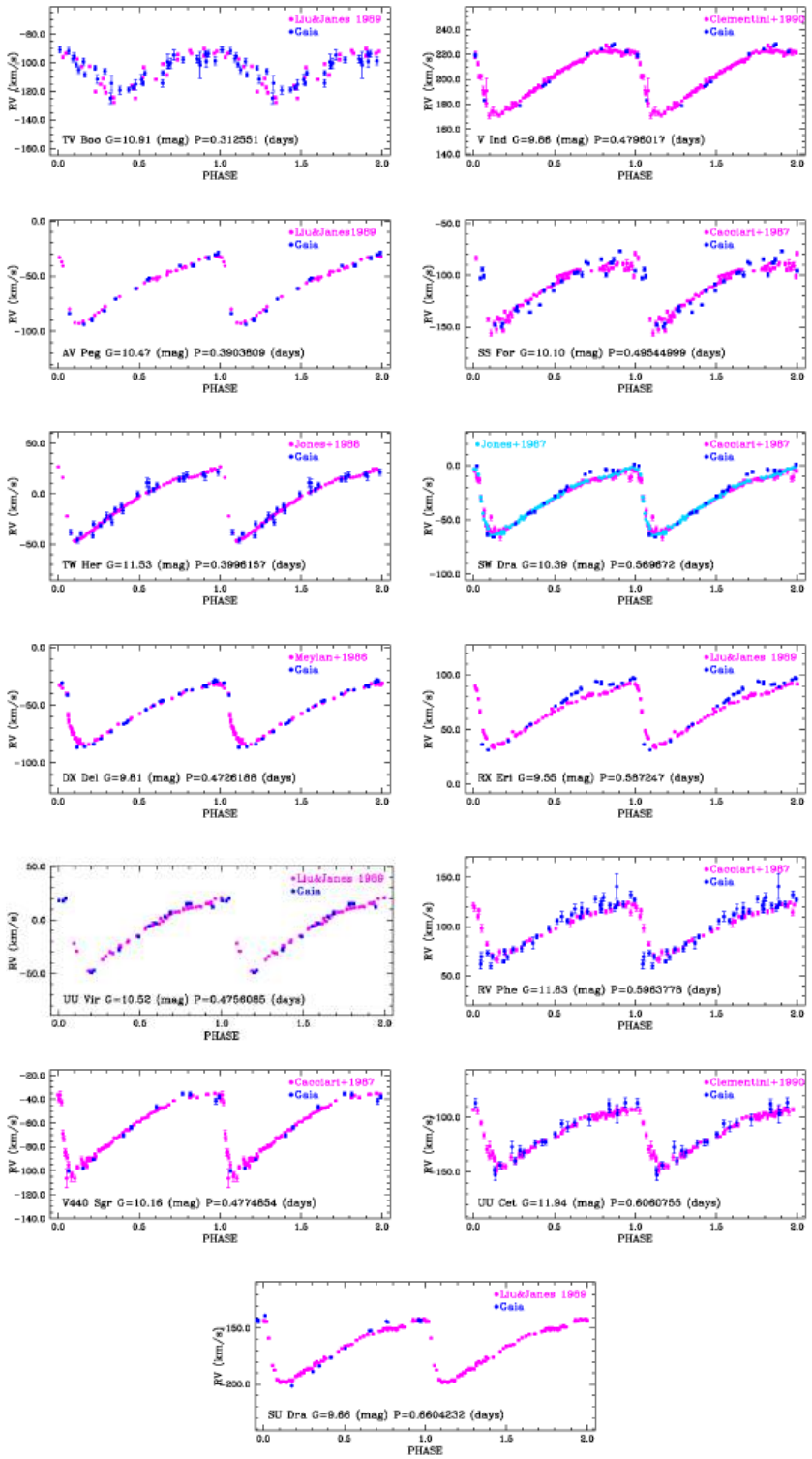

Fig. A.1. Same as in Fig. 18 for the remaining 13 RR Lyrae stars in the sample of 19 sources discussed in Sect. 4.3. The Gaia RV curves of TW Her and UU Vir were shifted by −4 km/s, the curve of TV Boo was shifted by +5 km/s, and the curve of AV Peg was shifted by −3 km/s to better match the literature RV curves.

A.3. Atlas of the light curves and RV curves for the RR Lyrae stars with RVS time-series data published in DR3.

We show G, G_{BP}, and G_{RP} light curves and RV curves for a total sample of 1100 sources for which RVS time-series RVs are released in DR3. The sample includes 1096 bona fide RR Lyrae stars and four sources that were reclassified as different variable types during validation. Specifically, source 5337626858335118O was reclassified as DCEP_1O (see Sect. 6.5), and the sources 4130380472726484608, 3062985235999231104, and 5734183009797858l7 were reclassified as ECLs (see Sect 6.9).

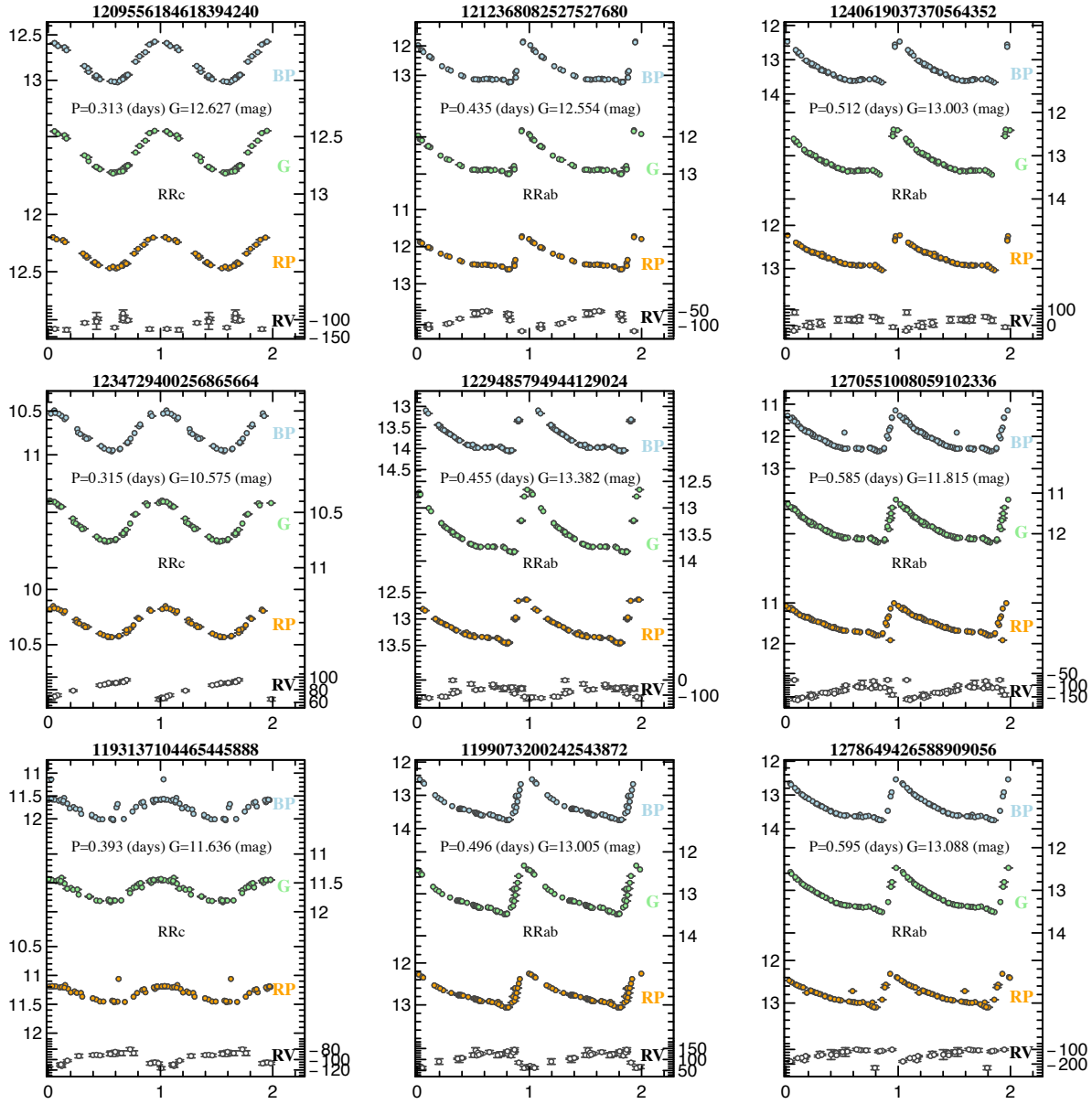

Fig. A.2. G_{BP}, G, and G_{RP} light curves and RV curves for RR Lyrae stars with RVS time-series data published in DR3. The atlas is published in its entirety only at the CDS.

Appendix B: Tests of the astrophysical parameters for RR Lyrae stars

B.1. Metallicities

In this section we present comparisons of the SOS Cep&RRL photometric metallicities with metal abundances from high-resolution spectra of RR Lyrae stars in Clementini et al. (1995), Lambert et al. (1996), Pancino et al. (2015), and with the metal abundances reported in column 10 of Table A.3 for the 19 RR Lyrae stars used to validate the RV curves from the RVS.

B.2. Absorption and metallicity values from the GSP_Phot module of Apsis

RR Lyrae stars have unusually large flux errors in their time-averaged BP/RP spectra compared to non-variable sources. The reason is that when the mean BP/RP spectra are computed, the amplitude of the light variation, which can range in the G band from ∼0.2 mag for RRc to more than one magnitude for RRab stars, enters the computed time-averaged BP/RP spectra as an additional flux error. This is clearly shown by the comparison of the S/Ns (median of each sample in each pixel) of the continuous BP/RP spectra of a sample of 1 000 RR Lyrae stars with $14 < \langle G \rangle < 16$ extracted from the `vari_rrlyrae` table and the continuous BP/RP spectra of a comparison sample composed of 1 000 random sources again within $14 < G < 16$ presented in Fig. B.3.

The larger BP/RP flux uncertainties cause larger uncertainties in the temperatures derived for RR Lyrae stars, thus opening space for temperature-extinction degeneracies in the GSP_Phot absorption estimates for RR Lyrae stars and causing large uncertainties and systematic offsets in the GSP_Phot metallicities for these variable stars.

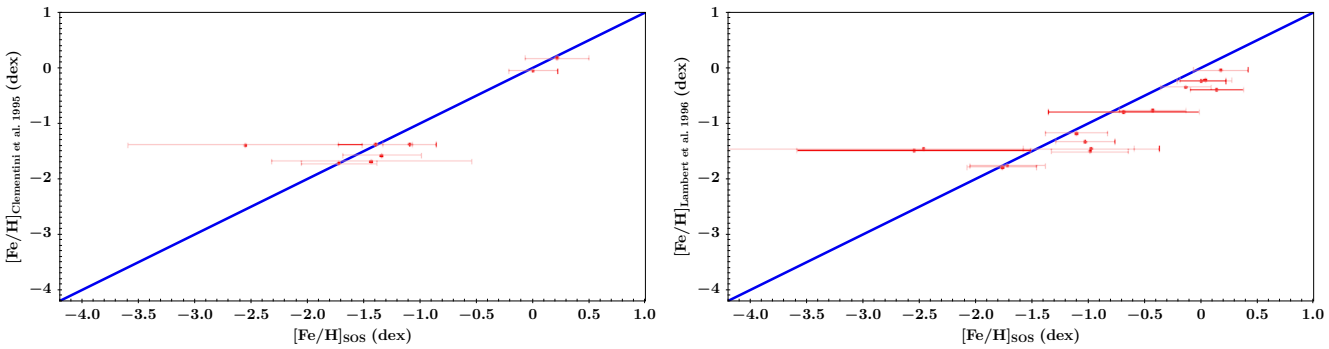

Fig. B.1. Comparison of the photometric metallicities derived by the SOS Cep&RRL pipeline and the metal abundances from high-resolution spectra of 8 RR Lyrae stars in Clementini et al. (1995) (left panel) and metal abundances from high-resolution spectra of 15 RR Lyrae stars in Lambert et al. (1996) (right panel).

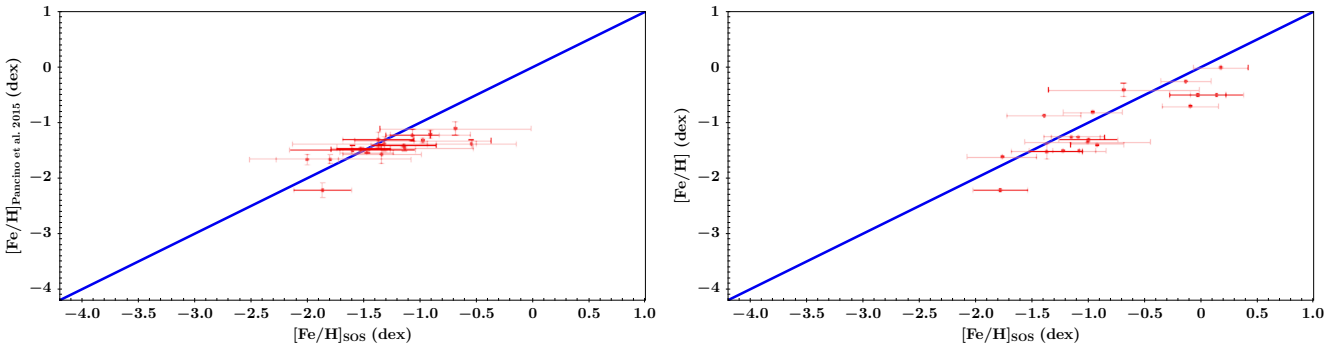

Fig. B.2. Comparison of the photometric metallicities derived by the SOS Cep&RRL pipeline and the metal abundances from high-resolution spectra of 16 RR Lyrae stars in Pancino et al. (2015) (left panel) and the metal abundances listed in Column 10 of Table A.3 of 19 RR Lyrae stars used to validate the RV curves from the RVS (right panel).

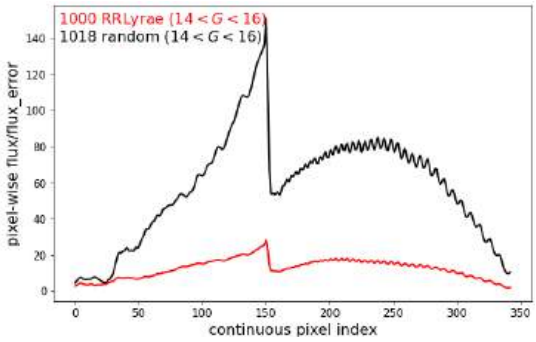

Fig. B.3. Comparison of the S/Ns (median of each sample in each pixel) of the continuous *BP*/*RP* spectra of a sample of 1 000 RR Lyrae stars with $14 < \langle G \rangle < 16$ mag extracted from the `vari_rrlyrae` table (red line) and the continuous *BP*/*RP* spectra of a control sample composed by 1 000 random non-variable sources with $14 < G < 16$ mag. The random sources (black line) have a much higher pixel-wise S/N than the RR Lyrae stars (red line), even though both samples are drawn from the same apparent *G* range.

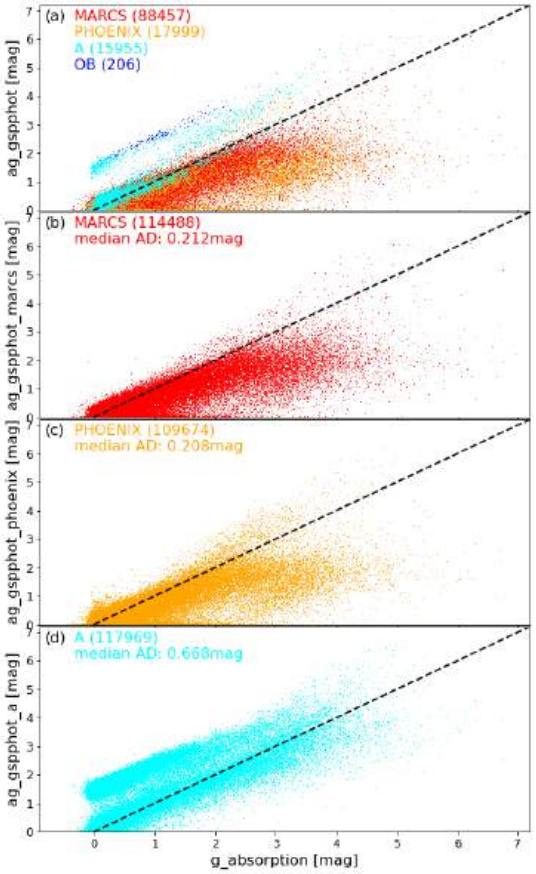

Fig. B.4. Same as in Fig. 25, but now the sources are colour-coded according to the GSP_Phot best library [Panel (a)]. The numbers next to each library name indicate how often each library is "best". The outlier group above the one-to-one relation consists of OB stars and some A stars (although other A stars fall nicely onto the 1-1 relation). Panels (b) to (d) show the results from each library individually (not best) as taken from the `astrophysical_parameters_supp` table in the *Gaia* archive. Panels (b) and (c) show that the MARCS and PHOENIX libraries do not have the outlier group above the identity relation, but for high SOS Cep&RRL $A(G)$ values, the GSP_Phot absorption appears to be lower. The median absolute differences (AD) are also plotted in panels (b) to (d). They are 0.212 mag for MARCS and 0.208 mag for PHOENIX.

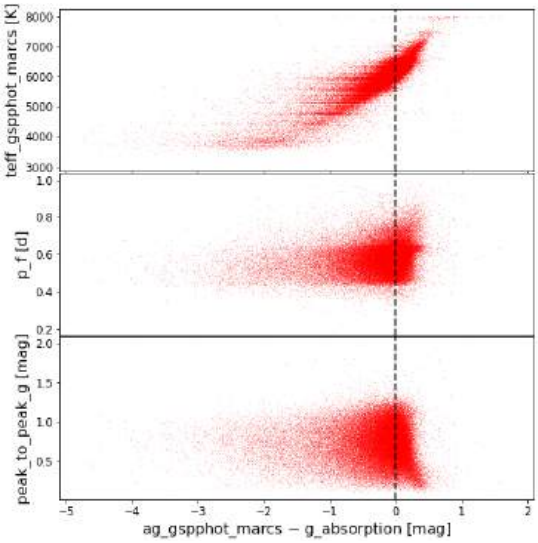

Fig. B.5. Run of the GSP_Phot $T_{\rm eff}$, pulsation period (Pf), and peak-to-peak amplitude in the G band [Amp(G)] of RR Lyrae stars for which both the GSP_Phot and the SOS Cep&RRL G absorption [$A(G)$] values are available as a function of the difference between the two absorption estimates, using for GSP_Phot only the MARCS library results in the `astrophysical_parameters_supp` table of the DR3 archive. The absorption differences are clearly unrelated to the pulsation period or the G peak-to-peak amplitude. The top panel clearly shows that large absorption differences are caused by an incorrect temperature in GSP_Phot MARCS. The absorption estimates agree for $6\,300 \lesssim T_{\rm eff} \lesssim 6\,800$ K, which is the typical mean temperature range of RRab stars (see also Column 11 in Table A.3). The variability (0.2-1.0 mag peak-to-peak amplitude in the G band) of the RR Lyrae stars is absorbed as increased flux uncertainties in the time-averaged BP/RP spectra. Through the unusually large BP/RP flux uncertainties, the χ^2 is flattened, and thus space for degeneracies is opened. In particular, a temperature-extinction degeneracy takes place that would explain the difference between the SOS Cep&RRL and the GSP_Phot absorption estimates for RR Lyrae stars.

Appendix C: Parameters for 14 RR Lyrae that are missing in the `vari_rrlyrae` table.

We provide the parameters that were computed with the SOS Cep&RRL pipeline for 14 bona fide RR Lyrae stars that were not published in the DR3 `vari_rrlyrae` table in Table C.1 (see Sect. 6.6).

Table C.1. Main parameters computed by the SOS Cep&RRL pipeline for 14 RR Lyrae stars that do not appear in the DR3 `vari_rrlyrae` table (see Sect. 6.6).

Main parameters computed by the SOS Cep&RRL pipeline													
Source ID	Type	Pf $\sigma(Pf)$	$P1O$ $\sigma(P1O)$	E[a] (G)	$\langle G\rangle/\langle G_{BP}\rangle/\langle G_{RP}\rangle$	Amp(G)/Amp(G_{BP})/Amp(G_{RP}) σAmp($G/G_{BP}/G_{RP}$)	$\phi_{21}(G)$ $\sigma[\phi_{21}(G)]$	$R_{21}(G)$ $\sigma[R_{21}(G))]$	$\phi_{31}(G)$ $\sigma[\phi_{31}(G)]$	R_{31} $\sigma[R_{31}(G)]$	[Fe/H][b] σ[Fe/H]	A(G)[c] σA(G)	$N_{G/G_{BP}/G_{RP}}$
4092009204924599040	RRc	- -	0.2581538 ±5x10^{-7}	1716.555440	15.4824/15.9069/14.866 ±9.7x10^{-4}/±0.0023/±0.0033	0.126/0.156/0.085 ±0.002/±0.007/±0.006	4.806 ±0.232	0.070 ±0.012	- -	- -	- -	- -	24/22/23
4120414435009794048	RRc	- -	0.256715 ±1x10^{-6}	1748.953931	17.317/18.136/16.401 ±0.006/±0.018/0.012	0.380/0.385/0.303 ±0.019/±0.040/±0.019	4.687 ±0.173	0.174 ±0.042	- -	- -	- -	- -	24/12/13
4144246349481643392	RRab	0.81001 ±1x10^{-5}	- -	1713.903329	17.216/18.149/16.119 ±0.003/±0.026/±0.018	0.225/0.251/0.200 ±0.013/±0.076/±0.064	4.859 ±0.130	0.281 ±0.045	- -	- -	- -	2.827 ±0.100	25/24/23
5797652730842515968	RRc	- -	0.2167765 ±4x10^{-7}	1700.798893	16.3430/16.5870/15.8778 ±7x10^{-4}/±0.0056/±0.0030	0.158/0.197/0.107 ±0.002/±0.017/±0.008	4.511 ±0.182	0.067 ±0.012	- -	- -	- -	- -	56/53/54
5797917193442176640	RRc	- -	0.2637340 ±4x10^{-7}	1701.161373	15.6366/15.8718/15.2366 ±0.0005/±0.00196/±0.00245	0.147/0.170/0.101 ±0.001/±0.009/±0.010	4.707 ±0.130	0.083 ±0.010	- -	- -	- -	- -	57/48/47
5846086424210395520	RRc	- -	0.2933843 ±5x10^{-7}	1700.684493	16.6451/16.8922/16.2396 ±0.0008/±0.0036/±0.0035	0.156/0.186/0.118 ±0.002/±0.011/±0.010	5.00 ±0.178	0.080 ±0.015	- -	- -	- -	- -	52/47/46
5917239841741208576	RRab	0.638600 ±2x10^{-6}	- -	1705.946735	16.3224/16.6628/15.8031 ±0.0005/±0.0026/±0.0024	0.147/0.188/0.116 ±0.001/±0.009/±0.006	4.422 ±0.050	0.189 ±0.007	2.937 ±0.229	0.040 ±0.011	−0.25 ±0.344	0.415 ±0.051	81/80/76
5991733644318583424	RRc	- -	0.258867 ±1x10^{-6}	1707.080357	16.444/17.10244/15.636 ±0.013/±0.004/±0.004	0.135/0.178/0.123 ±0.003/±0.014/±0.012	4.378 ±0.483	0.074 ±0.015	- -	- -	- -	- -	53/53/50
6017924835910361344	RRc	- -	0.268742 ±2x10^{-6}	1708.808652	17.762/18.319/17.037 ±0.002/±0.011/±0.006	0.214/0.294/0.183 ±0.007/±0.023/±0.013	4.847 ±0.184	0.178 ±0.046	- -	- -	- -	- -	32/32/30
6069336998880602240	RRab	0.73337 ±5x10^{-6}	- -	1699.822497	16.3183/16.6855/15.7082 ±0.0008/±0.0157/±0.0057	0.181/0.265/0.152 ±0.004/±0.052/±0.019	4.516 ±0.087	0.242 ±0.020	- -	- -	- -	0.712 -	37/35/36
6707009423228603904	RRc	- -	0.306965 ±1x10^{-6}	1709.373150	16.16385/16.3367/15.7239 ±0.0009/±0.0155/±0.0261	0.154/0.138/0.245 ±0.022/±0.043/±0.086	4.778 ±0.320	0.048 ±0.012	- -	- -	- -	- -	27/25/26
5935214760885709440	RRc	- -	0.340823 ±4x10^{-6}	1706.070130	19.0373/20.624/17.757 ±0.004/±0.092/±0.011	0.158/0.819/0.113 ±0.018/±0.301/±0.044	5.373 ±0.495	0.193 ±0.065	- -	- -	- -	- -	40/24/27
4362766825101261952	RRc	- -	0.2631889 ±5x10^{-7}	1716.317264	16.3937/16.9315/15.6715 ±0.0008/±0.0071/±0.0036	0.140/0.153/0.115 ±0.002/±0.027/±0.011	4.849 ±0.380	0.0518 ±0.019	- -	- -	- -	- -	43/40/41
5967334102579505664	RRab	0.62513 ±2x10^{-5}	- -	1707.700232	18.426/19.999/17.229 ±0.005/±0.040/±0.012	0.130/0.372/0.124 ±0.013/±0.310/±0.059	- -	- -	- -	- -	- -	3.429 ±0.090	37/38/37

Notes. The G, G_{BP}, G_{RP} time series photometry of these sources can be retrieved from the `gaiadr3.vari_classifier_results` table.
[a]The BJD of the epoch of maximum light is offset by JD 2455197.5 d (= J2010.0). [b]Photometric metal abundance derived from the ϕ_{31} Fourier parameter of the light curve of RR Lyrae stars (see Sects. 5.1 and 7). [c]Absorption in the G band computed from a relation that links the star intrinsic colour to the period and the amplitude of the G-band light variation of RR Lyrae stars (see Sects. 5.3 and 7).

Appendix D: OGLE-IV, ASAS-SN, and CATALINA control samples

Figures D.1, D.2, and D.3 show the footprints of RR Lyrae control samples drawn from the OGLE-IV, ASAS-SN, and CATALINA catalogues, respectively, that were used to estimate the completeness (and contamination, only OGLE) of the final clean catalogue of 270 905 RR Lyrae stars that are released in DR3.

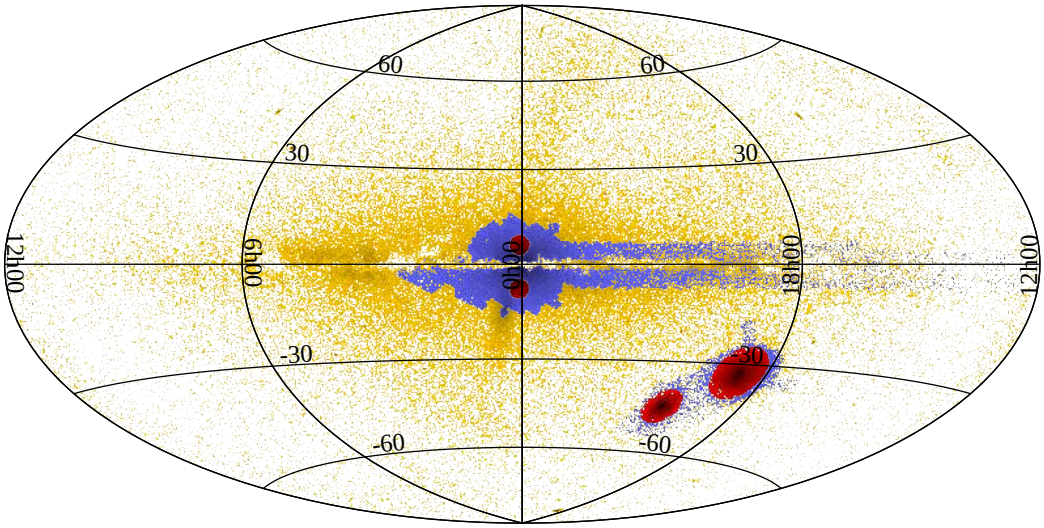

Fig. D.1. Regions (red areas) in the footprint of the OGLE-IV RR Lyrae stars (violet symbols) that we used to estimate the completeness, contamination, and percentage of new discoveries of the final clean catalogue of DR3 RR Lyrae stars (orange symbols) in the LMC, SMC, and in the Galactic bulge. For the LMC, we used a circular region with 8.3° in radius centred at (RA=81.5° Dec=−70.1°), for the SMC a region with 5.6° in radius centred at (RA=13.2°, Dec=−72.9°), and for the MW bulge, we used two regions with 3° degree in radius centred at (RA=274.7°, Dec=−31.8°; bulge-up) and (RA=261.2°, Dec=−24.9°; bulge-down).

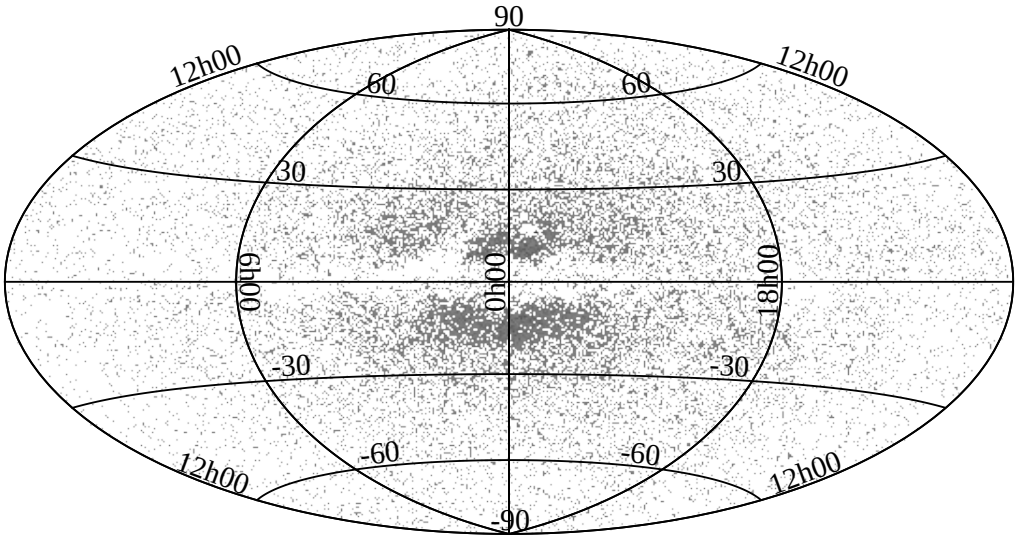

Fig. D.2. Footprint of the RR Lyrae stars in the ASAS-SN survey that we used to estimate the completeness of the *Gaia* DR3 RR Lyrae clean catalogue. In the region shown in the map lie 28 377 all-sky RR Lyrae stars observed by ASAS-SN with magnitudes in the range $10.4 < V < 17.4$ mag. In the RR Lyrae clean catalogue, we recover 20 921 of them, using a cross-match radius of 2.5 arcsec.

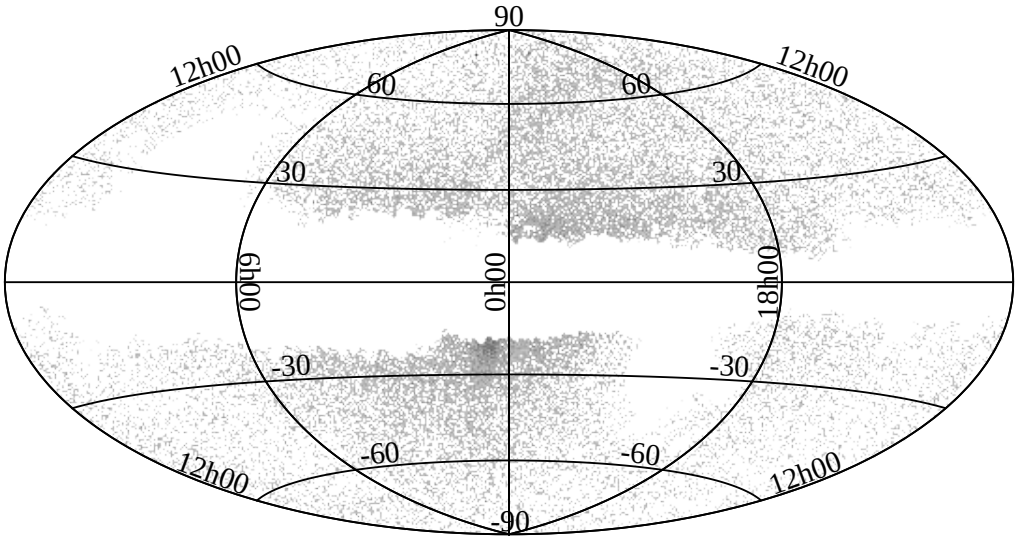

Fig. D.3. Footprint of the RR Lyrae stars of the CATALINA survey that we used to estimate the completeness of the *Gaia* DR3 RR Lyrae clean catalogue. In the region shown in the map lie 42 775 RR Lyrae observed by CATALINA, with magnitudes in the range $11 < V < 21.1$ mag. In the RR Lyrae clean catalogue, we recover 36 576 of them, using a cross-match radius of 2.5 arcsec.

Appendix E: Examples of *Gaia* archive queries

Table E.1. Queries to retrieve DR3 information on the RR Lyrae stars from the *Gaia* archive in the Astronomical Data Query Language (Osuna et al. 2008).

Query to retrieve the sourceid of all RR Lyrae stars confirmed with the SOS Cep&RRL pipeline in the *Gaia* DR3.

```
select gaia.source_id from gaiadr3.gaia_source as gaia
inner join gaiadr3.vari_rrlyrae as rrl on gaia.source_id=rrl.source_id
```

Query to retrieve the number of processed observations and SOS Cep&RRL-computed parameters of all RR Lyrae in the *Gaia* DR3.

```
select rrl.*,vs.num_selected_g_fov,vs.num_selected_bp,vs.num_selected_rp
from gaiadr3.vari_rrlyrae rrl
inner join gaiadr3.vari_summary vs on rrl.source_id=vs.source_id
```

Appendix F: Acronyms

Table F.1. List of acronyms used in this paper. Each acronym is also defined at its first occurrence in the paper.

Acronym	Description
ACEP	Anomalous Cepheid
$A(G)$	Absorption in the G band
AGN	Active Galactic Nuclei
All_Sky	The celestial region excluding the LMC, SMC, M31 and M33 regions
Amp(G)	Amplitude of the light variation in the G band
Amp(G_{BP})	Amplitude of the light variation in the G_{BP} band
Amp(G_{RP})	Amplitude of the light variation in the G_{RP} band
Amp(RV)	Amplitude of the RVS radial velocity variation
B-W	Baade-Wesselink
CMD	Colour Magnitude Diagram
DCEP	Classical Cepheid (Population I)
DPAC	Data Processing and Analysis Consortium
dSph	Dwarf spheroidal galaxy
DR	Data Release
EDR3	Early Data Release 3
ECL	Eclipsing binary
ELL	Ellipsoidal variable
F	Fundamental mode of pulsation
[Fe/H]	Iron abundance
FO or 1O	First overtone mode of pulsation
G	Gaia photometric G-band
G_{BP}	Gaia photometric G_{BP} band
G_{RP}	Gaia photometric G_{RP} band
G_{RVS}	Gaia photometric G_{RVS} band
GC	Globular cluster
LMC	Large Magellanic Cloud
LZ	Luminosity–Metallicity
M31	Andromeda galaxy
M33	Triangulum galaxy
MAD	Median Absolute Deviation
M_{G_0}	Absolute G magnitude
[M/H]	Total metal abundance
MORO	MultibandOutlierRemovalOperator
MW	Milky Way
PA	Period–Amplitude
Paper I	Clementini et al. (2016)
Paper II	Clementini et al. (2019)
PL	Period–Luminosity
PLZ	Period–Luminosity–Metallicity
PW	Period–Wesenheit
QSO	Quasi Stellar Object
ROFABO	RemoveOutliersFaintAndBrightOperator
RRab	RR Lyrae star of ab type
RRc	RR Lyrae star of c type
RRd	double-mode RR Lyrae star
RV	Radial Velocity
RVS	Radial Velocity Spectrometer
SEAPipe	Source Environment Analysis Pipeline
SMC	Small Magellanic Cloud
SOS	Specific Object Study
T2CEP	Type II Cepheid (Population II)
UFD	Ultra-faint dwarf galaxy